Impaired mRNA splicing and proteostasis in preadipocytes in obesity-related metabolic disease

Julia Sánchez-Ceinos[1,2], Rocío Guzmán-Ruiz[1,2*], Oriol A. Rangel-Zúñiga[2,3], Jaime López-Alcalá[1,2], Elena Moreno-Caño[1], Mercedes del Río-Moreno[2,4], Juan L. Romero-Cabrera[3], Pablo Pérez-Martínez[3], Elsa Maymo-Masip[5], Joan Vendrell[5], Sonia Fernández-Veledo[5], José M. Fernández-Real[2,6], Jurga Laurencikiene[7], Mikael Rydén[7], Antonio Membrives[8], Raúl M. Luque[2,4], José López-Miranda[2,3], and María M. Malagón[1,2*]

[1]Department of Cell Biology, Physiology, and Immunology, Instituto Maimónides de Investigación Biomédica de Córdoba (IMIBIC)/University of Córdoba/Reina Sofia University Hospital, 14014 Córdoba, Spain. [2]CIBER Fisiopatología de la Obesidad y Nutrición (CIBERobn), Instituto de Salud Carlos III, Spain. [3]Lipids and Atherosclerosis Unit, Department of Internal Medicine, IMIBIC/Reina Sofia University Hospital/University of Córdoba, 14004, Spain. [4]OncObesity and Metabolism Group. Department of Cell Biology, Physiology and Immunology, IMIBIC/University of Cordoba/Reina Sofía University Hospital. Córdoba, 14004, Spain. [5]Hospital Universitari de Tarragona Joan XXIII, Institut d´Investigació Sanitària Pere Virgili Universitat Rovira i Virgili, Tarragona, Spain; CIBER de Diabetes y Enfermedades Metabólicas Asociadas (CIBERdem), Instituto de Salud Carlos III, Madrid, Spain. [6]Department of Diabetes, Endocrinology and Nutrition, Dr. Josep Trueta University Hospital, and Eumetabolism and Health Group, Girona Biomedical Research Institute (IdibGi), Girona, Spain. [7]Lipid Laboratory. Department of Medicine Huddinge/Karolinska Institute (KI)/Karolinska University Hospital. Stockholm, 14186, Sweden. [8]Unidad de Gestión Clínica de Cirugía General y Digestivo. Sección de Obesidad. IMIBIC/Reina Sofia University Hospital, Córdoba, 14004, Spain.

***For correspondence:**

Dr. María M. Malagón, Department of Cell Biology, Physiology, and Immunology, IMIBIC//University of Córdoba/Reina Sofia University Hospital, 14004 Córdoba, Spain, Tel: +34-957213777; E-mail: bc1mapom@uco.es. ORCID iD: 0000-0002-2419-2727.

Dr. Rocío Guzmán-Ruiz, Department of Cell Biology, Physiology, and Immunology, IMIBIC//University of Córdoba/Reina Sofia University Hospital, 14004 Córdoba, Spain, Tel: +34-957213778; E-mail: bc2gurur@uco.es. ORCID iD: 0000-0001-8020-4676.

Abstract

Preadipocytes are crucial for healthy adipose tissue expansion. Preadipocyte differentiation is altered in obese individuals, which has been proposed to contribute to obesity-associated metabolic disturbances. Here, we demonstrate that impaired alternative splicing and dysregulated endoplasmic reticulum (ER)-associated protein degradation (ERAD) represent marker pathways of dysfunctional preadipocytes in obese individuals with insulin resistance (IR)/type 2 diabetes (T2D). Down-regulation of a key member of the major spliceosome, *PRFP8*/PRP8, as observed in IR/T2D preadipocytes from subcutaneous (SC) fat, prevented adipogenesis by altering both the expression and splicing patterns of adipogenic transcription factors and lipid droplet-related proteins, while adipocyte differentiation was restored upon recovery of *PRFP8*/PRP8 normal levels. Adipocyte differentiation was also compromised under conditions of ERAD hyperactivation, as occurs in SC and omental (OM) preadipocytes in IR/T2D obesity. Thus, targeting mRNA splicing and ER proteostasis in preadipocytes could improve adipose tissue function and thus contribute to metabolic health in obese individuals.

Introduction

Adipose precursor cells, the preadipocytes, are essential for the maintenance of adipose tissue homeostasis, regeneration, and expansion (***Berry et al., 2016***). Preadipocytes differentiation into adipocytes, i.e. adipogenesis, enables adipocyte turnover and adipose tissue growth and ensures adipose tissue plasticity to accommodate surplus energy ***(Arner et al., 2010; Sarjeant and Stephens, 2019***; ***Spalding et al., 2008***). It has been proposed that the inability for recruiting new adipose cells together with the functional impairment of hypertrophied adipocytes that occur in obesity contribute to lipid spill over from the adipose tissue (***Lessard and Tchernof, 2012***). Ectopic fat deposition and lipotoxicity in non-adipose organs have been associated with the development of insulin resistance (IR) and type 2 diabetes (T2D) (***Engin and Engin, 2017***). Thus, increasing adipogenesis appears as a valuable strategy to facilitate healthy adipose tissue expansion and ensure metabolic health (***Ghaben and Scherer, 2019***).

Adipocyte differentiation involves striking changes in size, metabolism, and responsiveness to signals. This process, in turn, relies on major changes in gene expression programs regulating mRNA and protein production (***de Sá et al., 2017***). An Increasing body of evidence shows that mRNA processing and, in particular, alternative splicing, is crucial for genome reprogramming during cell differentiation ***(Fiszbein and Kornblihtt, 2017***). In this line, the recent identification of PPARγ protein variants with opposing effects on preadipocyte differentiation, supports a role for alternative splicing in adipogenesis (***Aprile et al., 2020, 2018, 2014***). However, the splicing components relevant to adipogenesis and the cellular events regulated by alternative splicing during

76 adipocyte differentiation have been scarcely explored (***Lin, 2015***), and it is yet to
77 be established whether alternative splicing is modified in human obesity.
78 Another crucial mechanism preserving precursor cell function relates to protein
79 homeostasis (i.e., proteostasis), which maintains the capacity of cells to expand
80 in order to sustain tissue growth and regeneration (***Noormohammadi et al.,***
81 ***2018***). Several lines of evidence support an important role for the endoplasmic
82 reticulum (ER) protein quality control system in the regulation of adipogenesis
83 (***Lowe et al., 2011***). In fact, the unfolded protein response (UPR) is perturbed in
84 the obese adipose tissue and has been proposed to contribute to the pathology
85 of obesity (***Yilmaz, 2017***). By contrast, it is still unknown whether the other
86 component of the protein control system, the ER-associated protein degradation
87 (ERAD), which is crucial for protecting cells against accumulation of
88 misfolded/unfolded proteins and proteotoxicity ***(Hwang and Qi, 2018***), is altered
89 in the obese adipose tissue. Importantly, genetic ablation of the core ERAD
90 protein, SEL1L, in mouse adipocytes causes lipodystrophy and postprandial
91 hyperlipidaemia (***Sha et al., 2014***).
92 Here, we set out an iTRAQ-LC-MS/MS proteomic approach for the analysis of
93 subcutaneous (SC) and omental (OM) preadipocytes from obese individuals with
94 normoglycaemia (NG) and T2D in order to identify altered molecular pathways
95 that may contribute to metabolic disease in obesity. Down-regulation of multiple
96 components of the splicing machinery was observed in SC preadipocytes from
97 obese individuals with insulin resistance (IR) or T2D, as compared to NG obesity.
98 This, together with the observation that adipogenesis can be modulated by
99 regulating the expression levels of a key spliceosome component, *PRFP8*/PRP8,
100 support a role for alternative splicing in the development of obesity-associated

101 metabolic complications. In addition, our studies show that not only the UPR but
102 also the ERAD system are altered in human SC and OM preadipocytes from
103 IR/T2D obese subjects, and that this condition (i.e., hyperactivated ERAD), when
104 mimicked *in vitro*, prevented adipogenesis. Our results provide novel mechanistic
105 explanations for the impaired adipogenic capacity observed in IR/T2D obesity
106 that relates to both mRNA and ER-proteostasis disturbance.
107

108 **Results**

109 **Preadipocytes display distinct features in obesity-related IR/T2D**

110 Preadipocytes from SC and OM adipose tissue were isolated from 78 morbidly
111 obese subjects (BMI <40 kg/m^2) (hereinafter referred to as obese individuals)
112 (***Table 1***), who were subclassified into three groups [normoglycemic (NG Obese):
113 Glucose <100 mg/dL, HbA1c <5.7 %; impaired fasting glucose (IFG Obese):
114 Glucose 100-126 mg/dL, HbA1c 5.7-6.5 %; and with type 2 diabetes (T2D
115 Obese): Glucose >126 mg/dL, HbA1c >6.5 %], according to the criteria of the
116 American Diabetes Association (***ADA, 2021***). IFG individuals exhibited
117 significantly higher HOMA-IR values than NG individuals and they will be referred
118 to as insulin-resistant (IR) subjects (***Díaz-Ruiz et al., 2015***; ***Tam et al., 2012***). No
119 significant differences were found among groups in blood pressure, inflammation,
120 or lipid parameters except triglycerides, whose levels were enhanced in T2D *vs.*
121 NG obese groups.

122 Paired SC and OM adipose tissue samples were processed for the isolation of
123 the stroma-vascular fraction (SVF) and mature adipocytes. Microscopic analysis
124 of freshly isolated mature adipocytes revealed that these cells were larger in
125 IR/T2D than in NG obese individuals (***Table 1—Figure supplement 1A***).

126 SC and OM preadipocytes were obtained after serial passaging (2-3
127 passages) of the corresponding SVFs following established methods (***Bunnell et***
128 ***al., 2008***; ***Palumbo et al., 2018***; ***Serena et al., 2016***; ***Zhu et al., 2013***). The purity
129 of the preadipocyte cultures was confirmed by the presence of the preadipocyte
130 marker DLK1/PREF1 and the absence of the blood cell markers CD45 and CD14
131 (***Table 1—Figure supplement 1B***). Expression levels of the proliferation marker,
132 *KI67*, and the proliferation rate, as assessed by cell count, were higher in SC than
133 in OM preadipocytes, and both parameters decreased in IR/T2D (***Table 1—***
134 ***Figure supplements 1C and 1D***). Preadipocyte proliferation rate negatively
135 correlated with obesity and IR markers (BMI, glucose, insulin, and HbA1c) (***Table***
136 ***1—Supplementary file 1***).
137 Microscopic observation of lipid droplets (LDs) showed that both SC and OM
138 preadipocytes from NG obese subjects differentiated well, while those from
139 IR/T2D obese groups differentiated poorly (***Table 1—Figure supplement 1E***). In
140 this line, the mRNA levels of the adipocyte markers, *PPARG*, *FABP4,* and
141 *ADIPOQ* were lower in IR obese subjects than in their NG counterparts
142 throughout differentiation (***Table 1—Figure supplement 1F***).

143 **Comparative proteomics of human obese preadipocytes**

144 In order to identify marker pathogenic pathways of dysfunctional preadipocytes
145 in obesity-associated metabolic disease, we employed iTRAQ proteomics of SC
146 and OM preadipocytes from obese individuals with extreme metabolic
147 phenotypes, NG *vs.* T2D. This study enabled the identification of a total of 1,758
148 proteins that were present in both SC and OM fat from NG and T2D obese
149 individuals, thus defining the human obese preadipocyte proteome. According to
150 GO Biological Process annotation, 55.5% of these proteins were related to

151 cellular and metabolic processes (***Figure 1—Figure supplement 2A***), including
152 metabolism of mRNA, proteins, glucose, and lipids (***Figure 1—Figure***
153 ***supplement 2B***). All the proteomic data related to this study are available at the
154 ProteomeXchange Consortium via the Proteomics IDEntifications (PRIDE)
155 partner repository ***(Perez-Riverol et al., 2019***) with the dataset identifier
156 PXD015621.

157 Comparison of proteomic data from SC and OM preadipocytes revealed
158 marked differences between the two types of cells regarding the number of
159 differentially expressed proteins and protein-related functional pathways (***Figure***
160 ***1—Figure supplement 3***, and ***Figure 1—Source data 1***). To investigate
161 enrichment for functional pathways in each depot, canonical pathway analysis of
162 the proteomic data was performed using IPA. Among the top ten IPA canonical
163 pathways that were overrepresented in SC preadipocytes in T2D obesity (***Figure***
164 ***1—Source data 2***), the highest ranked down-regulated pathway was the
165 spliceosomal cycle (***Figure 1B***). The unfolded protein response (UPR) was also
166 modified in SC preadipocytes from T2D obese group (***Figure 1B***), while
167 pathways related to ER stress were up-regulated in OM preadipocytes (***Figure***
168 ***1C***) in T2D *vs.* NG obesity.

169 Based on these findings, we next characterized the splicing machinery and ER
170 control system in preadipocytes and their contribution to adipocyte differentiation.

171 **Splicing dysregulation as a marker of SC preadipocytes in obesity-related**
172 **metabolic disease**

173 To complement our proteomic observations, we assessed the expression of
174 splicing-related genes in human preadipocytes using a microfluidic-based
175 dynamic qPCR array comprising 45 splicing-related components (***Gahete et al.,***

176 ***2018***). Preadipocytes isolated from the SC and OM fat pads of NG, IR, and T2D
177 obese individuals were employed for this study. Analysis of gene expression
178 profiles by hierarchical clustering revealed a marked gene expression shift
179 between NG and IR/T2D SC preadipocytes, which was not evident for OM
180 preadipocytes (***Figure 2A***). SC preadipocytes from IR/T2D obese individuals
181 exhibited lower expression levels of splicing-related genes than NG obese
182 subjects, including components of major spliceosome (*PRPF8*, *RNU5*, *SF3B1*
183 *tv1*, *TCERG1*, and *U2AF1*), and splicing factors (*CELF1*, *MAGOH*, *RBM3*,
184 *RBM45*, *SFPQ*, and *SNW1*) (***Figures 2A*** and ***2B***, and ***Figure 2—Figure***
185 ***supplement 4***). Notably, only the minor spliceosome component, *RNU12*, was
186 up-regulated in T2D *vs.* NG SC preadipocytes (***Figure 2A*** and ***Figure 2—Figure***
187 ***supplement 4B***). No differences in OM preadipocytes were observed among the
188 three groups of obese individuals (***Figure 2*** and ***Figure 2—Figure supplement***
189 ***4***). These observations were largely confirmed in a second independent subset
190 of samples obtained from additional obese individuals using RT-PCR (***Figure 2—***
191 ***Figure supplement 5***).
192 The splicing machinery was also investigated in preadipocytes from a second
193 cohort, comprising lean subjects (BMI <25 kg/m^2) and NG and T2D individuals
194 with simple obesity (BMI 30-35 kg/m^2) (hereinafter referred to as simple obesity)
195 (***Figure 2C*** and ***Figure 2—Figure supplement 6***). These results revealed
196 significantly higher expression levels of main components of the major
197 spliceosome (*PRPF8* and *SF3B1 tv1*) in SC preadipocytes from NG obese *vs.*
198 lean individuals (***Figure 2C*** and ***Figure 2—Figure supplement 6A***). A trend to
199 increase was also observed for the minor spliceosome component, *RNU12*, and
200 the splicing factors, *CELF1* and *SNW1*, although this did not reach statistical

201 significance (***Figure 2—Figure supplements 6B*** and ***6C***). Notably, and similar
202 to that observed for morbidly obese individuals from cohort 1 (***Figure 2A*** and
203 ***Figure 2—Figure supplements 4 and 5***), a significant decrease in the
204 expression levels of all the genes tested, except *RNU12*, was observed in T2D
205 *vs.* NG individuals with simple obesity (***Figure 2C*** and ***Figure 2—Figure***
206 ***supplement 6***). No differences were observed in OM preadipocytes when groups
207 of cohort 2 were compared (***Figure 2C*** and ***Figure 2—Figure supplement 6***).

208 ***PRPF8*/PRP8 expression studies in human preadipocytes**

209 One of the most highly expressed genes in SC preadipocytes from NG obese
210 individuals that was significantly down-regulated in both IR and T2D obese
211 subjects as compared to NG SC preadipocytes, was *PRPF8*/PRP8. Specifically,
212 mRNA and protein levels of this key component of the major spliceosome were
213 reduced by 51% and 56%, respectively, in IR SC preadipocytes, and by 49% and
214 82% in T2D SC preadipocytes as compared to NG levels (***Figures 2A*** and ***2B***).
215 No differences in *PRPF8*/PRP8 expression were observed among groups in OM
216 preadipocytes (***Figures 2A*** and ***2B***). Differentiation studies revealed that while
217 *PRPF8* expression levels remained low throughout adipogenesis in IR
218 preadipocytes, *PRPF8* levels peaked at day 3 (D3) of differentiation and
219 thereafter remained above D0 levels in NG preadipocytes (***Figure 2D***). *PRPF8*
220 mRNA remained constant or decreased at the end of differentiation of NG and IR
221 OM preadipocytes, respectively (***Figure 2D***).

222 ***PRPF8*/PRP8 down-regulation in SGBS preadipocytes impairs**
223 **adipogenesis**

224 We employed a siRNA strategy to down-regulate *PRPF8* gene expression levels
225 in preadipocytes to mimic the conditions found in IR/T2D obese SC
226 preadipocytes as compared to NG obesity. These studies were carried out using
227 the human SC adipocyte cell line, SGBS cells. As observed for NG SC human
228 primary preadipocytes, *PRPF8* mRNA levels reached a peak at early stages of
229 SGBS cell differentiation (D4) (***Figure 3A***).

230 siRNA treatment of SGBS preadipocytes (D4) decreased by 67% and 65%
231 *PRPF8* mRNA and protein levels, respectively, at day 3 post-transfection (D7),
232 without changing cell viability (**Figure 3—*Figure supplements 7A-C***).
233 Morphometric evaluation of Oil-Red O staining in confocal micrographs revealed
234 that *PRPF8*-silenced preadipocytes accumulated more but smaller LDs than
235 control cells, which resulted in an increase in the total lipid content in cells
236 exposed to *PRPF8* siRNA (***Figure 3C***). *In silico* analysis of CLIP_Seq data using
237 ENCORI (The Encyclopedia of RNA Interactomes) (***Li et al., 2013***) revealed both
238 adipogenic (*PPARG* and *SREBF1)* and LD biogenesis and growth markers
239 (*BSCL2*, *CIDEB*, and *CIDEC*) as PRP8 target genes (***Figure 3—Source data 3***).
240 Enrichment analysis of PRP8-RNA interactions revealed pathways such as
241 insulin signalling, adipokine signalling, and fatty acid metabolism to be
242 significantly overrepresented (***Figure 3—Source data 3***). Similarly, the
243 HumanBase tool (***Greene et al., 2015***) identified several adipogenesis-related
244 genes, including *ADIPOQ*, *CAV1*, and *CD36*, among the Top10 genes showing
245 functional interactions with *PRPF8* (***Figure 3—Source data 4***). In accordance
246 with the *in silico* data, expression of total *PPARG* and *SREBF1* transcript contents

247 and the abundances of some of their isoforms were altered in *PRPF8*-silenced
248 cells (***Figures 3D*** and ***3E***). In particular, mRNA and protein levels of the fat
249 specific *PPARG* isoform, *PPARG-2*, were up-regulated upon *PRPF8* silencing
250 (***Figures 3D*** and ***3E***). Decreased levels and/or altered splicing patterns of
251 *BSCL2*, *CIDEB*, and *CIDEC,* were also observed in silenced cells (***Figure 3F***).
252 Other genes showing significant changes in *PRPF8*-silenced cells included
253 enzymes involved in lipid synthesis (FAS and DGAT2), and the LD-associated
254 protein, ADRP, while neither PLIN1 nor HSL/pHSL were modified (***Figure 3G***).
255 *PRPF8* silencing also activated stress responses in SGBS adipocytes, as
256 indicated by the increased protein levels of the ER stress marker, CHOP, the
257 immunoproteasome component, PSMB8, and CASP3/Pro-CASP3 ratio (***Figure***
258 ***3G***). Contrarily to control cells, *PRPF8*-silenced cells did not respond to an insulin
259 challenge (***Figure 3H***). Most of the effects depicted for silenced SGBS cells at
260 D7 remained significant at D10 (***Figure 3—Figure supplement 7***). Nevertheless,
261 silenced cells at D10 still exhibited abundant LDs but of small size, thus resulting
262 in a drastic decrease in the total amount of lipids stored in *PRPF8* siRNA-treated
263 cells as compared with controls (***Figure 3I***). *PPARG-2* mRNA and protein, and
264 the late adipocyte markers, *ADIPOQ* and *FABP4*, were down-regulated at D10 in
265 *PRPF8*-silenced cells (***Figure 3—Figure supplements 7D-E*** and ***7H***).
266 Notably, recovery of PRP8 protein levels by co-transfection of *PRPF8*-silenced
267 SGBS cells with an expression vector coding for this protein (*PRPF8*-pcDNA3.1)
268 reverted the effects induced by *PRPF8* silencing on adipocyte and LD markers,
269 both at D7 (data not shown) and D10 (***Figure 3—Figure supplement 7***).
270 Silencing-induced changes in both LD number and size were also reverted in
271 rescue experiments by *PRPF8* re-expression (***Figure 3I***). Silencing experiments

272 using human adipose-derived stem cells (hADSCs) gave similar results to those
273 observed in SGSB cells (***Figure 3—Figure supplements 8***).
274 We also examined the contribution of other splicing genes to adipocyte
275 differentiation, namely the SF3B complex and the splicing factor, SFPQ.
276 Specifically, since SC preadipocytes from IR/T2D obese individuals showed
277 diminished *SF3B1 tv1* expression levels (***Figure 3—Figure supplements 4*** *and*
278 ***5***), we exposed SGBS cells to pladienolide-B, which binds to the SF3B complex
279 and inhibits pre-mRNA splicing via targeting splicing factor SF3B1 ***(Aouida et al.,***
280 ***2016***; ***Cretu et al., 2018***). Exposure to pladienolide-B impaired lipid accumulation
281 in SGBS cells (***Figure 3—Figure supplement 9A***). This concurred with, among
282 other changes, diminished expression levels of *PPARG-1*, *PPARG-2*, and both
283 total *SREBF1* and *SREBF1-1*, while *PPARG-4* and *BSCL2-2/3* expression
284 increased (***Figure 3—Figure supplements 9B*** and ***9C***). On the other hand,
285 *SFPQ* down-regulation by siRNA treatment of SGBS cells caused significant
286 changes in the expression of only a few genes, i.e., up-regulation of total *SREBF1*
287 and *SREBF1-1* and down-regulation of *PPARG-4* (***Figure 3—Figure***
288 ***supplements 9D-G***). Nevertheless, silenced SGBS cells exhibited reduced lipid
289 content, mostly due to the increase in the number of LDs (2.4-fold), while LD size
290 decreased as compared with control cells (2.7-fold) (***Figure 3—Figure***
291 ***supplement 9E***).

292 **Analysis of *PRPF8*/PRP8 effects on human primary preadipocytes**

293 Based on our findings in SGBS preadipocytes, we carried out targeted
294 silencing and overexpression studies of *PRPF8*/PRP8 in primary preadipocytes
295 obtained from SC adipose tissue samples of NG, IR, and T2D obese individuals
296 (***Figure 4***).

297 First, we examined the effect of *PRPF8* silencing in SC preadipocytes from
298 obese NG patients using a specific siRNA as a mean to mimic the down-
299 regulation of this gene found in SC preadipocytes from obese subjects with
300 IR/T2D (***Figures 2A*** and ***2B***, ***Figure 1—Figure supplements 4*** and ***5***). As shown
301 in ***Figure 4B***, SC preadipocytes from NG obese individuals exhibited lower lipid
302 content and changes in LD size and number when silenced for *PRPF8*. In
303 addition, *PRPF8* down-regulation caused numerical decreases, that in most
304 cases reached statistical significance, in the expression levels of both total
305 *PPARG* and *SREBF1* and their isoforms as compared to mock-transfected SC
306 preadipocytes from NG obese subjects (***Figures 4C-D***). Notably, rescue
307 experiments by transfection of silenced NG obese preadipocytes with the
308 *PRPF8*-pcDNA3.1 expression vector showed restored expression of most of the
309 genes tested, which was accompanied by a recovery of LD content (***Figure 4***).
310 Second, in order to test whether recovery of *PRPF8*/PRP8 levels could
311 improve the differentiation capacity of IR and T2D obese SC preadipocytes,
312 overexpression studies using the *PRPF8*-pcDNA3.1 expression vector were
313 carried out (***Figure 4***). After transfection, both IR and T2D obese SC
314 preadipocytes exhibited *PRPF8* expression levels comparable to those of SC
315 preadipocytes from obese NG patients (***Figure 4A***). *PRPF8* expression recovery
316 upon *PRPF8*-pcDNA3.1 transfection increased the expression of several *PPARG*
317 isoforms (*PPARG-2*, *PPARG-3*, *PPARG-4*, and *γORF4*) to control levels (i.e., SC
318 preadipocytes in NG obesity), especially in IR preadipocytes (***Figure 4C***). Similar
319 results were observed for both total *SREBF1* and *SREBF1-1* (***Figure 4D***). In all,
320 these results indicate that the expression of *PPARG* and *SREBF1* could be
321 recapitulated in SC preadipocytes from obese IR/T2D patients by *PRPF8*

322 complementation. In line with these findings, confocal microscopy studies
323 showed that *PRPF8*-pcDNA3.1 expression increased total lipid content in SC
324 preadipocytes from obese subjects with IR/T2D by increasing LD size, while
325 decreasing LD number (***Figure 4B***). Analysis of markers of LD biogenesis and
326 growth (*BSCL-2*, *CIDEB*, *CIDEC*), showed similar trends to those observed for
327 *PPARG* and *SREBF1* upon manipulation of *PRPF8* expression in SC
328 preadipocytes from either NG or IR/T2D obese individuals (***Figures 4E-G***).

329 **The UPR is altered in preadipocytes of IR/T2D obese subjects**

330 As mentioned earlier, pathway analysis of iTRAQ proteomic data indicated that
331 ER stress-related pathways were altered in both SC and OM preadipocytes from
332 T2D obese individuals when compared to NG obese subjects (***Figures 1B*** and
333 ***1C***).

334 Immunoblotting studies of additional human preadipocyte samples to those
335 employed for iTRAQ studies, confirmed and extended the proteomic data by
336 demonstrating altered mRNA/protein levels of UPR components in both SC and
337 OM preadipocytes from IR/T2D obese groups as compared to NG obesity
338 (***Figures 1B*** and ***1C***, and ***Figure 5***). To be more specific, SC and OM
339 preadipocytes from T2D obese individuals exhibited enhanced levels of the ER
340 stress-inducible gene, BiP (***Figure 5A*** and ***Figure 1—Source data 2***). IR/T2D
341 modified the protein content of p90 and p50, and cleaved/full-length ATF6 ratio
342 in OM preadipocytes, and decreased this ratio in SC preadipocytes in IR *vs*. NG
343 (***Figure 5B***). In addition, pPERK and pPERK/PERK ratio were up-regulated in
344 SC and OM preadipocytes in relation to IR and/or T2D (***Figure 5C***). However,
345 peIF2α and peIF2α/eIF2α ratio as well as the eIF2α-target, CHOP, were
346 significantly reduced in OM preadipocytes in relation to IR/T2D (***Figures 5C*** and

347 ***5E***). We observed enhanced IRE1α levels and decreased pIRE1α/IRE1α ratio in
348 IR *vs*. NG OM preadipocytes (***Figure 5F***). IR OM preadipocytes and IR/T2D SC
349 preadipocytes also exhibited higher levels of the spliced form of *XBP1* than NG
350 preadipocytes (***Figure 5G***). Finally, the ER chaperones, GRP94 and PDI, were
351 more abundant in T2D preadipocytes than in NG preadipocytes from both SC
352 and OM fat (***Figure 5H***). Our proteomic study revealed enhanced levels of 11
353 additional ER chaperones in T2D SC preadipocytes (***Figure 1—Source data 2***).

354 **Dysregulation of ER-associated protein degradation (ERAD) in IR/T2D**
355 **obese preadipocytes**

356 In association with the UPR, the ERAD represents a key quality-control
357 machinery that recruits unfolded/misfolded ER proteins via ER chaperones and
358 targets these proteins for cytosolic degradation by the proteasome ***(Christianson***
359 ***and Ye, 2014***; ***Qi et al., 2017***). Given our results on the UPR, we next explored
360 the ERAD in human preadipocytes and observed a marked up-regulation of
361 proteins involved in all the steps comprising this process, including protein
362 recognition (*BIP*; ***Figure 6A***), retrotranslocation through the ER membrane
363 (*DERL1*, *SEC61A1*, *STT3A*, and *STT3B*; ***Figure 6B***), ubiquitination (*HRD1* and
364 *RNF185*; ***Figure 6C***), and targeting of misfolded proteins to the proteasome
365 (*RAD23A* and *UBQLN1*; ***Figure 6D***) in IR/T2D *vs.* NG obesity. These changes
366 occurred in both SC and OM preadipocytes, which split into two clusters (NG and
367 IR/T2D) when ERAD data was represented in a two-way hierarchical clustering
368 heatmap (***Figure 6E***). In this line, when the ERAD process was explored during
369 adipocyte differentiation, higher overall transcript contents of ERAD genes in IR
370 preadipocytes than in NG preadipocytes (measured as AUC) were observed
371 ***(Figure 6—Figure supplement 10)***.

372 Finally, when preadipocytes from individuals of cohort 2 were examined, a
373 trend to increase in representative genes of ERAD in T2D individuals with simple
374 obesity *vs*. their NG counterparts and lean individuals was observed (***Figure 6—***
375 ***Figure supplement 11***). Nevertheless, the expression of some of these ERAD-
376 related genes, such as *RAD23A*, which was higher in SC preadipocytes from NG
377 individuals with simple obesity as compared to lean individuals, decreased in the
378 transition from NG to T2D in obesity (***Figure 6—Figure supplement 11D***), an
379 effect that was also observed in morbid obesity (***Figure 6D***).

380 **Regulation of ER proteostasis in preadipocytes**

381 In order to unveil the regulation of ERAD in preadipocytes , *in vitro* models of
382 hyperglycaemia/hyperinsulinemia, inflammation, and hypertrophy due to lipid
383 overload, were developed using SGBS cells (***Figure 7—Figure supplement 12***).
384 Specifically, preadipocytes were exposed to high concentrations of glucose and
385 insulin (HGHI), TNFα, or fatty acids (palmitate or oleate), respectively (***Díaz-Ruiz***
386 ***et al., 2015***). None of the treatments compromised cell viability (data not shown)
387 and, except for oleate, they impaired insulin-induced Akt phosphorylation (***Figure***
388 ***7—Figure supplement 12C***). Exposure to HGHI increased the expression of BiP
389 and nearly all the other ERAD components tested (***Figure 7—Figure***
390 ***supplement 13A***). As shown in ***Figure 7—Figure supplement 13B***, expression
391 levels of ERAD genes enabled discrimination of HGHI-treated from control SGBS
392 cells. Given these observations, we next examined the activity of the protein
393 degradation machinery in the cytosol, the proteasome (***Bard et al., 2018***), in cells
394 exposed to HGHI. These studies showed that hyperglycaemic/hyperinsulinemic
395 conditions decreased the activity of the 26S proteasome while increasing the

396 amount of ubiquitinated proteins in SGBS preadipocytes (***Figure 7—Figure***
397 ***supplements 13C*** and ***13H***).

398 The naturally occurring bile acid, tauroursodeoxycholic acid (TUDCA), has
399 been shown to restore ER homeostasis in ER-stressed cells (***Zhang et al., 2018***).
400 We thus tested whether exposure of SGBS preadipocytes to TUDCA prior to
401 HGHI treatment could prevent HGHI-induced up-regulation of ERAD genes and
402 accumulation of ubiquitinated proteins in these cells, which was proven to be the
403 case (***Figure 7—Figure supplements 13D and 13E***). TUDCA also reverted
404 HGHI inhibitory effects on PPARγ and FABP4 expression levels (***Figure***
405 ***7—Figure supplement 13F***).

406 Finally, TUDCA was also able to reduce the enhanced expression levels of
407 ERAD-related genes and decreased mRNA levels of adipogenic markers induced
408 by BiP overexpression in SGBS preadipocytes (***Figure 7—Figure supplement***
409 ***14***).

410 Based on the results obtained in SGBS preadipocytes, we next tested whether
411 exposure to HGHI could induce an IR-like phenotype in primary preadipocytes
412 from OM adipose tissue of NG obese individuals (i.e., activation of ERAD). ***Figure***
413 ***7*** shows that, as for SGBS preadipocytes, exposure of OM preadipocytes from
414 NG obese subjects to HGHI increased the expression levels of genes involved in
415 all ERAD steps (recognition, retrotranslocation ubiquitination, and targeting to the
416 proteasome) in these cells (***Figures 7A-D***). On the other hand, TUDCA, which
417 did not alter essentially the expression of ERAD genes when administered alone,
418 reduced HGHI-induced gene expression increases to control levels (i.e., OM
419 preadipocytes from NG obese individuals exposed to medium alone) (***Figures***
420 ***7A-D***). HGHI also increased the accumulation of ubiquitinated proteins in OM

421 preadipocytes from NG obese individuals, while only a slight, not significant
422 decrease in ubiquitin-conjugated proteins was observed when HGHI was
423 combined with TUDCA (***Figure 7E***). Notably, the activity of the 26S proteasome
424 remained unchanged in all the experimental conditions tested (***Figure 7F***).
425 Morphometric quantification of micrographs from HGHI-treated OM
426 preadipocytes revealed a decrease in total lipid content as compared to their
427 control counterparts (***Figure 7G***). These changes were accompanied by
428 significant reductions in the expression of total *PPARG* and *PPARG-2* as well as
429 of *ADIPOQ* and *FABP4* mRNA levels (***Figures 7H*** and ***7I***). Exposure to TUDCA
430 reverted the effects of HGHI on both lipid content and on most of the adipogenic
431 genes examined (***Figures 7G-I***).
432 On the other hand, analysis of OM preadipocytes from both IR and T2D obese
433 individuals demonstrated that proteasome activity was decreased while levels of
434 ubiquitin-conjugated proteins were increased in these cells as compared to their
435 NG counterparts (***Figures 7E*** and ***7F***). Interestingly, TUDCA reverted both
436 effects in OM preadipocytes from IR obese patients but not in T2D preadipocytes
437 (***Figures 7E*** and ***7F***). TUDCA was also able to increase the expression of
438 markers of differentiation in preadipocytes from IR and, to a lower extent, also
439 from T2D obese individuals (***Figures 7H*** and ***7I***). In fact, this chaperone
440 enhanced the lipid content in OM preadipocytes of IR and T2D obese subjects to
441 the levels found in OM preadipocytes of NG obese subjects, though TUDCA-
442 treated T2D OM preadipocytes exhibited low LD numbers (***Figure 7G***).
443
444
445

446 **Discussion**

447 We found that alternative splicing in the SC adipose tissue, and the ER stress-
448 UPR-ERAD system in both SC and OM fat represent essential components of
449 the adipogenic process that are altered in obese individuals with IR/T2D. We
450 show novel evidence demonstrating that NG obesity involves the up-regulation
451 of splicing-related genes in SC preadipocytes as compared with lean individuals.
452 However, the development of IR/T2D, both in simple and morbid obesity, is
453 associated with a general decrease in the expression of splicing genes in SC
454 preadipocytes. In fact, decreasing the expression of a key component of the
455 major spliceosome, *PRPF8*/PRP8, by siRNA is sufficient to hamper the
456 expression of both markers of adipogenesis and regulators of LD biogenesis and
457 growth. Our results support a relevant role for this protein and the splicing
458 machinery in the regulation of adipocyte differentiation and highlight the biological
459 significance of alternative splicing in maintaining adipose tissue homeostasis and
460 metabolic health in obesity. Our results are also indicative of IR/T2D-dependent
461 ERAD hyperactivation in preadipocytes of the two major fat depots, SC and OM,
462 in obese individuals. Maladaptative UPR and ERAD signalling upon ER stress
463 induction may contribute to impair adipocyte differentiation and to the progression
464 of metabolic disease in obesity.

465 Alternative splicing of mRNA enables cells to acquire protein diversity, which
466 is essential for cell differentiation and tissue growth and identity ***(Baralle and***
467 ***Giudice, 2017***). It is accepted that both mRNA transcription and processing
468 contribute to the changes in gene expression patterns leading to the transition of
469 progenitor cells toward a mature phenotype (***Fiszbein and Kornblihtt, 2017***). In
470 this regard, recent reports suggest a role for alternative splicing in adipocyte

471 differentiation (***Lin, 2015***). It has been shown that inhibition of the splicing factor,
472 SF3B1, blocks 3T3-L1 adipocyte differentiation (***Kaida, 2019***), and recent RNA-
473 seq studies support the occurrence of alternative splicing events during
474 adipogenesis of bone marrow-derived human mesenchymal stem cells (***Yi et al.,***
475 ***2019***). Furthermore, certain naturally PPARγ isoforms generated by alternative
476 splicing act as dominant-negative isoforms that prevent adipocyte differentiation
477 (***Aprile et al., 2020, 2018, 2014***). However, few studies have addressed the
478 relevance of the splicing machinery in human preadipocytes and whether this
479 system is altered in obesity. To the best of our knowledge, this is the first study
480 demonstrating the deregulation of representative members of the two main
481 components of the splicing machinery, the major and minor spliceosome, and
482 associated splicing factors in human SC preadipocytes (and, occasionally, also
483 in OM preadipocytes) in relation to obesity-associated IR/T2D. To be more
484 specific, we show the up-regulation of several splicing-related genes in response
485 to simple obesity, especially in SC preadipocytes, in individuals that maintain an
486 adequate glycaemic control. This could represent an adaptive response to weight
487 gain that seems to be lost in obese or extremely obese individuals with IR/T2D.
488 In fact, our proteomic and gene expression results indicate that a high proportion
489 of splicing-related elements were down-regulated in SC preadipocytes from
490 obese individuals with IR/T2D as compared to those with a better metabolic
491 profile (NG). In all, our results strongly support the notion that the splicing process
492 is altered in obesity and related metabolic disease.

493 To analyse the relevance of alternative splicing on adipogenesis, we reduced
494 the expression of *PRPF8*/PRP8 in SC preadipocytes from NG obese individuals
495 to the levels found in their counterparts in IR/T2D obese individuals as well as in

496 the human preadipocyte cell line, SGBS cells. In this context, recent work
497 combining RNA-seq and proteomics demonstrated that PRP8 depletion altered
498 the expression of more than 1,500 proteins in Cal51 breast cancer cells,
499 supporting the relevance of this protein in defining the human proteome (***Liu et***
500 ***al., 2017***). In fact, as part of the core of the major spliceosome, PRP8 is
501 potentially involved in the removal of most introns from precursor mRNAs (99.5%
502 of non-coding regions are removed by the major spliceosome) (***Turunen et al.,***
503 ***2013***). Our studies showed that decreasing PRP8 protein levels in NG obese SC
504 preadipocytes or in SGBS preadipocytes evoked gene/protein expression
505 changes indicative of altered adipogenesis, which was confirmed by the
506 decreased accumulation of lipids observed in both cell types at late stages of
507 differentiation. These results were replicated in another SC adipocyte cell line,
508 hADSCs, derived from a lean donor, reinforcing the key contribution of
509 *PRPF8*/PRP8 to human adipocyte differentiation.

510 Two different yet functionally interrelated pathways were impaired in either NG
511 obese SC preadipocytes, SGBS preadipocytes or hADSCs cells silenced for
512 *PRPF8* in terms of both total gene expression levels and isoform balance of the
513 proteins involved, i.e., adipogenic transcriptional program, and LD biogenesis
514 and growth (***Figure 8***). Thus, PRP8 down-regulation altered the expression of
515 PPARγ and SREBP1, as well as of seipin and two members of the CIDE family
516 (CIDEB, CIDEC). In particular, the overall decrease in PPARγ and SREBP1
517 isoforms observed upon PRP8 down-regulation may account for the reduction
518 observed in mRNA and/or protein levels of known downstream target genes of
519 these transcription factors (adiponectin, FABP4, CIDEC, and FAS) (***Lowe et al.,***
520 ***2011***; ***Slayton et al., 2019***). Likewise, the dramatic changes in LD size and

521 number observed in *PRPF8*-silenced adipocytes might be related to the low
522 expression levels of the canonical seipin variant, seipin1 (***Craveiro Sarmento et***
523 ***al., 2018***), observed in these cells. Indeed, our observations are in line with
524 previous data on seipin knockout A431 cells, which also exhibited more
525 numerous but smaller LDs than controls (***Salo et al., 2016***). Interestingly, seipin
526 knock-down has been shown to suppress *PPARG* and *SREBF1* expression (***Fei***
527 ***et al., 2011***), thus suggesting that the phenotype of cells silenced for PRP8 may
528 be the result of the action of this spliceosome component on multiple key genes
529 contributing to adipogenesis and lipogenesis. In line with this notion, analysis of
530 CLIP-sep data in the ENCORI database revealed the presence of PRP8 binding
531 sites in *PPARG*, *SREBP1*, *BSCL2*, *CIDEB* and *CIDEC* mRNAs. Further research
532 is needed to fully establish the splicing targets for PRP8 in preadipocytes and to
533 characterize the relevance of the resulting protein isoforms (and/or their ratio) in
534 adipogenesis. Notwithstanding this, the observation that PRP8 re-expression in
535 *PRPF8*-silenced SGBS cells and, most notably, in SC preadipocytes from IR/T2D
536 obese individuals, can restore the expression and/or isoform balance of genes
537 such as *PPARG*, *BSCL2*, *CIDEB* or *CIDEC*, as well as normal LD content,
538 supports a prominent role for this protein in lipid accumulation in adipocytes. Our
539 data on *SFPQ* silencing and SF3B pharmacological inactivation would further
540 extend this role to the whole splicing machinery. In this scenario, it is reasonable
541 to propose that the decreased expression of splicing-related genes in SC
542 preadipocytes in IR/T2D obesity as compared to NG obesity could be
543 responsible, at least in part, of the loss of adipogenic capacity displayed by SC
544 preadipocytes from obese individuals with metabolic disease. The regulatory
545 mechanisms controlling the expression of splicing genes in preadipocytes under

546 physiological and pathological conditions remain to be elucidated. Studies from
547 our laboratory using *in vitro* models mimicking different obesogenic inputs
548 (hyperglycaemia/hyperinsulinemia, adipocyte hypertrophy, inflammation) failed
549 to modify *PRPF8* mRNA levels in preadipocytes (data not shown). Future studies
550 will be aimed at establishing whether other pathogenic processes causing
551 adipose tissue dysfunction in obese individuals (i.e., fibrosis, hypoxia) may alter
552 alternative splicing in these cells (***Figure 8***).

553 When viewed together, our data strongly support the notion that splicing
554 deregulation in SC preadipocytes may represent a pathogenic factor that
555 contributes to the development of obesity-related complications. As mentioned
556 earlier, changes in splicing components between groups were negligible in OM
557 preadipocytes as compared to their SC counterparts. These inter-depot
558 differences, which appear to be cell autonomous, might contribute, at least partly,
559 to the distinct differentiation capacity of SC and OM preadipocytes observed in
560 this and other studies (***Martyniak and Masternak, 2017***).Interestingly, along with
561 altered splicing, SC preadipocytes in IR/T2D obesity also exhibited molecular
562 features indicative of ER stress response failure, a hallmark process associated
563 with the development of metabolic diseases (***Bhattarai et al., 2020***). Our data
564 suggest that this pathogenic process also occurs in OM preadipocytes in IR/T2D
565 obesity. In accordance with these findings, previous studies from our laboratory
566 have established that IR obesity is associated with enhanced levels of ER stress
567 markers in mature adipocytes isolated from either SC or OM fat (***Díaz-Ruiz et al.,***
568 ***2015***). Herein we report, for the first time, that the three UPR signal transducers,
569 IRE1α, PERK, and ATF6 (***Hetz and Papa, 2018***), and two effector systems
570 downstream the UPR branches, CHOP and *XBP1* splicing, are dysregulated in

571 primary SC and OM preadipocytes in the transition from NG to IR/T2D in severe
572 obesity, in terms of total protein content and/or phosphorylation rate (i.e.,
573 activation). It is noteworthy that changes in these proteins did not always follow
574 the same trends between SC and OM preadipocytes in response to IR/T2D,
575 indicating the existence of depot-specific (mal)adaptative responses to obesity-
576 associated ER stress. Notwithstanding this notion, a feature common to SC and
577 OM preadipocytes was the up-regulation of both the master initiator of the UPR
578 signalling pathway, BiP, and *XBP1s/ XBP1u* ratio, in IR/T2D obesity. Given the
579 role of BiP in mediating the targeting of misfolded/unfolded ER proteins for
580 cytosolic degradation via ERAD, and the stimulatory effect of *XBP1s* on the
581 expression of ERAD components (***Karagöz et al., 2019***), these observations
582 supported that IR/T2D obesity could not only alter the UPR but also the activity
583 of this branch of the quality-control system in the ER ***(Hwang and Qi, 2018***).
584 Interestingly, ERAD is activated when the protein folding capacity of the ER is
585 exceeded ***(Hwang and Qi, 2018***), which seems to be the case for SC and OM
586 preadipocytes of IR/T2D morbidly obese individuals according to their enhanced
587 expression levels of ER chaperones as compared to NG obesity. In fact, our
588 studies show, for the first time, that SC and OM preadipocytes from IR/T2D obese
589 individuals, as compared to NG obese individuals, display enhanced levels of
590 proteins participating in all the steps comprising the ERAD, thus suggesting that
591 this pathway is hyperactivated in preadipocytes during the progression to IR/T2D
592 in obese individuals. Notably, our studies also revealed increased mRNA levels
593 of genes involved in protein retrotranslocation from the ER to the cytosol in
594 preadipocytes from individuals with simple obesity, especially in those with T2D,
595 as compared to lean individuals.

596 In all, our data on the UPR and ERAD strongly support the notion that
597 metabolic disease in obesity is characterized by the perturbation of ER
598 proteostasis network components in preadipocytes. They also support the link
599 between unresolved ER stress and adipogenesis dysregulation (***Longo et al.,***
600 ***2016***). Our studies using *in vitro* models mimicking different obesogenic inputs
601 indicate that inflammation, adipocyte hypertrophy and, specially,
602 hyperglycaemia/hyperinsulinemia (HGHI), as occurs in IR obese individuals, may
603 contribute to alter ER proteostasis in preadipocytes. To be more specific,
604 exposure to hyperglycaemic/hyperinsulinemic conditions induced ERAD
605 hyperactivation, as well as BiP expression, in both OM preadipocytes from NG
606 obese individuals and in SGBS preadipocytes. Intriguingly, HGHI-induced ERAD
607 expression was accompanied by a concomitant increase in ubiquitinated proteins
608 in preadipocytes and, in the case of SGBS cells, by a decrease in the activity of
609 the cell machinery involved in misfolded/unfolded protein degradation, the
610 proteasome. In this line are also our results on the decreased activity of the
611 proteasome in OM preadipocytes from obese individuals with IR/T2D. These
612 results suggest that the preadipocytes are unable to counteract the proteostatic
613 stress occurring under IR/T2D conditions, and proteotoxicity may ensue. In
614 agreement with these findings, we have reported the occurrence of proteotoxicity,
615 i.e., decreased activity of the proteasome and accumulation of ubiquitinated
616 proteins, in *in vitro* differentiated preadipocytes and in mature adipocytes isolated
617 from SC and OM fat of diet-induced obese mice as compared to lean animals, as
618 well as in mature adipocytes isolated from IR *vs*. NG obese individuals (***Díaz-***
619 ***Ruiz et al., 2015***). In all, our studies strongly support the notion that dysregulated
620 ERAD in preadipocytes represents a relevant pathological mechanism linked to

621 the development of metabolic disease in obese individuals (***Figure 8***). In this line,
622 altered ERAD expression levels in NG OM preadipocytes and SGBS cells
623 exposed to HGHI were accompanied by changes in adipogenic markers
624 demonstrative of impaired adipocyte differentiation. These effects were reverted
625 by pre-exposure of these cells to the ER stress-reducing agent, TUDCA (***Zhang***
626 ***et al., 2018***), which also reduced the enhanced expression levels of ERAD genes
627 found in OM preadipocytes of IR obese individuals or, though to a lesser extent,
628 in T2D OM preadipocytes. Together, these findings suggest that TUDCA may
629 represent a potentially useful treatment for preadipocyte damage prevention in
630 obesity, as it has been proposed for this bile acid in other ER stress-related
631 pathologies (***Kusaczuk, 2019***).

632 In summary, our results unveil an important role for alternative splicing in SC
633 preadipocyte differentiation thus paving the way for the development of novel
634 therapeutic strategies to modulate adipose tissue expansion. Our studies on
635 altered ER dynamics, that affect not only the UPR but also the ERAD pathway,
636 in SC and OM preadipocytes are in line with our previous results in mature
637 adipocytes (***Díaz-Ruiz et al., 2015***) and, in all, indicate that the maintenance of
638 ER proteostasis in adipose tissue cells is key to ensure metabolic health in
639 obesity.

640

641 **Materials and Methods**

642 **Subjects (Cohort 1)**

643 A total of 78 morbidly obese subjects (BMI >40 kg/m^2) undergoing bariatric
644 surgery were recruited at the General and Digestive Surgery Unit and the Lipids
645 and Atherosclerosis Unit of the Reina Sofía University Hospital (HURS; Córdoba,

646 Spain). Written consent was obtained from all the participants prior to recruitment,
647 and the experimental protocol was approved by the Ethics and Research
648 Committee of HURS following the Helsinki Declaration. Anthropometric and
649 biochemical parameters were obtained as described (***Díaz-Ruiz et al., 2015***).
650 Subjects are of Caucasian origin, aged 18-60 years. Type 2 diabetes mellitus
651 (T2D) in treatment with insulin, serious systemic disease not related to obesity
652 (infectious disease, cancer, kidney disease or severe liver disease) or major
653 cardiovascular disease in the 6 months prior to the inclusion of the study,
654 pregnancy, or breastfeeding and acute or chronic inflammatory diseases were
655 considered as exclusion criteria.

656 Subjects were matched by age and BMI and subclassified into three groups
657 [normoglycemic (NG Obese, n= 27; 13 females and 14 males): Glucose <100
658 mg/dL and HbA1c <5.7%; impaired fasting glucose (IFG Obese, n=25; 13
659 females and 12 males): Glucose 100–126 mg/dL and HbA1c 5.7-6.4%; and
660 diagnosed with type 2 diabetes (T2D Obese, n=17; 11 females and 6 males):
661 Glucose >126 mg/dL and HbA1c >6.4%], according to the criteria of the American
662 Diabetes Association (***ADA, 2021***). The clinical characteristics of the subjects are
663 shown in ***Table 1***. IFG individuals exhibited significantly higher HOMA-IR values
664 than NG individuals, as well as other clinical and plasma parameters that are
665 within the cut-off points for identifying insulin resistance in hyperinsulinemia-
666 euglycemic clamp studies (***Tam et al., 2012***). Thus, they will be referred to
667 hereinafter as insulin-resistant (IR) subjects (***Díaz-Ruiz et al., 2015***).

668 **Subjects (Cohort 2)**

669 43 subjects were recruited by the Endocrinology and Surgery departments at
670 the University Hospital Joan XXIII (Tarragona, Spain) as reported previously

671 (***Ejarque et al., 2017***). All subjects were of Caucasian origin and reported that
672 their body weight had been stable for at least 3 months before the study. They
673 had no systemic disease other than obesity, and all had been free of infection in
674 the previous month before the study. Primary liver disease, cardiovascular
675 disease, arthritis, acute inflammatory disease, infectious disease, neoplastic and
676 renal diseases were specifically excluded by biochemical work-up. Subjects were
677 classified by BMI according to World Health Organization criteria as lean (n=18,
678 BMI<25 kg/m^2) and obese (n=25, BMI>30 kg/m^2). Obese subjects were
679 subclassified into NG (n=15) and T2D (n=10) groups, as previously described
680 (***Serena et al., 2016***). OM and SC adipose tissue samples were obtained during
681 scheduled non-acute surgical procedures including laparoscopic surgery for
682 hiatus hernia repair or cholecystectomies in non-morbid obese population.
683 Anthropometric and biochemical variables from the cohort are presented in
684 ***Supplemental file 2***.

685 The hospital ethics committee approved the study and informed consent for
686 biobanking surgically removed tissue was obtained from all participants in
687 accordance with the Declaration of Helsinki.

688 **Adipose tissue processing**

689 Paired abdominal subcutaneous (SC) and omental (OM) adipose tissue
690 biopsies were obtained during bariatric surgery and processed as previously
691 described (***Díaz-Ruiz et al., 2015***; ***Peinado et al., 2010***). Samples were washed
692 with Dulbecco`s phosphate buffered saline (D-PBS) to remove blood
693 contaminants and mechanically dispersed in DMEM/F-12 (1:1). Next, samples
694 were enzymatically dispersed by incubation in DMEM/F-12 (1:1) containing 400
695 units/mL of collagenase type V at 37 ºC for 30 min in a shaking bath. Undigested

696 tissue was removed by filtering through a sterile 100 µm pore Cell Strainer
697 (BDFalcon, Cat#352360) and the remaining was centrifuged at 600 x g for 10 min
698 to separate the floating mature adipocyte layer and the pelleted stromal-vascular
699 fraction (SVF). SVF was resuspended in DMEM/F-12 (1:1), filtered through a 40
700 µm pore Cell Strainer (BDFalcon, Cat#352340) and centrifuged at 400 x g for 5
701 min. Then, pelleted SVF was resuspended in 500 µL of RBC Lysis Buffer and
702 incubated for 3 min at room temperature (RT). After centrifugation at 400 x g for
703 10 min, SVF was frozen in liquid nitrogen and stored at -80 ºC for further analysis
704 and/or seeded onto culture flasks.

705 Freshly isolated mature adipocytes were washed with DMEM/F-12 (1:1) and
706 added to lipolysis buffer [Krebs Ringer Phosphate (KRP) buffer: 0.9 % NaCl, 15
707 mM NaH_2PO_4, 6 mM KCl, 1.5 mM MgSO4, 1.6 mM $CaCl_2$ supplemented with 2%
708 bovine serum albumin (BSA), 1 mg/mL glucose and 0.1 mg/mL ascorbic acid; pH
709 7.4]. Fat cell volume and weight was determined as described (***Tchoukalova et***
710 ***al., 2003***) and discussed (***Lundgren et al., 2007***). In brief, light microscopy
711 images of 100 cells were captured with a coupled camera (Moticam 1080; Motic,
712 Barcelona, Spain) and their diameters (d) were measured in micrometres using
713 ImageJ 1.50b. Mature adipocytes are assumed to be spheres so that their volume
714 (expressed in picolitres) was calculated as ($[\pi \times d^3]/6$) where d is the cell diameter
715 in micrometres.

716 **Human primary preadipocytes**

717 Human primary preadipocytes were cultured as previously described (***Serena***
718 ***et al., 2016***; ***Guzmán-Ruiz et al., 2014***). SVF cells obtained from fresh SC and
719 OM adipose tissue samples were seeded in preadipocyte-proliferation medium
720 DMEM/F-12 (1:1) supplemented with 8 mM biotin, 18 mM d-pantothenate acid,

721 100 mM ascorbate, and 1% penicillin-streptomycin, and 10% new-born calf
722 serum (NCS) at 37 ºC in a humidified atmosphere with 95% air: 5% CO2. Medium
723 was replaced every 48 h until confluence. Once in confluence (>80%), the cells
724 were detached with trypsin- EDTA solution and subcultured at 4,000 cells/cm^2 2-
725 3 times to purify and amplify the cell culture following established methods
726 (***Bunnell et al., 2008***; ***Palumbo et al., 2018***; ***Zhu et al., 2013***). Thereafter,
727 preadipocytes were collected and frozen in liquid nitrogen and stored at -80 ºC
728 for immunophenotyping analysis, proliferation studies, or directly induced for
729 adipogenic differentiation, as indicated in detail in the following sections.

730 **Immunophenotyping analysis**

731 Freshly isolated SVF cells and cell cultures derived from SVF at passages 2-
732 3 were processed for detection of preadipocyte markers and immune cell markers
733 to assess the purity of the cell preparations employed for further analysis. To be
734 more specific, the protein content of DLK1/PREF1 (preadipocyte marker), CD45
735 (leukocyte marker), and CD14 (macrophage marker) was assessed in extracts
736 from the SVF and preadipocytes that were obtained from the same SC and OM
737 adipose tissue samples following the procedures indicated in the "Quantitative
738 immunoblotting" section below.

739 ***In vitro* differentiated human adipocytes**

740 Preadipocytes were seeded at 4.000 cells/cm^2 in preadipocyte proliferation
741 medium until they reached 70-80% of confluence. Then (day 0 of differentiation),
742 primary preadipocytes were differentiated keeping them in differentiation
743 medium: preadipocyte-proliferation medium with 3% NCS and 17.5 mM glucose,
744 supplemented with 10 µg/mL insulin, 0.1 µM dexamethasone, 1 µM rosiglitazone,
745 and 0.5 mM IBMX for the first 3 days. Then, medium was removed and replaced

746 by differentiation medium supplemented with 10 µg/mL insulin and 0.1 µM
747 dexamethasone for 4 more days (day 6), when the medium was refreshed and
748 maintained until day 10. The adipogenic process was monitored by the
749 appearance of doubly refractile lipid inclusions by light microscopy and images of
750 the cultures were taken with a coupled camera (Moticam 1080; Motic, Barcelona,
751 Spain). Experiments were carried out using cells from passages 3 to 4.

752 **Human adipose tissue cells lines**

753 In this study we employed SGBS cells, a human-derived preadipocyte cell line
754 isolated from the SVF of SC adipose tissue from a 3-months male infant with
755 Simpson-Gobali-Behmel syndrome, was kindly donated by Prof. Dr. Martin
756 Wabitsch (Ulm University, Germany). This cell model has been largely used in
757 studies pertaining to preadipocytes and differentiated adipocytes (***Allott et al.,***
758 ***2012***; ***Fischer-Posovszky et al., 2008***; ***Kalkhof et al., 2020***; ***Li et al., 2016***;
759 ***Newell et al., 2006***; ***Zandbergen et al., 2005***). SGBS cells growth and
760 differentiation into adipocytes were performed as previously described (***Moure et***
761 ***al., 2016***). Cells were seeded at a density of 4,000 cells/cm2 and proliferated to
762 80% confluence in basal medium: DMEM/F12 (1:1) supplemented with 32.7 µM
763 biotin, 16.78 µM d-panthothenic acid, and 1% penicillin-streptomycin.

764 Confluent SGBS cells (day 0 of differentiation) were differentiated keeping
765 them in differentiation medium: serum-free basal medium, supplemented with
766 0.01 mg/mL human transferrin, 20 nM human insulin, 100 nM hidrocortisone, 0.2
767 nM 3,3',5-triiodo-l-thyronine (T3), 25 nM dexamethasone, 0.5 mM IBMX, and 2
768 µM rosiglitazone for the first 4 days. Next, medium was removed and replaced by
769 differentiation medium supplemented with medium 0.01 mg/mL human
770 transferrin, 20 nM human insulin, 100 nM hidrocortisone, and 0.2 nM T3 for 6

771 days (day 10). Then, medium was refreshed, and cells were maintained in culture
772 until day 14. The differentiation process was monitored by microscopic
773 observation of LDs and expression analysis of known markers of adipogenesis
774 and LD biogenesis (data not shown).

775 We also employed an adipose-derived stem cell line (hADSCs) that was
776 isolated from SC adipose tissue of a male lean donor (aged 16 years, BMI 24
777 kg/m^2). This cell model was developed and validated in our previous works
778 (***Acosta et al., 2017***; ***Ehrlund et al., 2017b***, ***2017a***; ***Petrus et al., 2020***). Cells
779 were isolated, propagated, and differentiated into adipocytes as described (***Gao***
780 ***et al., 2014***, ***2017***). Cells were cultured at 20.000 cells/cm^2 in proliferation
781 medium [DMEM low glucose (1 g/L glucose), pyruvate supplemented with 1%
782 hepes buffer 1M, 0.5% penicillin/streptomycin (10,000 U/mL), and 10% FBS] with
783 2.5 ng/mL human FGF2. Cells were then proliferated until 80% of confluence and
784 the medium was replaced for proliferation medium without FGF2 for one more
785 day.

786 Cells at day 0 of differentiation were differentiated keeping them in
787 differentiation medium [serum-free proliferation medium:Ham's F-12 Nutrient Mix
788 (1:1)] supplemented with 5 µg/mL human insulin, 10 µg/mL transferrin, 0.2 nM
789 T3, 1 µM rosiglitazone, 100 µM IBMX, and 1 µM dexamethasone for the first 3
790 days. Next, at day 3 of differentiation, medium was removed and replaced by
791 differentiation medium supplemented with 5 µg/mL human insulin, 10 µg/mL
792 transferrin, 0.2 nM T3, and 1 µM rosiglitazone. The medium was refreshed each
793 2-3 days until day 6 and day 10 of differentiation. Differentiation process were
794 monitored by microscopic observations of LDs.

795 All the cells used tested negative for mycoplasma contamination using a
796 specific commercially available kit.

797 **iTRAQ labelling and high-resolution LC-MS/MS**

798 $1x10^6$ human SC and OM preadipocytes from NG and T2D obese subjects
799 were homogenized in lysis buffer containing 8 M urea, 4% CHAPS, 30 mM Tris
800 base, sonicated, and quantified by RcDc assay kit. Reduction and alkylation were
801 done by addition of 2 mM 1,4-dithiothreitol (DTT) and 7 mM iodoacetamide (IAA),
802 respectively, for 15 min at RT. Then, samples from 2-3 individuals per group and
803 fat depot were pooled and used for two separate iTRAQ experiments (n=5-6
804 subjects per group and fat depot). Protein samples were precipitated using 10%
805 trichloroacetic acid (TCA), diluted in tetraethylammonium bromide (TEAB) with
806 0.1% sodium dodecyl sulphate (SDS) and quantified. Samples were diluted 1:2
807 with TEAB and digested with 2% trypsin. Tryptic peptides (240 µg per group and
808 fat depot) were employed for proteomic analysis using 4-plex isobaric tags for
809 iTRAQ according to the manufacturer's instructions. Samples were tagged with
810 the corresponding iTRAQ reagent, mixed, desalted and fractionated by strong
811 cation exchange (SCX).

812 Six fractions were collected, and each fraction was desalted, evaporated to
813 dryness, and diluted in 20 µL of injection phase. Then, 8 µL of extract were diluted
814 with 5% methanol (MeOH)/1% formic acid and analysed by liquid
815 chromatography-tandem mass spectrometry (LC-MS/MS). The MS system used
816 was an Orbitrap XL (Thermo Scientific) equipped with a microESI ion source
817 (Proxeon; Madrid, Spain) and coupled to an Agilent 1200 series LC-system
818 (Agilent Technologies; Madrid, Spain). The SCX-fractions were loaded onto a
819 chromatographic system consisting of a C18 preconcentrating cartridge (Agilent

820 Technologies) connected to a 15 cm long, 100 μm i.d. C18 column (Nikkyo
821 Technos Co., Ltd.; Tokyo, Japan). The separation was performed at 0.4 μL/min
822 in a 90-min acetonitrile gradient from 3 to 40% [solvent A: 0.1% formic acid,
823 solvent B: acetonitrile with 0.1% formic acid]. The Orbitrap XL was operated in
824 the positive ion mode with a spray voltage of 2 kV. The scan range for full scans
825 was m/z 400-1800. The spectrometric analysis was performed in a data
826 dependent mode, acquiring a full scan followed by 8 MS/MS scans of the 4 most
827 intense signals detected in the MS scan. For each MS signal, two MS/MS spectra
828 were acquired using higher energy collisional dissociation (HCD) and ion-trap-
829 based collision-induced dissociation (CID) as fragmentation devices. The HCD
830 spectra were used to measure the intensity of iTRAQ fragments and the CID
831 spectra were used for database search and peptide identification. An exclusion
832 time of 30 sec and a spectral count of 2 were included to avoid repetitive MS/MS
833 analysis of the dominant MS signals.

834 **Database search and protein identification**

835 Peak lists were searched against the complete human proteome (UniProt
836 release 2014_08, with 68.049 proteins) using SEQUEST (Proteome Discoverer
837 1.3, ThermoFisher) as search engine. The search tolerances were set as follows:
838 peptide mass tolerance 10 ppm, fragment tolerance 0.8 Da, with trypsin as
839 enzyme (allowing up to two missed cleavages), methionine oxidation (+15.995
840 Da) and 4-plex iTRAQ (K, Y, N-terminal, +144.102) as variable modifications, and
841 cysteine carbamidomethylation (+57.021 Da) as fixed modification. Peptide
842 identifications were filtered for 0.5% FDR and only proteins identified with two or
843 more peptides were considered. All the raw data of mass spectrometry
844 measurements, together with protein identification have been deposited to the

845 ProteomeXchange Consortium via the PRIDE (***Perez-Riverol et al., 2019***)
846 partner repository with the dataset identifier PXD015621.

847 **Data normalization and statistical analysis**

848 Protein intensities, for each of the two iTRAQ experiments, were normalized
849 using protein median intensities in each comparison (iTRAQ reagents 115/116:
850 0.987, 115/117: 0.958, 116/114: 1.142, 117/114: 1.191 for replicate 1; and
851 115/116: 1.026, 115/117: 0.933. 116/114: 1.090, 117/114: 1.180 for replicate 2).
852 Protein identified in the two replicates were matched. To discard duplicate
853 proteins between replicates, the following parameters were considered: absence
854 of missing values, # unique peptides, # peptide and coverage (the higher, the
855 better). Proteins showing quantification values within a fixed average ratio (±1.5)
856 and a coefficient of variation (CV) under 20% were considered for further
857 statistical analysis. Specifically, the Perl module "Statistic R" was used to
858 calculate the average, the standard deviation (SD), the coefficient of variation
859 (CV), and the fold change ratios for each protein between groups. Data normality
860 was tested by Shapiro-Wilk test, and a Student's t test was performed to obtain
861 the statistical significance (*p-value*).

862 **Bioinformatics analysis**

863 Gene Ontology (GO) analysis of the proteomic results was conducted using
864 online open-source software PANTHER (Protein ANalysis THrough Evolutionary
865 Relationships) classification system 14.1 that annotated proteins to biological
866 processes (***Mi et al., 2019a***, 2***019b***). Significant over- and under-represented GO
867 terms and pathways were identified by Fisher's Exact with FDR multiple test
868 correction < 0.05 taking all the Homo sapiens genes in the data set as a reference
869 list. To determine quantitative changes in this study, a ±1.5-fold change, with

870 p<0.05 (determined by t-test) in two replicates, was set as the threshold for
871 categorizing up-regulated and down-regulated proteins. Pathway and upstream
872 regulator analysis were performed using IPA (Ingenuity Pathways Analysis)
873 software 49309495. Canonical pathway analysis identified the pathways from the
874 IPA library of canonical pathways that were most significant to the data set. The
875 significance of the association between the data set and the canonical pathway
876 was measured in 2 ways: 1) A ratio of the number of proteins from the data set
877 that mapped to the pathway divided by the total number of proteins that mapped
878 to the canonical pathway displayed. 2) Fisher's exact test was used to calculate
879 a p-value determining the probability that the association between the proteins in
880 the dataset and the canonical pathway was explained by chance alone, and
881 p<0.05 was considered statistically significant. The authors thankfully
882 acknowledge the computer resources, technical expertise and assistance
883 provided by the PAB (Andalusian Bioinformatics Platform) centre located at the
884 University of Málaga (www.scbi.uma.es). mRNA binding sites and adipose
885 tissue-specific functional interactions of *PRPF8*, *SF3B1*, and *SFPQ* were
886 investigated using ENCORI (The Encyclopedia of RNA Interactomes;
887 http://starbase.sysu.edu.cn/index.php) (***Li et al., 2013***) or SpliceAid-F
888 (http://srv00.recas.ba.infn.it/SpliceAidF/) (***Giulietti et al., 2013***) and HumanBase
889 tool (https://hb.flatironinstitute.org/) (***Greene et al., 2015)***, respectively.

890 **Silencing studies in preadipocytes**

891 Primary human SC preadipocytes from NG obese individuals (cohort 1) and
892 SGBS preadipocytes, cultured on 6-wells or 12-wells plates, were stably
893 transfected at day 4 of differentiation with targeted double stranded siRNA
894 oligonucleotides against the major spliceosome component, *PRPF8,* the splicing

895 factor, *SFPQ*, or their corresponding specific negative control siRNA using
896 Lipofectamine RNAiMAX Transfection Reagent following manufacturer's
897 instructions. Transfection efficiency was checked by RT-PCR, western blotting
898 and, when possible, by cotransfecting cells with N-terminal end of phrGFP-N1,
899 as a reporter (***Moreno-Castellanos et al., 2017***) using Lipofectamine 2000
900 Transfection Reagent. Briefly, the cells were washed twice with D-PBS and
901 submerged into 1 mL of OPTI-MEMTM medium containing 100 nM of the
902 corresponding siRNA and, when required, 3 µg of phrGFP-N1 during 24 h.
903 Thereafter, the transfection medium was removed, and fresh culture medium was
904 added. Finally, after 3-5 days of transfection, silenced cells were stained with Oil
905 Red-O. The effects of *PRPF8* and *SFPQ* silencing were also explored by RT-
906 PCR and quantitative immunoblotting. In another series of experiments, *PRPF8*
907 siRNA-treated SGBS cells were exposed to 100 mM insulin for 15 min.
908 hADSCs were transfected one day before differentiation induction through
909 electroporation by Kit Neon™ Transfection System (***Kim et al., 2008***). The cells
910 were trypsinised and washed with D-PBS (without Ca^{2+} and Mg^{2+}) and
911 resuspended in Resuspension Buffer R at a final density of $1x10^6$ cells/mL. The
912 NEON system (Invitrogen) 10-µL electroporation tips were used with 10^6 cells per
913 reaction. One pulse (1,200 V, 40 ms) was used to transfect a final concentration
914 of 40 nmol/L siRNA to cells, which were seeded in medium without
915 antibiotic/antimycotic. Twenty-four h after electroporation, the medium was
916 replaced, and differentiation started following the standard protocol. Finally, the
917 effects of PRPF8 silencing were evaluated at different days of differentiation (0,
918 3, 6 and 10 days of differentiation).
919

920 **Overexpression studies in preadipocytes**

921 Primary human SC preadipocytes from NG obese individuals (cohort 1) and
922 SGBS preadipocytes, cultured on 6-wells or 12-wells plates, were stably
923 transfected at day 3-4 of differentiation with a plasmid vector coding for *PRPF8*
924 (*PRPF8*-pcDNA3.1), *SFPQ* (*SFPQ*-pcDNA3.1), their corresponding empty
925 plasmid vector alone (pcDNA3.1) as a negative control, or co-transfected in
926 combination with their corresponding siRNA using Lipofectamine 2000
927 Transfection Reagent following manufacturer's instructions. In another sets of
928 experiments, SGBS preadipocytes were stably transfected with a plasmid vector
929 coding for *BIP* (pCMV *BiP*-Myc-KDEL-wt) or its corresponding empty vector
930 (pCMV-Myc), Transfection efficiency was checked by RT-PCR, western blotting
931 and, when needed, by co-transfecting cells with N-terminal end of phrGFP-N1,
932 as a reporter (***Moreno-Castellanos et al., 2017***). Briefly, the cells were washed
933 twice with D-PBS and submerged into 1 mL of OPTI-MEM™ medium containing
934 3 µg of corresponding plasmid vector and 100 nM of the siRNA during 24 h.
935 Thereafter, the transfection medium was removed, and fresh culture medium was
936 added. Finally, after 3-5 days of transfection, silenced cells were stained with Oil
937 Red-O.

938 The effects of *PRPF8* overexpression were also explored in primary human
939 SC preadipocytes from IR/T2D obese individuals (cohort 1) by RT-PCR and
940 quantitative immunoblotting. These techniques were also employed to study the
941 effects of BiP overexpression in SGBS preadipocytes. All constructs were verified
942 by DNA sequencing.

943

944

945 **Lipid droplet (LD) morphometric analysis**

946 Oil Red-O staining of cellular lipids was performed in human preadipocytes
947 and SGBS cells grown on glass coverslips under different conditions as
948 previously described (***Pulido et al., 2011***). Cells were washed with D-PBS and
949 fixed with 4% paraformaldehyde for 8 min at RT. Coverslips were washed with
950 60% isopropanol and then left to dry completely. Subsequently, an Oil Red-O
951 stock solution was prepared: 0.35 g Oil Red-O was dissolved in 100 mL 100%
952 isopropanol. Before use, the solution was diluted 6:4 with distilled water, allowed
953 to stand for 10 min, and then filtered through Whatman no. 1 paper. Cells were
954 exposed to this solution for 30 min at RT in darkness and the unbound dye was
955 rinsed with distilled water. Images were captured with an inverted light
956 microscope coupled to a camera. For morphometric studies of the lipid droplets
957 (LDs), coverslips were mounted on slides with fluorescent mounting medium
958 containing 1 µg/mL DAPI, to visualize the nuclei, and examined by confocal
959 microscopy as described previously (***Pulido et al., 2011***). At least 30 cells were
960 randomly selected for each experimental condition and the LD number and size
961 were then estimated by using ImageJ 1.50b (***Deutsch et al., 2014***; ***Mohan et al.,***
962 ***2019***). Analysis was performed by converting the 8-bit image into a binary image,
963 that consists of the pixels comprising the LDs. Following binarization, the image
964 was subjected to watershed object separation for image processing, which is
965 used to identify borders of adjacent LDs (***Abdolhoseini et al., 2019***). After
966 separation, the binary image was manually compared with the original image for
967 consistency and correct binary conversion. After setting the scale of the image,
968 the amount and individual size of the LDs in the image, displayed by ImageJ as
969 surface area in µm2, were measured. Incomplete LDs located at the edge of the

970 image were excluded. The sum of the areas of all the LDs present in a cell was
971 used as the total lipid content.
972 Staining of neutral lipid and DNA was performed in hADSCs cultured on 96-
973 wells plates under PRPF8-silencing as previously described (***Pettersson et al.,***
974 ***2015***). hADSCs were washed with PBS and fixed with 4% paraformaldehyde
975 solution (PFA) containing 0.123 mol/L $NaH_2PO_4x2H_2O$, 0.1 mol/L NaOH and 0.03
976 mol/L glucose for 10 min at RT. Fixed cells were washed with PBS and stained
977 with Bodipy 500/510 (0.2 µg/ml PBS) and Hoechst (2 µg/ml PBS, Molecular
978 probes) for 20 min at RT. After washing with PBS, accumulation of intracellular
979 lipids (Bodipy staining) and cell number (Hoechst staining for nuclei) were
980 quantified with Cell Insight CX5 High-Content Screening (HCS) Platform (Thermo
981 Fisher Scientific) and High-Content Screening (HCS) Studio Cell Analysis
982 Software 2.0. Total lipid content, LD number and size were normalised by cell
983 number.
984 **Experimental treatments**
985 To evaluate the contribution of the SF3B complex to adipogenesis, we
986 employed pladienolide-B, a natural product that binds to this complex and inhibits
987 pre-mRNA splicing via targeting splicing factor SF3B1 *(**Aouida et al., 2016;***
988 ***Cretu et al., 2018***). SGBS cells at day 4 of differentiation were treated with
989 pladienolide-B or vehicle for 24 h (***Jiménez-Vacas et al., 2019***). Pladienolide-B
990 was initially used in the 10^{-11} to 10^{-7} M range, being 10^{-8} M the higher dose that
991 did not compromise cell viability (data not shown).
992 SGBS preadipocytes at day 4 of differentiation were exposed for 30 h, to
993 different treatments inducing IR as previously described (***Díaz-Ruiz et al., 2015***):
994 the inflammatory cytokine tumor necrosis factor alpha (TNFα, 5 nM), a

995 combination of high glucose (4.5 g/L) and high insulin (100 nmol/L) (HGHI),
996 palmitic acid (sodium salt; 500 μM), or oleic acid (500 μM). Palmitic and oleic acid
997 solutions contained 2% fatty acid-free BSA. One sample per experiment was
998 used to obtain control responses in the presence of the solvent. After the
999 treatments, control and TNFα-, HGHI-, palmitic, and oleic acid-treated SGBS
1000 cells were stimulated with insulin (100 nM) for 15 min. Primary human OM
1001 preadipocytes from NG obese individuals (cohort 1) at day 3 of differentiation
1002 were also exposed to HGHI conditions (24 h).

1003 In a second series of experiments, the effect of a bile acid known to reduce ER
1004 stress, tauroursodeoxycholic acid (TUDCA) (***Uppala et al., 2017***; ***Xia et al., 2017***;
1005 ***Zhang et al., 2018***), was tested in human OM preadipocytes from NG obese
1006 individuals and SGBS cells exposed to HGHI conditions as well as in human OM
1007 preadipocytes from IR/T2D obese individuals. To this end, cells at day 3-4 of
1008 differentiation were exposed to 0.5 mg/mL TUDCA for 14 h before culture in
1009 medium alone or in the presence of glucose (4.5 g/L) and insulin (100 nmol/L)
1010 (HGHI) for 24-30 h. At the end of the experiments, cells were processed for
1011 immunoblotting, RNA isolation, and Oil Red-O staining.

1012 **Confocal immunofluorescence microscopy**

1013 Samples were visualized by confocal microscopy under an LSM 5 Exciter
1014 confocal microscope fitted with Immersol™ immersion oil. Depending on the cell
1015 depth, 5-8 stacks per channel were collected and projected in a single image.
1016 After acquisition, images underwent a deconvolution process with the software
1017 package Huygens Professional 2.4.4.

1018

1019

1020 **RNA extraction and real-time PCR (RT-PCR)**

1021 Total RNA isolation and purification from human preadipocytes were
1022 performed using the RNeasy Kit. RNA from primary preadipocytes and SGBS
1023 cells under the different experimental conditions tested was isolated using TRIzol
1024 Reagent following the manufacturers' protocols, and subsequently treated with
1025 DNase. Quantification of recovered RNA was assessed using NanoDrop2000
1026 spectrophotometer. One µg of RNA was retrotranscribed to cDNA as previously
1027 described (***Peinado et al., 2010***) using with the Revertaid First Strand cDNA
1028 Synthesis kit. Transcript levels were quantified by RT-PCR with GoTaq qPCR
1029 Master Mix kit. Previously validated specific primers (***Supplemental file 3***) were
1030 designed using Primer3 Input 4.1.0 and purchased from Metabion (Steinkirchen,
1031 Germany). Primers or encompassing fragments of the areas from the extremes
1032 of two exons were designed to ensure the detection of the corresponding
1033 transcripts avoiding genomic DNA amplification. The cDNA was amplified with a
1034 thermal profile at the following conditions: hot-start activation at 95 ºC for 2 min,
1035 followed by 40 cycles of denaturation (95 ºC for 15 sec), then annealing/extension
1036 (60 ºC for 60 sec), and finally, a dissociation cycle (melting curve; 60 ºC to 95 ºC,
1037 increasing 0.5 ºC / 30 sec) to verify that only one product was amplified, using
1038 the Light-Cycler 96 instrument (Roche; Basilea, Switzerland). The primer
1039 concentrations were 500 nM. To allow for variation in the amount of RNA used
1040 and the efficiency of the reverse-transcription reaction, all results were
1041 normalized by the expression of three house-keeping genes (*ACTB*, *GAPDH* and
1042 *HPRT*) and relative quantification was calculated using the ΔCT formula (***Catalán***
1043 ***et al., 2007***). All samples for each experiment were run in the same plate in
1044 triplicate and the average values were calculated.

1045 **qPCR dynamic array**

1046 A qPCR dynamic array based on microfluidic technology for simultaneous
1047 determination of the expression of 45 transcripts in 36 samples (Fluidigm; San
1048 Francisco, CA) was employed (***del Río-Moreno et al., 2019***). Specific primers
1049 for human transcripts including components of the major (n=13) and minor
1050 spliceosome (n=4), associated splicing factors (n=28), and three housekeeping
1051 genes (*ACTB*, *GAPDH*, and *HPRT*) were specifically designed with the Primer3
1052 software and StepOneTM Real-Time PCR System software v2.3 (Applied
1053 Biosystems, Foster City, CA). Preamplification, exonuclease treatment, and
1054 qPCR dynamic array based on microfluidic technology were implemented as
1055 recently reported (***Gahete et al., 2018***; ***del Río-Moreno et al., 2019***), following
1056 manufacturer's instructions using the Biomark System and the Real-Time PCR
1057 Analysis Software (Fluidigm). The panel of splicing machinery components was
1058 selected on the basis of two main criteria: 1) the relevance of the given
1059 spliceosome components in the splicing process (such as the components of the
1060 spliceosome core), and 2) their demonstrated participation in the generation of
1061 splicing variants implicated in the pathophysiology of metabolic diseases (as is
1062 the case of the 28 splicing factors selected in this study) (***Gahete et al., 2018***;
1063 ***del Río-Moreno et al., 2019***)

1064 Briefly, following manufacturer's instructions, 12.5 ng of cDNA of each sample
1065 were pre-amplified using 1 µL of all primers mix (500 nM) in a T100 Thermal
1066 cycler (BioRad, Hercules, CA), using the following program: 1) 2 min at 95 ºC; 2)
1067 15 sec at 94 ºC and 4 min at 60 ºC (14 cycles). Then, samples were treated with
1068 2 µL of 4 U/µL Exonuclease I solution following the manufacturer's instructions.
1069 Next, samples were diluted with 18 µL of TE Buffer, and 2.7 µL were mixed with

1070 3 µL of EvaGreen Supermix and 0.3 µL of cDNA Binding Dye Sample Loading
1071 Reagent. Primers were diluted to 5 µM with 2 X Assay Loading Reagent. Control
1072 line fluid was charged in the chip and Prime script program was run into the IFC
1073 controller MX. Finally, 5 µL of each primer and 5 µL of each sample were pipetted
1074 into their respective inlets on the chip and the Load Mix script in the IFC controller
1075 software was run. Thereafter, the qPCR was run in the Biomark System following
1076 the thermal cycling program: 1) 9 ºC for 1 min; 2) 35 cycles of denaturing (95 ºC
1077 for 5 sec) and annealing/extension (60 ºC for 20 sec); and 3) a last cycle where
1078 final PCR products were subjected to graded temperature-dependent
1079 dissociation (60 ºC to 95 ºC, increasing 1 ºC/3 sec). Data were processed with
1080 Real-Time PCR Analysis Software 3.0.

1081 Finally, to control for variations in the efficiency of the retrotranscription
1082 reaction, mRNA copy numbers of the different transcripts analysed were adjusted
1083 by normalization factor (NF), calculated with the expression levels of the three
1084 housekeeping genes mentioned above using GeNorm 3.3 software. This
1085 selection was based on the stability of these housekeeping genes among the
1086 experimental groups to be compared, wherein the expression of these
1087 housekeeping genes was not significantly different among groups.

1088 **Quantitative immunoblotting**

1089 Human preadipocytes isolated from SC and OM adipose tissue of NG, IR and
1090 T2D obese individuals were disrupted in BLC buffer containing 150 mM NaCl, 20
1091 mM Tris-HCl pH 7.4, 1% Triton-X-100, 1 mM EDTA, and 1 µg/mL anti-protease
1092 cocktail CLAP (Chymostatin, Leupeptin, Antipain and Pepstatin A). Protein
1093 content was measured by Bradford assay and 30 mg of protein per sample were
1094 loaded into 4-20 % precast SDS-PAGE gels (Bio-Rad) under denaturing

1095 conditions. SGBS cells were homogenized in SDS-DTT buffer containing 62.5
1096 mM Tris-HCL pH 7.6, 2 % SDS, 100 mM DTT, 20% Glycerol. Protein content was
1097 separated by 10 % SDS-PAGE under denaturing conditions. In both cases,
1098 samples were transferred to nitrocellulose membranes (Bio-Rad). After Ponceau
1099 staining to ensure equal sample loading, membranes were blocked in Tris-buffer
1100 saline (TBS) consisting of 25 mM Tris, 150 mM NaCl with 0.05% Tween 20
1101 (TTBS) containing 5 % non-fat dry milk for 1 h at RT. Blots were then incubated
1102 overnight at 4 ºC with the corresponding primary antibody (***Appendix 1—key***
1103 ***resource table***). Immunoreactive bands were visualized using horseradish
1104 peroxidase (HRP)-conjugated secondary antibodies (***Appendix 1—key***
1105 ***resource table***) and the enhanced chemiluminescence ECL Plus detection
1106 system. Quantification of band intensities was carried out on digital images of
1107 membrane samples provided by LAS4000 gel documentation system (GE
1108 Healthcare; Barcelona, Spain) using ImageJ software (1.50b, NIH, Bethesda,
1109 MA), and normalized with Ponceau density values as previously described
1110 (***Jimenez-Gomez et al., 2013***; ***Peinado et al., 2011***). All comparative
1111 experiments were performed under identical conditions.

1112 **Proteasome activity assay**

1113 The 26S proteasome (ATP stimulated) and/or 20S (SDS stimulated) activities
1114 were measured in primary human OM preadipocytes from NG, IR, and T2D
1115 obese individuals (cohort 1) and SGBS preadipocytes upon exposure to HGHI
1116 (***Díaz-Ruiz et al., 2015***; ***Li et al., 2008***). Assays for proteasome activity were
1117 performed using Suc-LLVY-AFC product, which is proteolyzed by the
1118 chymotrypsin-like (ChT-L) active site of the proteasome forming a fluorogenic
1119 substrate (AFC) (***Keita et al., 2014***).

1120 Cells were washed with D-PBS and scraped from plates in BLC buffer without
1121 DTT, TX-100 or protease inhibitors because these compounds interfere with the
1122 assay. The reaction was conducted in 250 µL of activity assay buffer in a 96-well
1123 plate containing 50 µg/ml protein lysate in Proteasome buffer (20 mM Tris–HCl,
1124 pH 7.8, 1 mM EDTA, 0.5 mM DTT, 5 mM MgCl2, and 50 µM Suc-LLVY-AFC) plus
1125 2 mM ATP or 0.02% SDS for the determination of the 26S or 20S proteasome,
1126 respectively. In order to confirm the specificity of the findings for proteasome
1127 activity, parallel reactions containing the proteasome inhibitor, MG-132 (25 µM),
1128 were run as controls. The reaction mixture was incubated for 3 h at 37 ºC and the
1129 fluorescence of the released AMC product was kinetically followed each 10 min
1130 in a Flex Station 3 at an emission wavelength of 355 nm and an excitation
1131 wavelength of 460 nm. The background fluorescence values obtained by
1132 incubating the lysates with MG132 were subtracted from activity values. Results
1133 were analysed with the SoftMax Pro 2.2.1 and the values reported for
1134 proteasome peptidase activity are expressed as relative fluorescence arbitrary
1135 units/min/mg of total protein.

1136 **Cell viability and cytotoxicity assays**

1137 Cell viability of SGBS cell cultures was assessed by the MTT assay. Briefly,
1138 cells were incubated for 2 h with 0.1 mg/ml of (3-(4,5-dimetililtiazol-2-ilo)-2,5-
1139 difeniltetrazol de bromuro (MTT), dissolved in D-PBS. Washing with D-PBS (1
1140 mL) was followed by the addition of DMSO (1 mL) and gentle shaking for 10 min
1141 so that complete dissolution was achieved. Aliquots (200 µL) of the resulting
1142 solutions were transferred to 96-well plates and absorbance was recorded at 570
1143 nm using a Flex Station 3. Results were analysed with the SoftMax Pro 2.2.1 and
1144 are presented as percentage of the control siRNA values.

1145 Cytotoxicity of PRPF8-silencing in hADSCs was evaluated by Cytotoxicity
1146 Detection Kit Plus. The culture medium was aspirated and centrifugated at 3,000
1147 rpm for 10 min to obtain a cell free supernatant. Aliquots of media and warm
1148 reagent were mixed in a 96-well plate and absorbance was recorded using a
1149 microplate reader (Tecan Infinite 2000; Männedorf, Switzerland). Results were
1150 analysed with Magellan software 7.2 SP1.

1151 **Measurement of cell proliferation rate**

1152 Cell counting in culture flasks was carried out to monitor growth rates of the
1153 preadipocytes in culture. At passage 3, cells were detached from the culture
1154 flasks and an aliquot was stained with trypan blue and cells were counted in a
1155 Neubauer chamber. Cell proliferation was calculated as the total number of live
1156 cells per initial seeding number (***Morten et al., 2016***).

1157 **Statistical analysis**

1158 For *in vitro* experiments, at least three replicates were obtained for each
1159 condition. Data are presented as mean ± standard error of the mean (S.E.M.) and
1160 statistical analysis was performed using GraphPad Prism 7. To determine the
1161 normality distribution of the samples, Shapiro-Wilk normality test was used. To
1162 determine significance, either unpaired t test for parametric data or Mann Whitney
1163 test for non-parametric data were employed for comparisons between two
1164 groups. For comparison of more than two groups either one-way ANOVA with
1165 Tukey's multiple comparisons test for parametric data or Kruskal-Wallis with
1166 Dunn's multiple comparisons test for non-parametric were used. A two-way
1167 ANOVA was used to identify significant differences between experimental
1168 conditions in the response to insulin or during differentiation. Values were

1169 considered significant at $P<0.05$. Statistical details and significance can be found
1170 in the figure legends.
1171

1172 **Acknowledgments**

1173 The authors are grateful to the Proteomics Facilities of the SEPBIO/Autonomous
1174 University of Barcelona (UAB; Spain) and David Ovelleiro (Proteomics Unit,
1175 IMIBIC) for the iTRAQ-LC-MS/MS analysis and the Andalusian Bioinformatics
1176 Platform (PAB) centre located at the University of Málaga (Spain) for the
1177 Ingenuity Pathway Analysis (IPA) software. We thank Dr Wabitsch (Ulm
1178 University, Germany) for sharing SGBS cells. We thank Rafael Serrano-Berzosa
1179 (IMIBIC) for his technical help.

Additional information

Funding

Funder	Grant reference number	Author
Ministerio de Ciencia, Innovación y Universidades/FEDER	BFU2013-44229-REDT; BFU2016-76711-REDT; BFU2017-90578-REDT	M.M.M.
Ministerio de Ciencia, Innovación y Universidades/FEDER	RTI2018-093919-B-I00	S.F.-V.
Consejería de Salud y Bienestar Social/Junta de Andalucía/FEDER	PI-0200/2013	M.M.M.
Consejería de Salud y Bienestar Social/Junta de Andalucía/FEDER	PI-0159-2016	R.G.-R.
Instituto de Salud Carlos III (ISCIII)/FEDER	PIE14/00005	J.L.-M. and M.M.M.
Instituto de Salud Carlos III (ISCIII)/FEDER	PI16/00264	R.M.L.
Instituto de Salud Carlos III (ISCIII)/FEDER	PI17/0153	J.V.
Fondo de Investigación Sanitaria/ISCIII/FEDER Miguel Servet tenure-track program	CP10/ 00438 and CPII16/00008	S.F.-V.
Research Plan of University of Córdoba	Mod 2.5, 2019	R.G-R.
Co-funded by European Regional Development Fund/European Social Fund "Investing in your future"); and Consejería de Economía, Conocimiento, Empresas y Universidad/Junta de Andalucía/FEDER (BIO-0139). CIBEROBN is an initiative of the ISCIII, Spain.		
The funders had no role in study design, data collection and interpretation, or the decision to submit the work for publication.		

1183 **Author contributions**

1184 M.M.M. and R.G.-R. designed research. J.L.-M., O.A.R.-Z., A.M., J.L.R-C., and
1185 P.P.-M. selected the patients from cohort 1. E.M.-M., S.F.-V., and J.V. selected
1186 the patients from cohort 2 and performed preadipocyte isolation. J.M.F.-R.
1187 participated in SGBS experiments. J.S.-C., E.M.-C., M.d.R.-M., and J.L.-A.
1188 performed research and analysed data. R.M.L. coordinated the splicing array
1189 study. M.R. and J.L. coordinated the transcriptomic analysis studies. R.G.-R.,
1190 S.F.-V., J.L.-M., R.M.L., M.R., and J.L. reviewed/edited the manuscript. M.M.M.
1191 and J.S.-C. wrote the manuscript. All the authors discussed the results and the
1192 manuscript.

1193 **Author ORCIDs**

1194 María M. Malagón, ORCID iD: 0000-0002-2419-2727.

1195 Rocío Guzmán-Ruiz, ORCID iD: 0000-0001-8020-4676.

1196 **Ethics**

1197 Human subjects: Written consent was obtained from all the participants prior to
1198 recruitment, and the experimental protocol was approved by the Ethics and
1199 Research Committee of Reina Sofía University Hospital (HURS; Córdoba,
1200 Spain), and University Hospital Joan XXIII (Tarragona, Spain) following the
1201 Helsinki Declaration.

1202 **Data availability**

1203 The proteomic dataset generated during this study are available at
1204 ProteomeXchange Consortium via the PRIDE partner repository with the dataset
1205 identifier PXD015621. All other data generated during the study are included in
1206 the manuscript and supporting files. Source data has been provided for ***Figure 1***
1207 and ***3***.

1208 **References**

1209 ADA. 2021. 2. Classification and Diagnosis of Diabetes: Standards of
1210 Medical Care in Diabetes—2021. *Diabetes Care* **44**:S15 LP-S33.
1211 doi:10.2337/dc21-S002

1212 Aouida M, Eid A, Mahfouz MM. 2016. CRISPR/Cas9-mediated target validation
1213 of the splicing inhibitor Pladienolide B. *Biochimie open* **3**:72–75.
1214 doi:10.1016/j.biopen.2016.02.001

1215 Aprile M, Ambrosio MR, D'Esposito V, Beguinot F, Formisano P, Costa V,
1216 Ciccodicola A. 2014. PPARG in human adipogenesis: Differential
1217 contribution of canonical transcripts and dominant negative isoforms. *PPAR*
1218 *Research* **2014**:18–20. doi:10.1155/2014/537865

1219 Aprile M, Cataldi S, Ambrosio MR, D'Esposito V, Lim K, Dietrich A, Blüher M,
1220 Savage DB, Formisano P, Ciccodicola A, Costa V. 2018. PPARγΔ5, a
1221 Naturally Occurring Dominant-Negative Splice Isoform, Impairs PPARγ
1222 Function and Adipocyte Differentiation. *Cell Reports* **25**:1577-1592.e6.
1223 doi:10.1016/j.celrep.2018.10.035

1224 Aprile M, Cataldi S, Perfetto C, Ambrosio MR, Italiani P, Tatè R, Blüher M,
1225 Ciccodicola A, Costa V. 2020. In-Vitro-Generated Hypertrophic-Like
1226 Adipocytes Displaying PPARG Isoforms Unbalance Recapitulate Adipocyte
1227 Dysfunctions In Vivo. *Cells* **9**:1284. doi:10.3390/cells9051284

1228 Arner E, Westermark PO, Spalding KL, Britton T, Rydén M, Frisén J, Bernard S,
1229 Arner P. 2010. Adipocyte turnover: Relevance to human adipose tissue
1230 morphology. *Diabetes* **59**:105–109. doi:10.2337/db09-0942

1231 Baralle FE, Giudice J. 2017. Alternative splicing as a regulator of development
1232 and tissue identity. *Nature Reviews Molecular Cell Biology* **18**:437–451.

1233 doi:10.1038/nrm.2017.27
1234 Bard JAM, Goodall EA, Greene ER, Jonsson E, Dong KC, Martin A. 2018.
1235 Structure and Function of the 26S Proteasome. *Annual Review of*
1236 *Biochemistry* **87**:697–724. doi:10.1146/annurev-biochem-062917-011931
1237 Berry DC, Jiang Y, Graff JM. 2016. Emerging Roles of Adipose Progenitor Cells
1238 in Tissue Development, Homeostasis, Expansion and Thermogenesis.
1239 *Trends in Endocrinology and Metabolism* **27**:574–585.
1240 doi:10.1016/j.tem.2016.05.001
1241 Bhattarai KR, Chaudhary M, Kim H-R, Chae H-J. 2020. Endoplasmic Reticulum
1242 (ER) Stress Response Failure in Diseases. *Trends in Cell Biology* **30**:672–
1243 675. doi:https://doi.org/10.1016/j.tcb.2020.05.004
1244 Bunnell BA, Flaat M, Gagliardi C, Patel B, Ripoll C. 2008. Adipose-derived stem
1245 cells: isolation, expansion and differentiation. *Methods (San Diego, Calif)*
1246 **45**:115–120. doi:10.1016/j.ymeth.2008.03.006
1247 Chong J, Soufan O, Li C, Caraus I, Li S, Bourque G, Wishart DS, Xia J. 2018.
1248 MetaboAnalyst 4.0: Towards more transparent and integrative
1249 metabolomics analysis. *Nucleic Acids Research* **46**:W486–W494.
1250 doi:10.1093/nar/gky310
1251 Christianson JC, Ye Y. 2014. Cleaning up in the endoplasmic reticulum:
1252 Ubiquitin in charge. *Nature Structural and Molecular Biology* **21**:325–335.
1253 doi:10.1038/nsmb.2793
1254 Craveiro Sarmento AS, de Azevedo Medeiros LB, Agnez-Lima LF, Lima JG, de
1255 Melo Campos JTA. 2018. Exploring Seipin: From Biochemistry to
1256 Bioinformatics Predictions. *International Journal of Cell Biology*
1257 **2018**:5207608. doi:10.1155/2018/5207608

1258 Cretu C, Agrawal AA, Cook A, Will CL, Fekkes P, Smith PG, Lührmann R,
1259 Larsen N, Buonamici S, Pena V. 2018. Structural Basis of Splicing
1260 Modulation by Antitumor Macrolide Compounds. *Molecular Cell* **70**:265-
1261 273.e8. doi:10.1016/j.molcel.2018.03.011
1262 de sá PM, Richard AJ, Hang H, Stephens JM. 2017. Transcriptional regulation
1263 of adipogenesis. *Comprehensive Physiology* **7**:635–674.
1264 doi:10.1002/cphy.c160022
1265 Díaz-Ruiz A, Guzmán-Ruiz R, Moreno NR, García-Rios A, Delgado-Casado N,
1266 Membrives A, Túnez I, El Bekay R, Fernández-Real JM, Tovar S, Diéguez
1267 C, Tinahones FJ, Vázquez-Martínez R, López-Miranda J, Malagón MM.
1268 2015. Proteasome Dysfunction Associated to Oxidative Stress and
1269 Proteotoxicity in Adipocytes Compromises Insulin Sensitivity in Human
1270 Obesity. *Antioxidants & Redox Signaling* **23**:597–612.
1271 doi:10.1089/ars.2014.5939
1272 Ejarque M, Ceperuelo-Mallafré V, Serena C, Pachón G, Núñez-Álvarez Y,
1273 Terrón-Puig M, Calvo E, Núñez-Roa C, Oliva-Olivera W, Tinahones FJ,
1274 Peinado MA, Vendrell J, Fernández-Veledo S. 2017. Survivin, a key player
1275 in cancer progression, increases in obesity and protects adipose tissue
1276 stem cells from apoptosis. *Cell death & disease* **8**:e2802.
1277 doi:10.1038/cddis.2017.209
1278 Engin AB, Engin A. 2017. Obesity and Lipotoxicity. doi:10.1007/978-3-319-
1279 48382-5
1280 Fei W, Li H, Shui G, Kapterian TS, Bielby C, Du X, Brown AJ, Li P, Wenk MR,
1281 Liu P, Yang H. 2011. Molecular characterization of seipin and its mutants:
1282 implications for seipin in triacylglycerol synthesis. *Journal of lipid research*

1283 **52**:2136–2147. doi:10.1194/jlr.M017566
1284 Fiszbein A, Kornblihtt AR. 2017. Alternative splicing switches: Important players
1285 in cell differentiation. *BioEssays* **39**:1–11. doi:10.1002/bies.201600157
1286 Gahete MD, del Rio-Moreno M, Camargo A, Alcala-Diaz JF, Alors-Perez E,
1287 Delgado-Lista J, Reyes O, Ventura S, Perez-Martínez P, Castaño JP,
1288 Lopez-Miranda J, Luque RM. 2018. Changes in Splicing Machinery
1289 Components Influence, Precede, and Early Predict the Development of
1290 Type 2 Diabetes: From the CORDIOPREV Study. *EBioMedicine* **37**:356–
1291 365. doi:10.1016/j.ebiom.2018.10.056
1292 Gao H, Mejhert N, Fretz JA, Arner E, Lorente-Cebrián S, Ehrlund A, Dahlman-
1293 Wright K, Gong X, Strömblad S, Douagi I, Laurencikiene J, Dahlman I,
1294 Daub CO, Rydén M, Horowitz MC, Arner P. 2014. Early B Cell Factor 1
1295 Regulates Adipocyte Morphology and Lipolysis in White Adipose Tissue.
1296 *Cell Metabolism* **19**:981–992.
1297 doi:https://doi.org/10.1016/j.cmet.2014.03.032
1298 Gao H, Volat F, Sandhow L, Galitzky J, Nguyen T, Esteve D, Åström G, Mejhert
1299 N, Ledoux S, Thalamas C, Arner P, Guillemot JC, Qian H, Rydén M,
1300 Bouloumié A. 2017. CD36 Is a Marker of Human Adipocyte Progenitors
1301 with Pronounced Adipogenic and Triglyceride Accumulation Potential. *Stem*
1302 *Cells* **35**:1799–1814. doi:10.1002/stem.2635
1303 Ghaben AL, Scherer PE. 2019. Adipogenesis and metabolic health. *Nature*
1304 *Reviews Molecular Cell Biology* **20**:242–258. doi:10.1038/s41580-018-
1305 0093-z
1306 Giulietti M, Piva F, D'Antonio M, D'Onorio De Meo P, Paoletti D, Castrignanò T,
1307 D'Erchia AM, Picardi E, Zambelli F, Principato G, Pavesi G, Pesole G.

1308 2013. SpliceAid-F: a database of human splicing factors and their RNA-
1309 binding sites. *Nucleic acids research* **41**:D125–D131.
1310 doi:10.1093/nar/gks997
1311 Greene CS, Krishnan A, Wong AK, Ricciotti E, Zelaya RA, Himmelstein DS,
1312 Zhang R, Hartmann BM, Zaslavsky E, Sealfon SC, Chasman DI, Fitzgerald
1313 GA, Dolinski K, Grosser T, Troyanskaya OG. 2015. Understanding
1314 multicellular function and disease with human tissue-specific networks.
1315 *Nature Genetics* **47**:569–576. doi:10.1038/ng.3259
1316 Hetz C, Papa FR. 2018. The Unfolded Protein Response and Cell Fate Control.
1317 *Molecular Cell* **69**:169–181. doi:10.1016/j.molcel.2017.06.017
1318 Hwang J, Qi L. 2018. Quality Control in the Endoplasmic Reticulum: Crosstalk
1319 between ERAD and UPR pathways. *Trends in Biochemical Sciences*
1320 **43**:593–605. doi:10.1016/j.tibs.2018.06.005
1321 Jiménez-Vacas JM, Herrero-Aguayo V, Gómez-Gómez E, León-González AJ,
1322 Sáez-Martínez P, Alors-Pérez E, Fuentes-Fayos AC, Martínez-López A,
1323 Sánchez-Sánchez R, González-Serrano T, López-Ruiz DJ, Requena-Tapia
1324 MJ, Castaño JP, Gahete MD, Luque RM. 2019. Spliceosome Component
1325 SF3B1 as Novel Prognostic Biomarker and Therapeutic Target for Prostate
1326 Cancer. *Translational Research*. doi:10.1016/j.trsl.2019.07.001
1327 Kaida D. 2019. Spliceostatin A treatment inhibits mitotic clonal expansion and
1328 adipogenesis. *Biochemical and Biophysical Research Communications*
1329 **514**:848–852. doi:10.1016/j.bbrc.2019.04.180
1330 Karagöz GE, Acosta-Alvear D, Walter P. 2019. The Unfolded Protein
1331 Response: Detecting and Responding to Fluctuations in the Protein-
1332 Folding Capacity of the Endoplasmic Reticulum. *Cold Spring Harbor*

1333 *Perspectives in Biology* **11**:a033886. doi:10.1101/cshperspect.a033886
1334 Krämer A, Green J, Pollard J, Tugendreich S. 2014. Causal analysis
1335 approaches in ingenuity pathway analysis. *Bioinformatics* **30**:523–530.
1336 doi:10.1093/bioinformatics/btt703
1337 Kusaczuk M. 2019. Tauroursodeoxycholate-Bile Acid with Chaperoning Activity:
1338 Molecular and Cellular Effects and Therapeutic Perspectives. *Cells* **8**:1471.
1339 doi:10.3390/cells8121471
1340 Lessard J, Tchernof A. 2012. Depot- and obesity-related differences in
1341 adipogenesis. *Clin Lipidol* **7**:587–596.
1342 Li J-H, Liu S, Zhou H, Qu L-H, Yang J-H. 2013. starBase v2.0: decoding
1343 miRNA-ceRNA, miRNA-ncRNA and protein–RNA interaction networks from
1344 large-scale CLIP-Seq data. *Nucleic Acids Research* **42**:D92–D97.
1345 doi:10.1093/nar/gkt1248
1346 Lin JC. 2015. Impacts of alternative splicing events on the differentiation of
1347 adipocytes. *International Journal of Molecular Sciences* **16**:22169–22189.
1348 doi:10.3390/ijms160922169
1349 Liu Y, Gonzàlez-Porta M, Santos S, Brazma A, Marioni JC, Aebersold R,
1350 Venkitaraman AR, Wickramasinghe VO. 2017. Impact of Alternative
1351 Splicing on the Human Proteome. *Cell Reports* **20**:1229–1241.
1352 doi:10.1016/j.celrep.2017.07.025
1353 Longo M, Spinelli R, D'Esposito V, Zatterale F, Fiory F, Nigro C, Raciti GA,
1354 Miele C, Formisano P, Beguinot F, Di Jeso B. 2016. Pathologic
1355 endoplasmic reticulum stress induced by glucotoxic insults inhibits
1356 adipocyte differentiation and induces an inflammatory phenotype.
1357 *Biochimica et Biophysica Acta - Molecular Cell Research* **1863**:1146–1156.

1358 doi:10.1016/j.bbamcr.2016.02.019
1359 Lowe CE, O'Rahilly S, Rochford JJ. 2011. Adipogenesis at a glance. *Journal of*
1360 *Cell Science* **124**:3726. doi:10.1242/jcs.101741
1361 Martyniak K, Masternak MM. 2017. Changes in adipose tissue cellular
1362 composition during obesity and aging as a cause of metabolic
1363 dysregulation. *Experimental Gerontology* **94**:59–63.
1364 doi:10.1016/j.exger.2016.12.007
1365 Mi H, Muruganujan A, Ebert D, Huang X, Thomas PD. 2019a. PANTHER
1366 version 14: More genomes, a new PANTHER GO-slim and improvements
1367 in enrichment analysis tools. *Nucleic Acids Research* **47**:D419–D426.
1368 doi:10.1093/nar/gky1038
1369 Mi H, Muruganujan A, Huang X, Ebert D, Mills C, Guo X, Thomas PD. 2019b.
1370 Protocol Update for large-scale genome and gene function analysis with
1371 the PANTHER classification system (v.14.0). *Nature Protocols* **14**:703–721.
1372 doi:10.1038/s41596-019-0128-8
1373 Mitteer DR, Greer BD, Fisher WW, Cohrs VL. 2018. Teaching behavior
1374 technicians to create publication-quality, single-case design graphs in
1375 graphpad prism 7. *Journal of Applied Behavior Analysis* **51**:998–1010.
1376 doi:10.1002/jaba.483
1377 Noormohammadi A, Calculli G, Gutierrez-Garcia R, Khodakarami A, Koyuncu
1378 S, Vilchez D. 2018. Mechanisms of protein homeostasis (proteostasis)
1379 maintain stem cell identity in mammalian pluripotent stem cells. *Cellular*
1380 *and Molecular Life Sciences* **75**:275–290. doi:10.1007/s00018-017-2602-1
1381 Nowicki M, Bzhalava D, Bała P. 2018. Massively parallel implementation of
1382 sequence alignment with basic local alignment search tool using parallel

1383 computing in Java library. *Journal of Computational Biology* **25**:871–881.
1384 doi:10.1089/cmb.2018.0079
1385 Palumbo P, Lombardi F, Siragusa G, Cifone MG, Cinque B, Giuliani M. 2018.
1386 Methods of Isolation, Characterization and Expansion of Human Adipose-
1387 Derived Stem Cells (ASCs): An Overview. *International journal of molecular*
1388 *sciences* **19**:1897. doi:10.3390/ijms19071897
1389 Perez-Riverol Y, Csordas A, Bai J, Bernal-Llinares M, Hewapathirana S, Kundu
1390 DJ, Inuganti A, Griss J, Mayer G, Eisenacher M, Pérez E, Uszkoreit J,
1391 Pfeuffer J, Sachsenberg T, Yilmaz Ş, Tiwary S, Cox J, Audain E, Walzer M,
1392 Jarnuczak AF, Ternent T, Brazma A, Vizcaíno JA. 2019. The PRIDE
1393 database and related tools and resources in 2019: Improving support for
1394 quantification data. *Nucleic Acids Research* **47**:D442–D450.
1395 doi:10.1093/nar/gky1106
1396 Qi L, Tsai B, Arvan P. 2017. New Insights into the Physiological Role of
1397 Endoplasmic Reticulum-Associated Degradation. *Trends in Cell Biology*
1398 **27**:430–440. doi:10.1016/j.tcb.2016.12.002
1399 Salo VT, Belevich I, Li S, Karhinen L, Vihinen H, Vigouroux C, Magré J, Thiele
1400 C, Hölttä-Vuori M, Jokitalo E, Ikonen E. 2016. Seipin regulates ER –lipid
1401 droplet contacts and cargo delivery . *The EMBO Journal* **35**:2699–2716.
1402 doi:10.15252/embj.201695170
1403 Sarjeant K, Stephens JM. 2019. Adipogenesis 1–20.
1404 Schneider CA, Rasband WS, Eliceiri KW. 2012. NIH Image to ImageJ: 25 years
1405 of image analysis. *Nature Methods* **9**:671–675. doi:10.1038/nmeth.2089
1406 Serena C, Keiran N, Ceperuelo-Mallafre V, Ejarque M, Fradera R, Roche K,
1407 Nuñez-Roa C, Vendrell J, Fernández-Veledo S. 2016. Obesity and Type 2

1408 Diabetes Alters the Immune Properties of Human Adipose Derived Stem
1409 Cells. *Stem Cells* **34**:2559–2573. doi:10.1002/stem.2429
1410 Sha H, Sun S, Francisco AB, Ehrhardt N, Xue Z, Liu L, Lawrence P, Mattijssen
1411 F, Guber RD, Panhwar MS, Brenna JT, Shi H, Xue B, Kersten S,
1412 Bensadoun A, Péterfy M, Long Q, Qi L. 2014. The ER-associated
1413 degradation adaptor protein Sel1L regulates LPL secretion and lipid
1414 metabolism. *Cell metabolism* **20**:458–470. doi:10.1016/j.cmet.2014.06.015
1415 Slayton M, Gupta A, Balakrishnan B, Puri V. 2019. CIDE Proteins in Human
1416 Health and Disease. *Cells* **8**:238. doi:10.3390/cells8030238
1417 Spalding KL, Arner E, Westermark PO, Bernard S, Buchholz BA, Bergmann O,
1418 Blomqvist L, Hoffstedt J, Näslund E, Britton T, Concha H, Hassan M,
1419 Rydén M, Frisén J, Arner P. 2008. Dynamics of fat cell turnover in humans.
1420 *Nature* **453**:783–787. doi:10.1038/nature06902
1421 Tam CS, Xie W, Johnson WD, Cefalu WT, Redman LM, Ravussin E. 2012.
1422 Defining insulin resistance from hyperinsulinemic-euglycemic clamps.
1423 *Diabetes care* **35**:1605–1610. doi:10.2337/dc11-2339
1424 Turunen JJ, Niemelä EH, Verma B, Frilander MJ. 2013. The significant other:
1425 Splicing by the minor spliceosome. *Wiley Interdisciplinary Reviews: RNA*
1426 **4**:61–76. doi:10.1002/wrna.1141
1427 Untergasser A, Cutcutache I, Koressaar T, Ye J, Faircloth BC, Remm M, Rozen
1428 SG. 2012. Primer3-new capabilities and interfaces. *Nucleic Acids Research*
1429 **40**:1–12. doi:10.1093/nar/gks596
1430 Vandesompele J, De Preter K, Pattyn F, Poppe B, Van Roy N, De Paepe A,
1431 Speleman F. 2002. Accurate normalization of real-time quantitative RT-
1432 PCR data by geometric averaging of multiple internal control genes.

1433 *Genome biology* **3**:RESEARCH0034.
1434 Yi X, Yang Y, Wu P, Xu X, Li W. 2019. Alternative splicing events during
1435 adipogenesis from hMSCs. *Journal of Cellular Physiology* **235**:304–316.
1436 doi:10.1002/jcp.28970
1437 Yilmaz E. 2017. Endoplasmic Reticulum Stress and Obesity BT - Obesity and
1438 Lipotoxicity In: Engin AB, Engin A, editors. Cham: Springer International
1439 Publishing. pp. 261–276. doi:10.1007/978-3-319-48382-5_11
1440 Zhang Ying, Qu P, Ma X, Qiao F, Ma Y, Qing S, Zhang Yong, Wang Y, Cui W.
1441 2018. Tauroursodeoxycholic acid (TUDCA) alleviates endoplasmic
1442 reticulum stress of nuclear donor cells under serum starvation. *PloS one*
1443 **13**:e0196785–e0196785. doi:10.1371/journal.pone.0196785
1444 Zhu M, Heydarkhan-Hagvall S, Hedrick M, Benhaim P, Zuk P. 2013. Manual
1445 isolation of adipose-derived stem cells from human lipoaspirates. *Journal of*
1446 *visualized experiments : JoVE* e50585–e50585. doi:10.3791/50585
1447

1448 **Table 1. Anthropometric and biochemical characteristics of study subjects**

1449 **from cohort 1.**

	NG Obese	IR Obese	T2D Obese
N	30	30	18
Gender (female/male)	15 / 15	15 / 15	11 / 7
Post-menopause (n, %)	2 (13)	2 (13)	3 (27)
Lipid-lowering therapy (n, %)	0 (0)	5 (17)	4 (22)
Antidiabetic therapy (n, %)	0 (0)	3 (10)	8 (44)
Antihypertensive therapy (n, %)	1 (3)	6 (20)	5 (28)
Age (years)	43 ± 2	44 ± 2	46 ± 2
Weight (kg)	140.4 ± 7.0	153.4 ± 10.0	145.4 ± 7.5
Height (m)	1.67 ± 0.03	1.69 ± 0.02	1.65 ± 0.03
Body mass index (kg/m^2)	50.2 ± 2.1	52.8 ± 2.9	52.9 ± 1.9
Fat mass (%)	43.1 ± 1.9	41.2 ± 2.0	42.1 ± 1.7
Lean mass (%)	39.1 ± 3.2	36.1 ± 1.1	35.0 ± 1.0
Water mass (%)	23.0 ± 3.5	22.7 ± 1.6	22.9 ± 1.3
Waist circumference (cm)	144.2 ± 5.9	156.1 ± 8.1	149.9 ± 4.6
Systolic pressure (mm/Hg)	128.1 ± 2.3	127.0 ± 3.5	122.1 ± 2.6
Diastolic pressure (mm/Hg)	78.5 ± 4.4	75.5 ± 3.1	71.5 ± 2.6
Fasting glucose (mg/dL)	89.1 ± 1.7	105.4 ± 2.0 ^{aaa}	157.3 ± 9.6 $^{aaa, bbb}$
Fasting glucose (mmol/L)	4.95 ± 0.10	5.85 ± 0.11 ^{aaa}	8.73 ± 0.54 $^{aaa, bbb}$
Fasting insulin (mU/L)	15.4 ± 1.8	25.9 ± 2.9 ^{aa}	17.9 ± 2.7 ^{b}
HbA1c (%)	5.44 ± 0.06	6.22 ± 0.10 ^{aaa}	8.43 ± 0.53 $^{aaa, bb}$
HbA1c (mmol/mol)	32.2 ± 0.6	40.9 ± 1.2 ^{aaa}	64.8 ± 5.7 $^{aaa, bb}$
HOMA-IR (units)	3.42 ± 0.44	6.77 ± 0.74 ^{aa}	6.74 ± 1.05 ^{aa}
Total cholesterol (mg/dL)	167.4 ± 10.0	181.6 ± 8.3	198.1 ± 8.6
LDL cholesterol (mg/dL)	122.9 ± 11.1	112.9 ± 6.6	124.2 ± 8.5
HDL cholesterol (mg/dL)	39.5 ± 3.3	36.3 ± 2.1	36.7 ± 1.6
Triglycerides (mg/dL)	108.2 ± 7.0	132.7 ± 12.2	152.0 ± 12.9 ^{a}
Free fatty acids (mmol/L)	66.7 ± 6.3	74.4 ± 7.2	83.5 ± 6.2
C-reactive protein (mg/L)	9.61 ± 1.68	11.4 ± 2.3	17.4 ± 5.3
Uric acid (mg/dL)	6.30 ± 0.32	7.03 ± 0.36	6.85 ± 0.68

1450 **NG**, normoglycemic; **IR**, insulin-resistant; **T2D**, type 2 diabetes; **LDL**, low-density

1451 lipoprotein; **HDL**, high-density lipoprotein; **HbA1c**, glycated hemoglobin; **HOMA-**

1452 **IR**, homeostasis model assessment of insulin resistance. ^{a}P<0.05, ^{aa}P<0.01,

1453 ^{aaa}P<0.001 *vs.* NG Obese; ^{b}P<0.05, ^{bb}P<0.01, ^{bbb}P<0.001 *vs.* IR Obese. One-

1454 way ANOVA with Tukey's multiple comparisons test or Kruskal-Wallis with Dunn's

1455 multiple comparisons test (for parametric or non-parametric data, respectively)

1456 were used. Normality distribution was determined by Shapiro-Wilk normality test.
1457 The online version of this article includes the following figure supplements for
1458 Figure 1: ***Table 1*—Figure supplement 1**.

1459

1460 **Figure legends**

1461 **Figure 1.** Comparative proteomic analysis of subcutaneous (SC) and omental
1462 (OM) preadipocytes from obese subjects with type 2 diabetes (T2D) *vs.*
1463 normoglycaemia (NG). Data correspond to individuals from cohort 1. (**A**) Venn
1464 diagrams showing overlap of differentially regulated proteins between T2D *vs.*
1465 NG obese subjects in SC and OM preadipocytes (left panel). Up-regulated and
1466 down-regulated proteins are indicated in the right panel. (**B**) Top10 over-
1467 represented canonical pathways in T2D *vs.* NG obese subjects in SC
1468 preadipocytes and (**C**) in OM preadipocytes according to Ingenuity Pathway
1469 Analysis (IPA). Blue and red bars indicate down-regulated and up-regulated
1470 pathways, respectively, in T2D *vs.* NG obese subjects. Numbers indicate the
1471 number of identified proteins/total proteins annotated to the pathway. Black line
1472 indicates -Log_2(*P value*). Samples from 2-3 individuals per group and fat depot
1473 were pooled and used for two separate iTRAQ experiments (n=5-6
1474 subjects/group/fat depot). Data normality was tested by Shapiro-Wilk test and
1475 Student´s t test was used, a ±1.5-fold change with $p<0.05$ was set as the
1476 threshold for categorizing up- and down-regulated proteins. Canonical pathway
1477 analysis was performed using IPA (see *Materials and Methods* section). The
1478 online version of this article includes the following figure supplements for Figure
1479 1: ***Figure 1*—Figure supplement 2** and ***Figure 1*—Figure supplement 3**; and

1480 the following source data for Figure 1: ***Figure 1*—Source data 1** and ***Figure 1*—**
1481 **Source data 2**.

1482 **Figure 2.** Downregulation of the splicing machinery in subcutaneous (SC)
1483 preadipocytes is associated with obesity-related insulin resistance (IR) and type
1484 2 diabetes (T2D). (**A**) Hierarchical clustering dendrogram heatmap analysis of
1485 splicing-related genes in SC (green) and OM (red) preadipocytes from
1486 normoglycemic (NG), IR, and T2D morbidly obese subjects (cohort 1) (n=6, 1
1487 technical replicate each) measured by qPCR dynamic array. Rows stand for
1488 splicing-related genes (white, mayor spliceosome; grey, minor spliceosome;
1489 black, splicing factors), while columns stand for subject groups. The scale in the
1490 colour bar represents -Log_2(Fold Change). (**B**) mRNA levels of *PRPF8* measured
1491 by qPCR dynamic array (upper graph) and representative blot and protein level
1492 quantification of PRP8 (lower graph) in SC and OM preadipocytes from NG, IR,
1493 and T2D morbidly obese subjects (cohort 1; n=6, 1 technical replicate each)
1494 *P<0.05, **P<0.01 *vs.* NG and/or IR subjects, ##P<0.01 *vs*. SC preadipocytes
1495 from the same subjects. (**C**) mRNA levels of *PRPF8* in SC and OM preadipocytes
1496 from lean, and NG and T2D subjects with simple obesity (cohort 2; n=5-11, 1
1497 technical replicate each). *P<0.05 *vs.* lean and/or NG obese subjects, #P<0.05
1498 *vs*. SC preadipocytes from the same subjects. (**D**) *PRPF8* mRNA levels and area
1499 under the curve (AUC) during *in vitro* differentiation of SC and OM preadipocytes
1500 from NG and IR morbidly obese subjects (cohort 1; n=6, 1 technical replicate
1501 each). *P<0.05, ***P<0.001 *vs. PRPF8* mRNA levels at Day 0; ###P<0.001 *vs.*
1502 *PRPF8* mRNA levels at Day 3; $P<0.05, $$P<0.01, $$$P<0.001 *vs.* NG. Data are
1503 presented as mean ± standard error of the mean (S.E.M.). One-way ANOVA with
1504 Tukey's multiple comparisons test or Kruskal-Wallis with Dunn's multiple

1505 comparisons test (for parametric or non-parametric data, respectively) were used
1506 for B and C; two-way ANOVA was used for D. Normality distribution was
1507 determined by Shapiro-Wilk normality test. The online version of this article
1508 includes the following figure supplements for Figure 2: ***Figure 2*—Figure**
1509 **supplement 4**, ***Figure 2*—Figure supplement 5** and ***Figure 2*—Figure**
1510 **supplement 6**.

1511 **Figure 3.** *PRPF8* silencing impairs adipogenesis in SGBS cells. (**A**) *PRPF8*
1512 mRNA levels in SGBS cells during adipogenesis. (**B**) Representative blot and
1513 protein quantification of PRP8 content in SGBS cells during adipogenesis. (4-6
1514 replicate studies, 3 technical replicates each). **ND**, non-detected. *P<0.05,
1515 **P<0.01, ***P<0.001 vs. preceding differentiation days. (**C**) Representative
1516 confocal micrographs of SGBS adipocytes three days post-transfection
1517 (differentiation day 7) with control or *PRPF8*-siRNA stained with Oil Red-O [lipid
1518 droplets (LDs), red] and DAPI (nucleus, blue). Morphometric analysis of LDs was
1519 carried out using ImageJ software. Scale bar = 10 μm. (6 replicate studies, 10
1520 cells each). mRNA levels of splicing variants of the transcription factors, *PPARG*
1521 and *SREBF1* (**D**), and representative blot and protein level quantification of
1522 PPARγ1 and PPARγ2 (**E**), and of the LD-related proteins, *BSCL2*, *CIDEB*, and
1523 *CIDEC* (**F**), in SGBS adipocytes 3 days post-transfection. (**G**) Representative
1524 blots and protein level quantification of ADRP, BiP, PSMB8, CHOP, DGAT2,
1525 FAS, PLIN1, pHSL$^{(Ser563)}$, HSL, Pro-caspase3, and Caspase-3 in SGBS
1526 adipocytes 3 days post-transfection. (3-6 replicate studies, 3 technical replicates
1527 each). *P<0.05, **P<0.01, ***P<0.001 *vs.* control; ##P<0.01 *vs. PRPF8*-siRNA;
1528 $P<0.05 *vs. PRPF8*-pcDNA3.1. (**H**) Representative blots and protein level
1529 quantification of pAKT$^{(Ser473)}$ and AKT in SGBS adipocytes 3 days post-

1530 transfection treated with/without insulin (100 nmol/L, 15 min). (3 replicate studies,
1531 3 technical replicates each). ***P<0.001 *vs.* Control-siRNA -Insulin; ###P<0.001
1532 *vs.* control-siRNA +Insulin. (**I**) Representative confocal micrographs of SGBS
1533 adipocytes five days post-transfection (day 10 of differentiation) with control,
1534 *PRPF8*-siRNA or *PRPF8*-pcDNA3.1 alone, or in combination (*PRPF8* Recovery)
1535 stained with Oil Red-O (LDs, red) and DAPI (nucleus, blue). Morphometric
1536 analysis of LDs was carried out using ImageJ software. Scale bar = 10 μm. (5
1537 replicate studies, 10 cells each). *P<0.05, **P<0.01, ***P<0.001 *vs.* control;
1538 #P<0.05, ##P<0.01, ###P<0.001 *vs. PRPF8*-siRNA; $P<0.05. $$P<0.01 *vs. PRPF8*-
1539 pcDNA3.1. Data are presented as mean ± standard error of the mean (S.E.M.).
1540 One-way ANOVA with Tukey's multiple comparisons test or Kruskal-Wallis with
1541 Dunn's multiple comparisons test (for parametric or non-parametric data,
1542 respectively) were used for A and B; unpaired t test or Mann Whitney test (for
1543 parametric or non-parametric data, respectively) were used for C-G and I; and
1544 two-way ANOVA was used for H. Normality distribution was determined by
1545 Shapiro-Wilk normality test. The online version of this article includes the
1546 following figure supplements for Figure 3: ***Figure 3*—Figure supplement 7**,
1547 ***Figure 3*—Figure supplement 8**, and ***Figure 3*—Figure supplement 9**, and the
1548 following source data for Figure 3: ***Figure 3*—Source data 3** and ***Figure 3*—**
1549 **Source data 3**.

1550 **Figure 4.** *PRPF8* silencing alters differentiation of human primary SC
1551 preadipocytes. Data corresponds to individuals from cohort 1. (**A**) Quantification
1552 of *PRPF8* mRNA levels in subcutaneous (SC) preadipocytes from
1553 normoglycemic (NG), insulin resistant (IR), and with type 2 diabetes (T2D)
1554 morbidly obese individuals transfected with control, *PRPF8*-siRNA, or *PRPF8*-

1555 pcDNA3.1, alone or in combination (*PRPF8* Recovery). (3 replicate studies, 4
1556 technical replicates each). (**B**) Representative confocal micrographs of SC
1557 preadipocytes from NG, IR, and T2D morbidly obese individuals after transfection
1558 with control, *PRPF8*-siRNA, or *PRPF8*-pcDNA3.1 alone or in combination
1559 (*PRPF8* Recovery) stained with Oil Red-O [lipid droplets (LDs), red] and DAPI
1560 (nucleus, blue). Morphometric analysis of LDs was carried out using ImageJ
1561 software. Scale bar = 10 µm. (12 replicate studies, 10 cells each). mRNA levels
1562 of *PPARG* (**C**), and *SREBF1* (**D**), and the LD-related proteins, *BSCL2* (**E**), *CIDEB*
1563 (**F**), and *CIDEC* (**G**) and their splicing forms in SC preadipocytes from NG, IR,
1564 and T2D morbidly obese individuals after transfection with control, *PRPF8*-siRNA
1565 or *PRPF8*-pcDNA3.1, alone or in combination (*PRPF8* Recovery). (3 replicate
1566 studies, 4 technical replicates each). *P<0.05, **P<0.01, ***P<0.001 *vs.* NG-
1567 Control; $^{\#}$P<0.05, $^{\#\#}$P<0.01, $^{\#\#\#}$P<0.001 *vs. PRPF8*-siRNA; $^{\$}$P<0.05. $^{\$\$}$P<0.01,
1568 $^{\$\$\$}$P<0.001 *vs. PRPF8*-pcDNA3.1; $^{@}$P<0.05, $^{@@}$P<0.01, $^{@@@}$P<0.001 *vs.*
1569 corresponding basal. Data are presented as mean ± standard error of the mean
1570 (S.E.M.). One-way ANOVA with Tukey's multiple comparisons test or Kruskal-
1571 Wallis with Dunn's multiple comparisons test (for parametric or non-parametric
1572 data, respectively) were used. Normality distribution was determined by Shapiro-
1573 Wilk normality test.

1574 **Figure 5.** Unbalanced Unfolded Protein Response (UPR) in preadipocytes is
1575 associated with obesity-related insulin resistance (IR) and type 2 diabetes (T2D).
1576 Data corresponds to individuals from cohort 1. Representative blots and protein
1577 level quantifications of BiP (**A**), ATF6α^{p90} and ATF6α^{p50} (**B**), pPERK$^{(Thr980)}$ and
1578 PERK (**C**), pEIF2α$^{(Ser51)}$ and EIF2α (**D**), CHOP €, pIRE1α$^{(Ser724)}$ and IRE1α (**F**),
1579 and PDI and GRP94 (**H**) in subcutaneous (SC) and omental (OM) preadipocytes

1580 from normoglycemic (NG), IR and T2D morbidly obese subjects (n=6-12, 1
1581 technical replicate each). (**G**) mRNA levels of *XBP1s* and *XBP1u* in SC and OM
1582 preadipocytes from NG, IR and T2D obese subjects (n=12, 1 technical replicate
1583 each). *P<0.05, **P<0.01, ***P<0.001 *vs.* NG and/or IR subjects; #P<0.05,
1584 ##P<0.01, ###P<0.001 *vs.* SC preadipocytes from the same subjects. Data are
1585 presented as mean ± standard error of the mean (S.E.M.). One-way ANOVA with
1586 Tukey's multiple comparisons test or Kruskal-Wallis with Dunn's multiple
1587 comparisons test (for parametric or non-parametric data, respectively,
1588 determined by Shapiro-Wilk normality test) were used.

1589 **Figure 6.** Activation of Endoplasmic Reticulum-Associated Degradation (ERAD)
1590 in preadipocytes is associated with obesity-related insulin resistance (IR) and
1591 type 2 diabetes (T2D). Data corresponds to individuals from cohort 1. mRNA
1592 levels of *BIP* (**A**), *DERL1*, *SEC61A1*, *STT3A* and *STT3B* (**B**), *HRD1*, *RNF185*
1593 and *SEL1L* (**C**), and *RAD23A* and *UBQLN1* (**D**), in subcutaneous (SC) and
1594 omental (OM) preadipocytes from normoglycemic (NG), IR and T2D morbidly
1595 obese subjects (n=12, 1 technical replicate each). *P<0.05, **P<0.01, ***P<0.001
1596 *vs.* NG and/or IR subjects; #P<0.05, #P<0.01, ###P<0.001 *vs.* SC preadipocytes
1597 from the same subjects. (**E**) Hierarchical clustering dendrogram heatmap
1598 analysis of ERAD-related genes in SC (green) and OM (red) preadipocytes from
1599 NG, IR and T2D obese subjects. Rows stand for ERAD-related steps (white,
1600 recognition; light grey, retrotranslocation; dark grey, ubiquitination; black,
1601 targeting to proteasome), while columns stand for subject groups. The scale in
1602 the colour bar represents -Log_2(Fold Change). One-way ANOVA with Tukey's
1603 multiple comparisons test or Kruskal-Wallis with Dunn's multiple comparisons
1604 test (for parametric or non-parametric data, respectively, determined by Shapiro-

1605 Wilk normality test) were used. The online version of this article includes the
1606 following figure supplements for Figure 6: ***Figure 6*—Figure supplement 10** and
1607 ***Figure 6*—Figure supplement 11**.

1608 **Figure 7.** Activation of ERAD in human primary omental (OM) preadipocytes from
1609 normoglyceimc (NG) morbidly obese individuals by hyperglycemic /
1610 hyperinsulinemic (HGHI) conditions and reversal of ERAD activation in human
1611 primary OM preadipocytes from insulin resistant (IR) and with type 2 diabetes
1612 (T2D) morbidly obese individuals by TUDCA. Data correspond to individuals from
1613 cohort 1. mRNA levels of *BIP* (**A**), *DERL1*, *SEC61A1*, *STT3A,* and *STT3B* (**B**),
1614 *HRD1*, *RNF185* and *SEL1L* (**C**), and *RAD23A* and *UBQLN1* (**D**). (3 replicate
1615 studies, 4 technical replicates each). Representative dot-blot and protein
1616 quantification of ubiquitin-conjugated proteins (**E**), and chymotrypsin-like
1617 peptidase activity of the 26S proteasome (+ATP) (**F**) in OM preadipocytes from
1618 NG, IR, and T2D morbidly obese individuals exposed 14 h to 0.5 mg/mL TUDCA,
1619 24 h to HGHI conditions, and/or a combination of both. (3-9 replicate studies, 3
1620 technical replicates each). (**G**) Representative confocal micrographs of OM
1621 preadipocytes from NG, IR, and T2D morbidly obese individuals under the
1622 indicated experimental conditions stained with Oil Red-O [lipid droplets (LDs),
1623 red] and DAPI (nucleus, blue). Morphometric analysis of LDs was carried out
1624 using ImageJ software. Scale bar = 10 μm. (12 replicate studies, 10 cells each).
1625 (**H-I**) mRNA levels of adipogenesis-related genes in OM preadipocytes from NG,
1626 IR and T2D morbidly obese individuals under the indicated experimental
1627 conditions. (3 replicate studies, 4 technical replicates each). *P<0.05, **P<0.01.
1628 ***P<0.001 *vs.* control; #P<0.05, ##P<0.01, ###P<0.001 *vs.* HGHI; $P<0.05,
1629 $$P<0.01 *vs.* TUDCA; @P<0.05, @@P<0.01, @@@P<0.001 *vs.* corresponding

1630 basal. Data are presented as mean ± standard error of the mean (S.E.M.). One-
1631 way ANOVA with Tukey's multiple comparisons test or Kruskal-Wallis with Dunn's
1632 multiple comparisons test (for parametric or non-parametric data, respectively)
1633 were used. Normality distribution was determined by Shapiro-Wilk normality test.
1634 The online version of this article includes the following figure supplements for
1635 Figure 7: ***Figure* 7—Figure supplement 12**, ***Figure* 7—Figure supplement 13**,
1636 and ***Figure* 7—Figure supplement 14**.
1637 **Figure 8.** Schematic representation of the proposed mechanisms of action of
1638 PRP8/splicing and UPR/ERAD on adipocyte differentiation. PRP8 mediates
1639 alternative splicing events in subcutaneous (SC) preadipocytes by regulating the
1640 expression and/or isoform balance of the master regulators of adipogenesis,
1641 SREBP1 and PPARγ (solid arrows), likely through a direct action on the
1642 corresponding pre-mRNAs. This, in turn, would result in changes in the
1643 expression of adipogenic genes down-stream SREBP1 and PPARγ (dashed
1644 arrows), yet a direct action of PRP8 on CIDEB splicing is also plausible. The
1645 observed down-regulation of PRP8 in SC preadipocytes from obese individuals
1646 with insulin resistance (IR) and type 2 diabetes (T2D) would contribute to the
1647 impaired adipogenic capacity of these cells. A second pathogenic mechanism is
1648 activated in SC preadipocytes from IR/T2D obese individuals that impairs
1649 adipogenesis, i.e., dysregulated ER proteostasis leading to UPR/ERAD
1650 activation. This mechanism, which is also triggered in omental (OM)
1651 preadipocytes under conditions of IR/T2D obesity, alters the adipogenic program
1652 by modifying the expression of key adipogenic transcripction factors and down-
1653 stream adipocyte markers. Splicing dysregulation and UPR/ERAD activation
1654 could be differentially triggered by obesogenic insults. The model is based on

1655 published molecular mechanisms, *in silico* analysis of ENCORI and HumanBase
1656 databases, and the main findings shown in this article. This figure was created
1657 using graphical elements from Servier Medical Art repository (SMART;
1658 https://smart.servier.com/).
1659
1660 **Legends to Figure supplements**
1661 **Table 1—Figure supplement 1.** (**A**) Cell size of SC and OM mature adipocytes
1662 from NG, IR, and T2D morbidly obese subjects (cohort 1; n=6-8, 20 cells each).
1663 *P<0.05, ***P<0.001 *vs.* NG and/or IR obese subjects; ##P<0.01, ###P<0.001 *vs.*
1664 SC preadipocytes from the same subjects. (**B**) Representative blot and protein
1665 level quantification of DLK1/PREF1, CD45, and CD14 in the stromal-vascular
1666 fraction (SVF) and preadipocytes (PreAds) from SC and OM adipose tissue from
1667 morbidly obese subjects (cohort 1; n=11, 1 technical replicate each). ***P<0.001
1668 *vs.* SVF. (**C**) *m*RNA levels of *KI67* in SC and OM preadipocytes from NG, IR, and
1669 T2D morbidly obese subjects (cohort 1; n=3-6, 1 technical replicate each).
1670 *P<0.05, ***P<0.001 *vs.* NG and/or IR obese subjects; ##P<0.01 *vs.* SC
1671 preadipocytes from the same subjects. (**D**) Proliferation rate of SC and OM
1672 preadipocytes from NG, IR, and T2D morbidly obese subjects (cohort 1; n=20-
1673 22, 1 technical replicate each). #P<0.05, ##P<0.01 *vs.* SC preadipocytes from the
1674 same subjects. (**E**) Representative phase-contrast microscopy images (x100
1675 magnification and zoom) during *in vitro* differentiation and representative confocal
1676 images at day 10 of differentiation of SC and OM preadipocytes from NG, IR and
1677 T2D morbidly obese subjects (cohort 1). Cells were stained with Oil Red-O (lipid
1678 droplets, red) and DAPI (nucleus, blue). Scale bar = 50 µm. (**F**) mRNA levels of
1679 *FABP4*, *ADIPOQ*, and *PPARG* during *in vitro* differentiation of SC and OM
1680 preadipocytes from NG and IR morbidly obese subjects (cohort 1); the values of

1681 the area under the curve (AUC) are also shown (n=3-12, 3 technical replicates
1682 each). *P<0.05, **P<0.01, ***P<0.001 *vs.* previous days; #P<0.05, ##P<0.01,
1683 ###P<0.001 *vs.* NG Obese. Data are presented as mean ± standard error of the
1684 mean (S.E.M.). One-way ANOVA with Tukey's multiple comparisons test or
1685 Kruskal-Wallis with Dunn's multiple comparisons test (for parametric or non-
1686 parametric data, respectively) were used for A, C, and D; unpaired t test or Mann
1687 Whitney test (for parametric or non-parametric data, respectively) were used for
1688 B and AUC values in F; and two-way ANOVA was used for time-course
1689 differentiation studies in F. Normality distribution was determined by Shapiro-Wilk
1690 normality test.

1691 ***Figure 1*—Figure supplement 2.** Characterization of the human preadipocyte
1692 proteome. Analysis of the proteins identified by iTRAQ-LC-MS/MS in the
1693 proteome of preadipocytes isolated from morbidly obese subjects (cohort 1).
1694 Samples from 2-3 individuals per group and fat depot were pooled and used for
1695 two separate iTRAQ experiments (n=5-6 subjects/group/fat depot). (**A**) Proteins
1696 were categorized according to biological processes using GO PANTHER
1697 classification system (http://www.pantherdb.org/). (**B**) The bar chart represents
1698 the GO classification and fold enrichment of significantly over- and under-
1699 represented Biological Processes (p≤0.05 Bonferroni test) in preadipocyte
1700 proteome. The black line represents the number of identified proteins per each
1701 GO term and the red line represents -Log_2(*P value*).

1702 **Figure 1—Figure supplement 3.** (**A**) Venn diagrams showing overlap of
1703 differentially regulated proteins between SC and OM preadipocytes from NG and
1704 T2D morbidly obese subjects (cohort 1). Over-represented canonical pathways
1705 in SC *vs.* OM preadipocytes from NG (**B**), and T2D (**C**) obese subjects according

1706 to Ingenuity Pathway Analysis (IPA). Blue and red bars indicate down- and up-
1707 regulated pathways, respectively, in SC *vs.* OM preadipocytes. Numbers indicate
1708 the number of identified proteins/total proteins annotated to the pathway. Black
1709 line indicates $-Log_2$(*P value*). Samples from 2-3 individuals per group and fat
1710 depot were pooled and used for two separate iTRAQ experiments (n=5-6
1711 subjects/group/fat depot). Data normality was tested by Shapiro-Wilk test and
1712 Student´s t test was used, a ±1.5-fold change with $p<0.05$ was set as the
1713 threshold for categorizing up- and down-regulated proteins. Canonical pathway
1714 analysis was performed using IPA (see *Materials and Methods* section).

1715 **Figure 2—Figure supplement 4.** mRNA levels of components of the major
1716 spliceosome (**A**), minor spliceosome (**B**), and splicing factors (**C**) in SC and OM
1717 preadipocytes from NG, IR, and T2D morbidly obese subjects (cohort1; n=6, 1
1718 technical replicate each) measured by qPCR dynamic array. Only the genes from
1719 the microarray that were significantly regulated are represented (27 out of 42;
1720 *PRPF8* is shown in ***Figure 2B***). *P<0.05, **P<0.01, ***P<0.001 *vs.* NG and/or
1721 IR subjects; #P<0.05, ##P<0.01, ###P<0.001 *vs.* SC preadipocytes from the same
1722 subjects. Data are presented as mean ± standard error of the mean (S.E.M.).
1723 One-way ANOVA with Tukey's multiple comparisons test or Kruskal-Wallis with
1724 Dunn's multiple comparisons test (for parametric or non-parametric data,
1725 respectively). Normality distribution was determined by Shapiro-Wilk normality
1726 test.

1727 **Figure 2—Figure supplement 5.** mRNA levels of components of the major
1728 spliceosome (**A**), minor spliceosome (**B**), and splicing factors (**C**) in SC and OM
1729 preadipocytes from NG, IR, and T2D morbidly obese subjects (cohort 1; n=6, 1
1730 technical replicate each) measured by RT-PCR. *P<0.05, **P<0.01, ***P<0.001

1731 *vs.* NG and/or IR subjects; #P<0.05, ##P< 0.01, ###P<0.001 *vs.* SC preadipocytes
1732 from the same subjects. Data are presented as mean ± standard error of the
1733 mean (S.E.M.). One-way ANOVA with Tukey's multiple comparisons test or
1734 Kruskal-Wallis with Dunn's multiple comparisons test (for parametric or non-
1735 parametric data, respectively). Normality distribution was determined by Shapiro-
1736 Wilk normality test.

1737 **Figure 2—Figure supplement 6.** mRNA levels of representative components of
1738 the splicing machinery, including the major spliceosome (*SF3B1 tv1*) (**A**), minor
1739 spliceosome (*RNU12*) (**B**), and splicing factors (*CELF1* and *SNW1*) (**C**) in SC and
1740 OM preadipocytes from lean individuals and NG and T2D subjects with simple
1741 obesity (cohort 2; n=5-11, 1 technical replicate each). *P<0.05 vs. lean and/or NG
1742 obese subjects; #P<0.05, ##P<0.01, ###P<0.001 vs. SC preadipocytes from the
1743 same subjects. Data are presented as mean ± standard error of the mean
1744 (S.E.M.). One-way ANOVA with Tukey's multiple comparisons test or Kruskal-
1745 Wallis with Dunn's multiple comparisons test (for parametric or non-parametric
1746 data, respectively). Normality distribution was determined by Shapiro-Wilk
1747 normality test.

1748 **Figure 3—Figure supplement 7.** mRNA levels of *PRPF8* in SGBS adipocytes
1749 at day 3 and at day 5 post-transfection (D7 and D10 of differentiation,
1750 respectively) (3 replicate studies, 4 technical replicates each) (**A**), and
1751 representative blot and protein level quantification of PRP8 in SGBS adipocytes
1752 at day 5 post-transfection (3 replicate studies, 3 technical replicates each) (**B**)
1753 with control, *PRPF8*-siRNA or *PRPF8*-pcDNA3.1, alone or in combination
1754 (*PRPF8* Recovery). Cell viability of SGBS adipocytes at day 3 and day 5 post-
1755 transfection (6 replicate studies, 3 technical replicates each) (**C**). mRNA levels of

1756 splicing variants of the transcription factors, *PPARG* and *SREBF1* (3 replicate
1757 studies, 4 technical replicates each) (**D**), representative blot and protein level
1758 quantification of PPARγ1 and PPARγ2 (3 replicate studies, 3 technical replicates
1759 each) (**E**), and mRNA levels of splicing variants of the lipid droplet-related
1760 proteins, *BSCL2*, *CIDEB*, and *CIDEC* (3 replicate studies, 4 technical replicates
1761 each) (**F**) in SGBS adipocytes 5 days post-transfection with control, *PRPF8*-
1762 siRNA or *PRPF8*-pcDNA3.1, alone or in combination (*PRPF8* Recovery).
1763 *P<0.05, **P<0.01, ***P<0.001 *vs.* control; #P<0.05, ##P<0.01, ###P<0.001 *vs.*
1764 *PRPF8*-siRNA; $P<0.05, $$P<0.01, $$$P<0.001 *vs.* *PRPF8*-pcDNA3.1.
1765 Representative blots and protein level quantification of ADRP and BiP (6 replicate
1766 studies, 3 technical replicates each) (**G**), and mRNA levels of the adipokines,
1767 *FABP4* and *ADIPOQ* (6 replicate studies, 4 technical replicates each) (**H**), in
1768 SGBS adipocytes at day 5 post-transfection. *P<0.05 *vs.* control. Representative
1769 blot and protein level quantification of pAKT$^{(Ser473)}$ and AKT in SGBS adipocytes
1770 5 days post-transfection treated with/without insulin (100 nmol/L, 15 min) (3
1771 replicate studies, 3 technical replicates each) (**I**). ***P<0.001 *vs.* without Insulin;
1772 ###P<0.001 *vs.* control-siRNA +Insulin. Data are presented as mean ± standard
1773 error of the mean (S.E.M.). One-way ANOVA with Tukey's multiple comparisons
1774 test or Kruskal-Wallis with Dunn's multiple comparisons test (for parametric or
1775 non-parametric data, respectively, determined by Shapiro-Wilk normality test)
1776 were used for A-F; unpaired t test or Mann Whitney test (for parametric or non-
1777 parametric data, respectively) were used for G and H; and two-way ANOVA was
1778 used for I.
1779 **Figure 3—Figure supplement 8.** (**A**) mRNA levels of *PRPF8* in hADSCs cells
1780 during differentiation (days 0-13) (6 replicate studies, 4 technical replicates each).

1781 (**B**) mRNA levels of *PRPF8* in hADSCs cells transfected with *PRPF8*-siRNA or
1782 Control-siRNA at day 1 of differentiation and observed at days 3-6-10 of
1783 differentiation; the values of the area under the curve (AUC) are also shown (3
1784 replicate studies, 4 technical replicates each). (**C**) Cytotoxicity assay of hADSCs
1785 cells transfected with *PRPF8*-siRNA or Control-siRNA (4-8 replicate studies, 3
1786 technical replicates each). (**D**) Representative micrographs of hADSCs cells
1787 transfected with *PRPF8*-siRNA or Control-siRNA after staining with BODIPY
1788 (LDs, red) and Hoechst (nucleus, blue) (8 replicate studies, 9 cell fields each).
1789 mRNA levels of splicing variants of the transcription factors, *PPARG* and
1790 *SREBF1* (**E**), and of the LD-related proteins, *BSCL2*, *CIDEB,* and *CIDEC* (**F**) (4
1791 replicate studies, 3 technical replicates each) in hADSCs cells transfected with
1792 *PRPF8*-siRNA or Control-siRNA. *P<0.05, **P<0.01, ***P<0.001 *vs.* day 3 of
1793 differentiation; #P<0.05, ##P<0.01, ###P<0.001 *vs.* day 6 of differentiation;
1794 $P<0.05, $$P<0.01, $$$P<0.001 *vs.* Control-siRNA of the same day of
1795 differentiation. Data are presented as mean ± standard error of the mean
1796 (S.E.M.). One-way ANOVA with Tukey's multiple comparisons test or Kruskal-
1797 Wallis with Dunn's multiple comparisons test (for parametric or non-parametric
1798 data, respectively) were used for A; two-way ANOVA was used for B-F; and
1799 unpaired t test or Mann Whitney test (for parametric or non-parametric data,
1800 respectively) were used for AUC values in F. Normality distribution was
1801 determined by Shapiro-Wilk normality test.

1802 **Figure 3—Figure supplement 9.** (**A**) Representative confocal micrographs of
1803 SGBS cells after exposition of vehicle (DMSO; control) or pladienolide-B 10^{-8} M
1804 for 24 h stained with Oil Red-O (LDs, red) and DAPI (nucleus, blue).
1805 Morphometric analysis of LDs was carried out using ImageJ software. Scale bar

1806 = 10 μm (5 replicate studies, 10 cells each). mRNA levels of splicing variants of
1807 the transcription factors, *PPARG* and *SREBF1* (**B**), and the LD-related proteins,
1808 *BSCL2, CIDEB*, and *CIDEC* (**C**) in SGBS cells after exposure to vehicle (DMSO;
1809 control) or pladienolide-B 10^{-8} M for 24 h. (3 replicate studies, 4 technical
1810 replicates each). *P<0.05, **P<0.01, ***P<0.001 *vs.* control. (**D**) Representative
1811 blot and protein level quantification of SFPQ in SGBS cells after transfection with
1812 control, *SFPQ*-siRNA or *SFPQ*-pcDNA3.1, alone or in combination (*SFPQ*-
1813 Recovery (3 replicate studies, 3 technical replicates each). (**E**) Representative
1814 confocal micrographs of SGBS cells after transfection with control, *SFPQ*-siRNA
1815 or *SFPQ*-pcDNA3.1, alone or in combination (*SFPQ*-Recovery) stained with Oil
1816 Red-O (LDs, red) and DAPI (nucleus, blue). Morphometric analysis of LDs was
1817 carried out using ImageJ software. Scale bar = 10 μm (5-6 replicate studies, 10
1818 cells each). mRNA levels of splicing variants of the transcription factors, *PPARG*
1819 and *SREBF1* (**F**), and the LD-related proteins, *BSCL2, CIDEB*, and *CIDEC* (**G**)
1820 of SGBS cells after transfection with control, *SFPQ*-siRNA or *SFPQ*-pcDNA3.1,
1821 alone or in combination (*SFPQ*-Recovery) (3 replicate studies, 4 technical
1822 replicates each). *P<0.05, **P<0.01 *vs.* control; #P<0.05, ##P<0.01, ###P<0.001
1823 *vs. SFPQ*-siRNA; $P<0.05. $$P<0.01 *vs. SFPQ*-pcDNA3.1; n = 3. Data are
1824 presented as mean ± standard error of the mean (S.E.M.). Unpaired t test or
1825 Mann Whitney test (for parametric or non-parametric data, respectively) were
1826 used for A-C; One-way ANOVA with Tukey's multiple comparisons test or
1827 Kruskal-Wallis with Dunn's multiple comparisons test (for parametric or non-
1828 parametric data, respectively) were used for D-G. Normality distribution was
1829 determined by Shapiro-Wilk normality test.

1830 **Figure 6—Figure supplement 10.** mRNA levels of ERAD-related genes during
1831 *in vitro* differentiation of SC and OM preadipocytes from NG and IR morbidly
1832 obese individuals (cohort 1; n=6, 1 technical replicate each). Area under the curve
1833 (AUC) is also shown. *P<0.05, **P<0.01, ***P<0.001 *vs.* day 0 of differentiation;
1834 #P<0.05, ##P<0.01, ###P<0.001 *vs.* day 3 of differentiation; @@@P<0.001 *vs.* day 6
1835 of differentiation; $P<0.05, $$P<0.01, $$$P<0.001 *vs.* NG Obese. Data are
1836 presented as mean ± standard error of the mean (S.E.M.). Two-way ANOVA was
1837 used; and unpaired t test or Mann Whitney test (for parametric or non-parametric
1838 data, respectively) was used for AUC values. Normality distribution was
1839 determined by Shapiro-Wilk normality test.

1840 **Figure 6—Figure supplement 11.** mRNA levels of representative components
1841 of the ERAD pathway, participating in the recognition (*BIP*) (**A**), retrotranslocation
1842 through the endoplasmic reticulum (ER) membrane (*DERL1* and *SEC61A1*) (**B**),
1843 ubiquitination (*RNF185*) (**C**), and targeting of misfolded proteins to the
1844 proteasome (*RAD23A*) (**D**) in SC and OM preadipocytes from lean individuals
1845 and NG and T2D subjects with simple obesity (cohort 2; n=5-11, 1 technical
1846 replicate each). *P<0.05, **P<0.01 *vs.* lean and/or NG obese subjects; #P<0.05,
1847 ##P<0.01 *vs.* SC preadipocytes from the same subjects. Data are presented as
1848 mean ± standard error of the mean (S.E.M.). One-way ANOVA with Tukey's
1849 multiple comparisons test or Kruskal-Wallis with Dunn's multiple comparisons
1850 test (for parametric or non-parametric data, respectively). Normality distribution
1851 was determined by Shapiro-Wilk normality test.

1852 **Figure 7—Figure supplement 12.** Representative phase-contrast microscopy
1853 (x100 magnification and zoom) and confocal micrographs of SGBS
1854 preadipocytes exposed during 30 h to a combination of glucose (4.5 g/L) and

1855 insulin (100 nM) (HGHI; white bars), 5 nM TNFα (grey bars), 500 μM Oleate (dark
1856 grey bars), or 500 μM Palmitate (black bars) (**A**). Cells were stained with Oil Red-
1857 O (LDs, red) and DAPI (nucleus, blue). Morphometric analysis of LDs was carried
1858 out in untreated and treated SGBS preadipocytes using ImageJ software. Scale
1859 bar = 10 μm (5 replicate studies, 10 cells each) (**B**). *P<0.05, **P<0.01,
1860 ***P<0.001 *vs.* corresponding control. Representative blots and protein level
1861 quantification of pAKT$^{(Ser473)}$ and AKT in SGBS preadipocytes after exposure to
1862 insulin (100 nM, 15 min) or medium alone (3 replicate studies, 3 technical
1863 replicates each) (**C**). **P<0.01, ***P<0.001 *vs.* corresponding control with insulin.
1864 Data are presented as mean ± standard error of the mean (S.E.M.). Unpaired t
1865 test or Mann Whitney test (for parametric or non-parametric data, respectively,
1866 determined by Shapiro-Wilk normality test) were used. Normality distribution was
1867 determined by Shapiro-Wilk normality test.
1868 **Figure 7—Figure supplement 13.** (**A**) mRNA levels of ERAD-related genes in
1869 SGBS preadipocytes exposed during 30 h to high glucose (4.5 g/L)/high insulin
1870 (100 nmol/L) (HGHI; white), 5 nM TNFα (light grey), 500 μM Oleate (dark grey)
1871 or 500 μM Palmitate (black) (6 replicate studies, 4 technical replicates each).
1872 *P<0.05, **P<0.01 *vs.* corresponding control. (**B**) Hierarchical clustering
1873 dendrogram heatmap analysis of ERAD-related genes in SGBS preadipocytes in
1874 control (green) and after exposure to HGHI, TNFα, Oleate or Palmitate (red).
1875 Rows stand for ERAD-related steps (white, recognition; light grey,
1876 retrotranslocation; dark grey, ubiquitination; black, targeting to proteasome),
1877 while columns stand for subject groups. The scale in the colour bar represents -
1878 Log_2(Fold Change). (**C**) Chymotrypsin-like peptidase activity of the 26S
1879 proteasome (+ATP) and 20S proteasome (+SDS) (3 replicate studies, 3 technical

1880 replicates each). mRNA levels of ERAD (**D**) and adipogenesis-related (**E**) genes
1881 (3 replicate studies, 4 technical replicates each), and representative dot-blot and
1882 protein quantification of ubiquitin-conjugated proteins (3 replicate studies, 3
1883 technical replicates each) (**F**) in SGBS preadipocytes exposed 14 h to 0.5 mg/mL
1884 TUDCA (TUDCA, grey), 30 h to HGHI conditions (white), or a combination of both
1885 (TUDCA+HGHI, black). **ND**, non-detected. *P<0.05, **P<0.01. ***P<0.001 *vs.*
1886 control; #P<0.05, ##P<0.01, ###P<0.001 *vs.* HGHI; $P<0.05, $$P<0.01 *vs.* TUDCA.
1887 Data are presented as mean ± standard error of the mean (S.E.M.). Unpaired t
1888 test or Mann Whitney test (for parametric or non-parametric data, respectively,
1889 determined by Shapiro-Wilk normality test) were used for A and C; one-way
1890 ANOVA with Tukey's multiple comparisons test or Kruskal-Wallis with Dunn's
1891 multiple comparisons test (for parametric or non-parametric data, respectively)
1892 were used for D-F. Normality distribution was determined by Shapiro-Wilk
1893 normality test.
1894 **Figure 7—Figure supplement 14.** mRNA levels of ERAD (**A**) and adipogenesis-
1895 related genes (**B**) in SGBS preadipocytes overexpressing BiP (pCMV-BIP,
1896 black), exposed 14 h to 0.5 mg/mL TUDCA (TUDCA, grey), or a combination of
1897 both (TUDCA+pCMV-BIP, white with black dots) (3 replicate studies, 4 technical
1898 replicates each). *P<0.05, **P<0.01. ***P<0.001 *vs.* control; #P<0.05, ##P<0.01,
1899 ###P<0.001 *vs.* pCMV-BIP; $P<0.05, $$P<0.01, $$$P<0.001 *vs.* TUDCA. Data are
1900 presented as mean ± standard error of the mean (S.E.M.). One-way ANOVA with
1901 Tukey's multiple comparisons test or Kruskal-Wallis with Dunn's multiple
1902 comparisons test (for parametric or non-parametric data, respectively) were
1903 used. Normality distribution was determined by Shapiro-Wilk normality test.
1904
1905

1906 **Legends to Source data**

1907 **Figure 1—Source data 1.** Common pathways of normoglycemic (NG) and with
1908 type 2 diabetes (T2D) morbidly obese subjects (cohort 1) in the subcutaneous
1909 (SC) *vs.* omental (OM) preadipocytes proteome according to Ingenuity Pathway
1910 Analysis (IPA).

1911 **Figure 1—Source data 2.** Fat depot-specific canonical pathways in the type 2
1912 diabetes (T2D) *vs.* normoglycemic (NG) morbidly obese subjects (cohort 1)
1913 proteome according to Ingenuity Pathway Analysis (IPA).

1914 **Figure 3—Source data 3.** Analysis of CLIP_Seq data (target binding sites and
1915 related pathways) from *PRPF8*-silenced HepG2 and K562 cells provided by The
1916 Encyclopedia of RNA Interactomes (ENCORI) database.

1917 **Figure 3—Source data 4.** Adipose tissue-specific network of the functional
1918 interactions of *PRPF8*, *SF3B1*, and *SFPQ* according to HumanBase tool
1919 database, and binding sites of SFPQ according to SpliceAid-F.

1920 **Supplement files**

1921 **Supplemental file 1. Lineal regression analyses of subcutaneous (SC) and**

1922 **omental (OM) preadipocytes proliferation rate and anthropometric and**

1923 **biochemical parameters, n = 24-58.**

	SC Preadipocytes		OM Preadipocytes	
	r	***P value***	**r**	***P value***
Age (years)	-0.024	0.875	0.240	0.113
Weight (kg)	-0.373	0.023 *	-0.461	0.004 **
Height (m)	-0.147	0.386	-0.152	0.369
BMI (kg/m^2)	-0.518	0.001 ***	-0.593	<0.0001 ***
Fat mass (%)	-0.585	0.024 *	-0.714	0.004 **
Lean mass (%)	-0.093	0.741	0.696	0.005 **
Water mass (%)	-0.161	0.567	0.436	0.105
Waist circumference (cm)	-0.201	0.341	-0.204	0.352
Systolic pressure (mm/Hg)	-0.617	0.001 **	-0.127	0.553
Diastolic pressure (mm/Hg)	-0.468	0.021 *	-0.053	0.805
Fasting glucose (mg/dL)	-0.324	0.028 *	-0.406	0.005 **
Fasting insulin (mU/L)	-0.418	0.019 *	-0.427	0.017 *
HbA1c (%)	-0.417	0.007 **	-0.442	0.004 **
HOMA-IR (units)	-0.546	0.002 **	-0.512	0.003 **
Total cholesterol (mg/dL)	0.112	0.474	0.075	0.632
LDL cholesterol (mg/dL)	0.160	0.365	0.074	0.679
HDL cholesterol (mg/dL)	0.030	0.865	0.116	0.514
Triglycerides (mg/dL)	-0.170	0.281	-0.337	0.029 *
Free fatty acids (mmol/L)	0.239	0.262	0.431	0.036 *
C-reactive protein (mg/L)	-0.225	0.259	-0.530	0.004 **
Uric acid (mg/dL)	0.047	0.782	0.107	0.527

1924

1925 r=Spearman's correlation coefficient. *P<0.05, **P<0.01, ***P<0.001. Normality

1926 distribution was determined by Shapiro-Wilk normality test.

1927 **Supplemental file 2. Anthropometric and biochemical characteristics of**

1928 **study subjects from cohort 2.**

	Lean	NG Obese	T2D Obese
N	18	15	10
Gender (female/male)	10 / 8	9 / 6	6 / 4
Antidiabetic therapy (n, %)	0 (0)	0 (0)	7 (70)
Age (years)	51 ± 13	54 ± 14	60 ± 8
Weight (kg)	65.6 ± 8.7	92.2 ± 10.7 [aaa]	90.0 ± 11.7 [aaa]
Height (m)	1.68 ± 0.07	1.66 ± 0.10	1.68 ± 0.12
Body mass index (kg/m^2)	23.3 ± 2.1	33.6 ± 2.7 [aaa]	32.1 ± 2.9 [aaa]
Systolic pressure (mm/Hg)	125.1 ± 17.3	138.7 ± 17.5	142.2 ± 15.0
Diastolic pressure (mm/Hg)	74.2 ± 8.3	76.2 ± 9.8	81.6 ± 12.3
Fasting glucose (mg/dL)	88.0 ± 13.2	97.3 ± 15.3	121.6 ± 41.4 [aa, b]
Fasting glucose (mmol/L)	5.51 ± 0.96	5.84 ± 0.80	8.24 ± 5.61 [aa, b]
Fasting insulin (mU/L)	11.4 ± 2.2	12.7 ± 6.7	18.4 ± 1.3
HOMA-IR (units)	2.82 ± 0.94	3.28 ± 1.81	6.91 ± 5.08
Total cholesterol (mg/dL)	184.7 ± 33.6	192.8 ± 51.8	172.2 ± 24.6
LDL cholesterol (mg/dL)	104.1 ± 37.1	124.8 ± 43.9	98.7 ± 10.5
HDL cholesterol (mg/dL)	54.0 ± 11.0	49.7 ± 16.1	43.0 ± 14.0
Triglycerides (mg/dL)	106.7 ± 62.1	142.3 ± 60.1	226.6 ± 162.5 [aa]
Urid acid (mg/dL)	4.65 ± 0.68	5.13± 0.97	6.48 ± 0.96 [aa, b]

1929

1930 **NG**, normoglycemic; **T2D**, type 2 diabetes; **LDL**, low-density lipoprotein; **HDL**,

1931 high-density lipoprotein; **HOMA-IR**, homeostasis model assessment of insulin

1932 resistance. [aa]P<0.01, [aaa]P<0.001 *vs.* Lean; [b]P<0.05 *vs.* NG Obese. One-way

1933 ANOVA with Tukey's multiple comparisons test or Kruskal-Wallis with Dunn's

1934 multiple comparisons test (for parametric or non-parametric data, respectively)

1935 were used. Normality distribution was determined by Shapiro-Wilk normality test.

1936 **Supplemental file 3. Sequences and transcript sizes of primers used for**

1937 **RT-PCR studies.**

	Primer sequences (5' → 3')		
Gene (NCBI reference)	**Forward**	**Reverse**	**Size (bp)**
Hsa ACTB (NM_001101.3)	ACTCTTCCAGCCTTCCTTCTT	CAGTGATCTCCTTCTGCATCC	176
Hsa ADIPOQ (NM_009605.4)	TGGAGAAGCCGCTTATGTGT	GTCCCGGAATGTTGCAGTAG	159
Hsa BiP (X87949.1)	CTATGAAGCCCGTCCAGAAA	GTCGAGCCACCAACAAGAAC	85
Hsa BSCL2-1 (NM_001122955.3)	TCAGATCCTGGAGCATACCAA	CAGGCAGTGAACTAGCGACA	94
Hsa BSCL2-2/3 (KU178595.1)	GCCTCCTGCTATTTGGCTTT	TCTTCAGGGCTCTCACCATC	309
Hsa CCL2 (NM_002982.4)	CTGGACAAGCAAACCCAAAC	GGGGAAAGCTAGGGGAAAA	90
Hsa CIDEB-1 (NM_001318807.2)	GCCTACAGCCTGCCTCTTTT	TTGTGTTTGAGGTGGGGTCT	72
Hsa CIDEB-2 (NM_014430.3)	GGGCCTACAGGACACAGAAA	TGGACGTGACAGAGATGTGAA	237
Hsa CIDEC-5 (NM_001321142.2)	GAGGCTGTGAGGGGGAGAA	CTTGTCAGCTGGACTGCGTT	154
Hsa CIDE$_{total}$ (NM_001321142.2)	ATGGGAGAGAGGAGGCTTTG	CACTGACACATGCCTGGAGA	147
Hsa DERL1 (NM_001134671.2)	AAGACAAGCAGCGGATGAAG	AGGAAACAAACACCCAGCAA	175
Hsa FABP4 (NM_001442.3)	TGCAGCTTCCTTCTCACCTT	GGCAAAGCCCACTCCTACTT	134
Hsa FABP5 (DN991192)	GAAGGAGCTAGGAGTGGGAATAG	TCTCTCCCAGGGTACAAGAAAA	146
Hsa GAPDH (NM_002046.5)	AATCCCATCACCATCTTCCA	AAATGAGCCCCAGCCTTC	122
Hsa HPRT (S79316.1)	TAATCCAGCAGGTCAGCAAAG	CTGAGGATTTGGAAAGGGTGT	157
Has HRD1 (AB085847.1)	TGATGGGCAAGGTGTTCTTT	GCCAGTGGAAACATTTGAGG	177
Hsa KI67 (NM_002417)	GACATCCGTATCCAGCTTCCT	GCCGTACAGGCTCATCAATAAC	233
***Hsa γORF4* (Aprile et al., 2014)**	AAACCCAAAACAACTTCCCG	CTTGCAGTGGGGATGTCTCA	279
Hsa PDGFRA (NM_006206.6)	CCTTTTTGTGACGGTCTTGG	AAAGGCTACATCTGGGTCTGG	148
***Hsa PPARG-1* (Aprile et al., 2014)**	CGAGGACACCGGAGAGGG	TGTGGTTTAGTGTTGGCTTCTT	69
Hsa PPARG-2 (NM_015869.4)	AGGAGTGGGAGTGGTCTTCC	TTTTAACGGATTGATCTTTTGC	255
Hsa PPARG-3 (NM_138711.3)	TGGGTGTGTAGTCGTGGTACTTT	CTCGGTTACTCCCCGTTTCT	82
Hsa PPARG-4 (NM_005037.6)	GCCGTGGCCGCAGAAA	CCACGGAGCTGATCCCAAAG	76
***Hsa PPARG$_{total}$* (Aprile et al., 2014)**	ATGGCCACCTCTTTGCTCT	GAGAAGGAGAAGCTGTTGGC	272
Hsa RAD23A (D21235.1)	TGGCCCAAATCTTTCCATC	TGAGCTGATGTTAGCCCTTCTC	100
Hsa RNF185 (NM_152267.3)	CAACAGGACCCCAGAGAGAA	CCACCATCTCCAAATCCAAA	101
Hsa SEC61A1 (NM_013336.3)	GAGTGGACCTGCCAATCAAG	AGCTGAGAGCATTTGGGAGA	146
Hsa SEL1L (AF052059.1)	CCTGCCACTTCCCTTTTCTT	CCATTTCTGCTTCCTGCATC	180
Hsa SREBF1-1 (NM_001005291.3)	GACCGACATCGAAGGTGAAG	GGTCAAATAGGCCAGGGAAG	158
Hsa SREBF1$_{total}$ (NM_001005291.3)	AGCTCAAGGATCTGGTGGTG	TGTGTTGCAGAAAGCGAATG	93
Hsa STT3A (NM_001278503.1)	AGCTATGGCAAACCGAACAA	CCTCCAAAAATGACCAGCAC	153
Hsa STT3B (NM_178862.2)	CCCTCCTCCTTTTTCTTCCTC	ACGACTTGTGCTTGCTCTCC	153
Hsa TGFB2 (NM_000660.6)	GCAACAATTCCTGGCGATAC	CTAAGGCGAAAGCCCTCAA	136
Hsa UBQLN1 (NM_013438.4)	CAACACACCAGGAATGCAGA	CTTCTCATGTAGGGGGCAGA	90
Hsa UPK3B (NM_030570.3)	TGCACTCAGGAGGGTTTAGG	ATGGTGGAGCAGGAGAGACA	135
Hsa XBP1s (NM_001079539.1)	TGGATGCCCTGGTTGCT	CACCTGCTGCGGACTCA	87
Hsa XBP1u (NM_005080.3)	CGCAGCACTCAGACTACGTG	CTGGGTCCAAGTTGTCCAGA	147
Mmu PRPF8 (NM_138659.2)	TACATGACGGCCAAGAACAA	TGCAATCCCAGTACAAGCAA	146

1938

1939 **bp,** base pairs**.**

1940 **Appendix 1—key resource table**

Reagent type (species) or resource	Designation	Source or reference	Identifiers	Additional information
Cell line (*Homo sapiens*)	Human preadipocytes from SC and OM adipose tissue	This paper	N/A	Primary cell line
Cell line (*Homo sapiens*)	Human adipose-derived stromal cells (hADSCs)	This paper and previous work from Dr. Mikael Rydén group	(***Gao et al., 2017***, ***2014***)	SC adipose tissue from a male donor (16 years old, BMI 24 kg/m^2)
Cell line (*Homo sapiens*)	Simpson-Golabi-Behmel syndrome (SGBS) cell line	Gift from Prof. Dr. José Manuel Fernández-Real (Institut d'Investigació Biomèdica; Girona, Spain)	N/A	
Biological sample (*Homo sapiens*)	Human SC and OM adipose tissue from NG, IR and T2D morbid obese individuals (cohort 1)	General and Digestive Surgery Unit and the Lipids and Atherosclerosis Unit of the Reina Sofía University Hospital (Córdoba, Spain)	Reina Sofía University Hospital Research Ethical Committee (439/2010)	
Biological sample (*Homo sapiens*)	Human SC and OM adipose tissue from lean, NG and, T2D obese individuals (cohort 2)	Endocrinology ad Surgery Departments at the University Hospital Joan XXIII (Tarragona, Spain)	(Ejarque et al., 2017; Serena et al., 2016)	
Antibody	ADRP (B-6) (mouse monoclonal)	Santa Cruz Biotechnology	sc-377429, N/A	(1:1000)
Antibody	AKT (rabbit polyclonal)	Cell Signaling Technology	9272, AB_329827	(1:1000)
Antibody	ATF6α (H-280) (rabbit polyclonal)	Santa Cruz Biotechnology	sc-22799, AB_2242950	(1:1000)
Antibody	CASPASE-3 (8G10) (rabbit monoclonal)	Cell Signaling Technology	9665, AB_2069872	(1:1000)
Antibody	CD14 (M-305) (rabbit polyclonal)	Santa Cruz Biotechnology	sc-9150, AB_2074171	(1:1000)
Antibody	CD45 (H-230) (rabbit polyclonal)	Santa Cruz Biotechnology	sc-25590, AB_2174143	(1:1000)
Antibody	CHOP (L63F7) (mouse monoclonal)	Cell Signaling Technology	2895, AB_2089254	(1:1000)
Antibody	DGAT2 (goat polyclonal)	Novus	NB100-57851, AB_921135	(1:1000)
Antibody	DLK/PREF1 (H-118) (rabbit polyclonal)	Santa Cruz Biotechnology	sc-25437, AB_2292943	(1:1000)
Antibody	eIF2α (3A7A8) (mouse monoclonal)	Santa Cruz Biotechnology	sc-517214, N/A	(1:1000)
Antibody	FAS (C-20) (goat polyclonal)	Santa Cruz Biotechnology	sc-16147, AB_2101097	(1:1000)
Antibody	BiP/GRP78 (A-10) (mouse monoclonal)	Santa Cruz Biotechnology	sc-376768, N/A	(1:1000)
Antibody	GRP94 (rabbit polyclonal)	Cell Signaling Technology	2104, AB_823506	(1:1000)
Antibody	HSL/LIPE (rabbit polyclonal)	Abcam	ab45422, AB_2135367	(1:1000)
Antibody	IRE1α (B-12) (mouse monoclonal)	Santa Cruz Biotechnology	sc-390960, N/A	(1:1000)
Antibody	PDI (C81H6) (rabbit monoclonal)	Cell Signaling Technology	3501, AB_2156433	(1:1000)

Antibody	PERK (B-5) (mouse monoclonal)	Santa Cruz Biotechnology	sc-377400, AB_2762850	(1:1000)
Antibody	Phospho-AKT (Ser473) (rabbit monoclonal)	Cell Signaling Technology	4060, AB_2315049	(1:750)
Antibody	Phospho-eIF2α (Ser51) (rabbit polyclonal)	Santa Cruz Biotechnology	sc-101670, AB_2096507	(1:750)
Antibody	Phospho-HSL/LIPE (Ser563) (rabbit polyclonal)	Cell Signaling Technology	4139, AB_2135495	(1:750)
Antibody	Phospho-IRE1α (Ser724) (rabbit polyclonal)	Abcam	ab48187, AB_873899	(1:750)
Antibody	Phospho-PERK (Thr981) (rabbit polyclonal)	Santa Cruz Biotechnology	sc-32577, AB_2293243	(1:750)
Antibody	PLIN1 (guinea pig polyclonal)	Progen	GP29, N/A	(1:1000)
Antibody	PPARγ (D69) (rabbit polyclonal)	Cell Signaling Technology	2430, AB_823599	(1:1000)
Antibody	PRP8 (E-5) (mouse monoclonal)	Santa Cruz Biotechnology	sc-55533, AB_831685	(1:1000)
Antibody	PSMB8/LMP7 (sheep polyclonal)	R&D Systems	AF7710, N/A	(1:1000)
Antibody	SFPQ (rabbit monoclonal)	Abcam	ab177149, N/A	(1:1000)
Antibody	UBIQUITIN (rabbit polyclonal)	Cell Signaling Technology	3933, AB_2180538	(1:1000)
Antibody	Goat/Sheep IgG (mouse monoclonal)	Sigma-Aldrich	A9452, AB_258449	(1:2500)
Antibody	Guinea Pig IgG (goat polyclonal)	Sigma-Aldrich	A7289, AB_258337	(1:2500)
Antibody	Mouse IgG (rabbit polyclonal)	Sigma-Aldrich	A9044, AB_258431	(1:2500)
Antibody	Rabbit IgG (goat polyclonal)	Sigma-Aldrich	A8275, AB_258382	(1:10000)
Recombinant DNA reagent	phrGFP-N1	Agilent Technologies	240036	
Recombinant DNA reagent	pcDNA3.1(+)	Invitrogen	V79020	
Recombinant DNA reagent	*PRPF8* (*NM_006445*) in pcDNA3.1(+)	GenScript	OHu19527C	
Recombinant DNA reagent	*SFPQ* (*NM_005066.3*) in pcDNA3.1(+)	GenScript	OHu23607C	
Recombinant DNA reagent	pCMV-Myc	Clontech	635689	
Recombinant DNA reagent	pCMV-BiP-Myc-KDEL-wt	AddGene	27164	
Sequence-based reagent	Primers for RT-PCR, see ***Supplemental file 3***	This paper	N/A	
Sequence-based reagent	Primers for splicing-machinery components array	(***Gahete et al., 2018***)	N/A	
Sequence-based reagent	*PRPF8* Silencer™ Select Validated siRNA	Ambion	4390824	
Sequence-based reagent	*SFPQ* Silencer™ Select Validated siRNA	Ambion	s224606	

Sequence-based reagent	Silencer™ Select Negative Control No. 1 siRNA	Ambion	4390843
Peptide, recombinant protein	3-Isobutyl-1-methylxanthine (IBMX)	Sigma-Aldrich	I5879
Peptide, recombinant protein	Antipain	Sigma-Aldrich	A6191
Peptide, recombinant protein	Biotin	Sigma-Aldrich	B4639
Peptide, recombinant protein	Bovine Serum Albumin (BSA)	Sigma-Aldrich	A8806, A7030
Peptide, recombinant protein	Chymostatin	Sigma-Aldrich	C7268
Peptide, recombinant protein	Collagenase Type V	Sigma-Aldrich	C9263
Peptide, recombinant protein	Dexamethasone	Sigma-Aldrich	D4902, D1756
Peptide, recombinant protein	Human 3,3',5-Trihydrochloride sodium salt (T3)	Sigma-Aldrich	T5516, T6397
Peptide, recombinant protein	Human FGF2	Sigma-Aldrich	F0291
Peptide, recombinant protein	Human Insulin	Sigma-Aldrich	I2643, I9278
Peptide, recombinant protein	Human Transferrin	Sigma-Aldrich	T8158
Peptide, recombinant protein	Human Tumor Necrosis Factor-α (TNFα)	Sigma-Aldrich	T6674
Peptide, recombinant protein	Hydrocortisone	Sigma-Aldrich	H0135
Peptide, recombinant protein	Leupeptin	Sigma-Aldrich	L2884
Peptide, recombinant protein	MG-132	Calbiochem	474790
Peptide, recombinant protein	N-Succinyl-Leu-Leu-Val-Tyr-7-Amido-4-Methylcoumarin (Suc-LLVY-AFC)	Sigma-Aldrich	S6510
Peptide, recombinant protein	Pepstatin A	Sigma-Aldrich	P4265
Peptide, recombinant protein	Rosiglitazone	Sigma-Aldrich	R2408
Chemical compound, drug	(+)-Sodium L-ascorbate	Sigma-Aldrich	A4034
Chemical compound, drug	1,4-dithiothreitol (DTT)	Thermo Scientific	R0862
Chemical compound, drug	Acetonitrile	Sigma-Aldrich	271004
Chemical compound, drug	Adenosine 5′-triphosphate (ATP) disodium salt hydrate	Sigma-Aldrich	A26209
Chemical compound, drug	BODIPY™ 500/510 C_1, C_{12} (4,4-Difluoro-5-Methyl-4-Bora-3a,4a-Diaza-s-Indacene-3-Dodecanoic Acid)	Invitrogen	D3823
Chemical compound, drug	Calcium chloride ($CaCl_2$)	Sigma-Aldrich	449709
Chemical compound, drug	CHAPS hydrate	Sigma-Aldrich	C3023

Chemical compound, drug	Chloroform	Sigma-Aldrich	C2432
Chemical compound, drug	Clarity Western ECL Substrate	Bio-Rad	1705061
Chemical compound, drug	D-(+)-Glucose	Panreac Applichem / Siga-Aldrich	1413411211, G8270
Chemical compound, drug	DAPI	Sigma-Aldrich	D9542
Chemical compound, drug	Dimethyl sulfoxide (DMSO)	Sigma-Aldrich	D4540
Chemical compound, drug	D-Pantothenic acid hemicalcium salt	Sigma-Aldrich	P5155
Chemical compound, drug	Dulbecco's Phosphate Buffered Saline (D-PBS) Solution	Sigma-Aldrich	D1408
Chemical compound, drug	Dulbecco's Phosphate Buffered Saline (D-PBS) Solution (-) Ca^{2+}, Mg^{2+}	HyClone	SH30028.02
Chemical compound, drug	Dulbecco's Modified Eagle Medium (DMEM)/F-12 (1:1)	Gibco	31330-038
Chemical compound, drug	EDTA disodium salt	Sigma-Aldrich	E5134
Chemical compound, drug	Exonuclease I Reaction Buffer	New England BioLabs	B0293S
Chemical compound, drug	Fluorescence Mounting Medium	Dako	S3023
Chemical compound, drug	Formic acid	Scharlau	AC10760050
Chemical compound, drug	Glycerol	VWR	97063-892
Chemical compound, drug	Ham's F-12 Nutrient Mix	Gibco	21765037
Chemical compound, drug	Hepes Buffer (1M)	Gibco	15630056
Chemical compound, drug	Hoechst 33342, Trihydrochloride, Trihydrate	Invitrogen	H3570
Chemical compound, drug	Immersol™ Immersion Oil	Carl Zeiss	518F
Chemical compound, drug	Iodoacetamide (IAA)	Sigma-Aldrich	I1149
Chemical compound, drug	Isopropanol	Sigma-Aldrich	33539
Chemical compound, drug	iTRAQ™ Reagents	Applied Biosystems	PN4351918
Chemical compound, drug	Lipofectamine 2000 Transfection Reagent	Invitrogen	11668019
Chemical compound, drug	Lipofectamine RNAiMAX Transfection Reagent	Invitrogen	13778150
Chemical compound, drug	Magnesium Chloride ($MgCl_2$)	Merck	5833
Chemical compound, drug	Magnesium Sulfate 7-hydrate ($MgSO_4$)	Panreac Applichem	141404
Chemical compound, drug	Methanol (MeOH)	VWR Chemicals	20864320
Chemical compound, drug	Newborn Calf Serum (NCS)	Gibco	16010159

Chemical compound, drug	Nonfat dried milk powder	Panreac Applichem	Cat# A0830
Chemical compound, drug	Oil Red O	Sigma-Aldrich	O0625
Chemical compound, drug	Oleic acid	Sigma-Aldrich	O1383
Chemical compound, drug	Opti-MEM™ I Reduced Serum Medium	Gibco	11058021
Chemical compound, drug	Paraformaldehyde (PFA)	Bosterbio	AR1068
Chemical compound, drug	Penicillin-Streptomycin (10,000 U/mL)	Sigma-Aldrich / Gibco	P4333, 15140122
Chemical compound, drug	Pladienolide-B	Santa Cruz Biotechnology	sc-391691
Chemical compound, drug	Potassium Chloride (KCl)	Merck	104936
Chemical compound, drug	Ponceau S	Sigma-Aldrich	P3504
Chemical compound, drug	RBC Lysis Buffer	Norgen Biotek Corp.	21201
Chemical compound, drug	RNase-Free DNase Set	Qiagen	79254
Chemical compound, drug	Sodium Chloride (NaCl)	Merk Millipore	7647145
Chemical compound, drug	Sodium Dodecyl Sulfate (SDS)	Sigma-Aldrich	L3771
Chemical compound, drug	Sodium Hydroxide (NaOH)	Sigma-Aldrich	S4085
Chemical compound, drug	Sodium Palmitate	Sigma-Aldrich	P9767
Chemical compound, drug	Sodium Phosphate Monobasic Monohydrate (NaH_2PO_4)	Fisher scientific	BP330-1
Chemical compound, drug	Sodium Phosphate Monobasic Monohydrate Dihydrate ($NaH_2PO_4x2H_2O$)	Sigma-Aldrich	71505
Chemical compound, drug	TE Buffer	Invitrogen	12090015
Chemical compound, drug	Tetraethylammonium Bromide (TEAB)	Sigma-Aldrich	241059
Chemical compound, drug	Thiazolyl Blue Tetrazolium Bromide (MTT)	Sigma-Aldrich	M5655
Chemical compound, drug	Trichloroacetic acid (TCA)	Sigma-Aldrich	T6399
Chemical compound, drug	Triton™ X-100	Sigma-Aldrich	T8787
Chemical compound, drug	Trizma® base (Tris base)	Sigma-Aldrich	T6066
Chemical compound, drug	Trizma® hydrochloride (Tris-HCl)	Sigma-Aldrich	T3253
Chemical compound, drug	TRIzol™ Reagent	Invitrogen	15596018
Chemical compound, drug	Trypan Blue solution	Sigma-Aldrich	T8154
Chemical compound, drug	Trypsin Gold, Mass Spectrometry Grade	Promega	V5280
Chemical compound, drug	Trypsin-EDTA solution	Sigma-Aldrich	T3924

Chemical compound, drug	Tween® 20	Panreac Applichem	A1389
Chemical compound, drug	Urea	Sigma-Aldrich	U1205
Commercial assay or kit	96.96 DNA Binding Dye Sample / Loading Kit	Fluidigm	BMK-M10-96.96-EG
Commercial assay or kit	AllPrep DNA/RNA/Protein Mini Kit	Qiagen	80004
Commercial assay or kit	Cytotoxicity Detection Kit Plus	Roche	4744926001
Commercial assay or kit	GoTaq® qPCR Master Mix	Promega	A6001
Commercial assay or kit	Mycoplasma gel detection kit	Biotools	4542
Commercial assay or kit	NEON™ Transfection System Kit	Invitrogen	MPK10096
Commercial assay or kit	Protein Assay Dye Reagent Concentrate	Bio-Rad	5000006
Commercial assay or kit	RC DC™ Protein Assay	Bio-Rad	5000122
Commercial assay or kit	RevertAid First Strand cDNA Synthesis Kit	Thermo Scientific	K1621
Commercial assay or kit	SsoFast™ EvaGreen® Supermix	Bio-Rad	1725200
Software, algorithm	Biomark & EP1 Software 4.5.2	Fluidigm	https://www.fluidigm.com/software
Software, algorithm	Basic Local Alignment Search Tool (BLAST)	NCBI (Nowicki et al., 2018)	https://blast.ncbi.nlm.nih.gov/Blast.cgi
Software, algorithm	ENCORI: The Encyclopedia of RNA Interactomes	(***Li et al., 2013***)	http://starbase.sysu.edu.cn/index.php
Software, algorithm	GeNorm 3.3	(***Vandesompele et al., 2002***)	https://genorm.cmgg.be/
Software, algorithm	GraphPad PRISM 7	GraphPad Software, Inc. (Mitteer et al., 2018)	https://www.graphpad.com
Software, algorithm	High-Content Screening (HCS) Studio Cell Analysis Software 2.0	Thermo Fisher Scientific	https://www.thermofisher.com/es/es/home/life-science/cell-analysis/cellular-imaging/high-content-screening/hcs-studio-2.html
Software, algorithm	Human Base tool	(***Greene et al., 2015***)	https://hb.flatironinstitute.org/
Software, algorithm	Huygens Professional 2.4.4	Scientific Volume Imaging	https://svi.nl/Huygens-Professional
Software, algorithm	ImageJ 1.50b	National Institute of Health (NIH) (***Schneider et al., 2012***)	https://imagej.nih.gov/ij/

Software, algorithm	Ingenuity Pathways Analysis (IPA) 49309495	Qiagen, provided by the Andalusian Bioinformatics Platform (PAB) center (University of Málaga, Spain; www.scbi.uma.es) (***Krämer et al., 2014***)	www.ingenuity.com
Software, algorithm	LightCycler® 96 1.1.0.1320	Roche Life Science	https://lifescience.roche.com/en_es/products/lightcycler-381711.html
Software, algorithm	Magellan™ software 7.2 SP1	Tecan	https://lifesciences.tecan.com/software-magellan
Software, algorithm	MetaboAnalyst 4.0	(***Chong et al., 2018***)	https://www.metaboanalyst.ca/docs/About.xhtml
Software, algorithm	Primer3 Input 4.1.0	(***Untergasser et al., 2012***)	http://bioinfo.ut.ee/primer3/
Software, algorithm	Protein ANalysis THrough Evolutionary Relationships (PANTHER) classification system 14.1	(***Mi et al., 2019a***, ***2019b***)	http://www.pantherdb.org/
Software, algorithm	Real-Time PCR Analysis Software 3.0	Fluidigm	https://www.fluidigm.com/
Software, algorithm	SoftMax Pro 2.2.1	Molecular Devices	https://www.moleculardevices.com/
Software, algorithm	SpliceAid-F	(***Giulietti et al., 2013***)	http://srv00.recas.ba.infn.it/SpliceAidF/
Software, algorithm	Statistic R module	Pearl software	https://www.pearlsoftware.com/
Software, algorithm	StepOne™ Real-Time PCR System 2.3	Thermo Scientific	https://www.thermofisher.com/es/es/home.html
Software, algorithm	Stratagene Mx3000p	Thermo Scientific	https://www.thermofisher.com/es/es/home.html
Software, algorithm	Venn Diagram Plotter	Pacific Northwest National Laboratory	https://omics.pnl.gov/software/venn-diagram-plotter

1941

Figure 1

A

T2D Obese *vs.* NG Obese

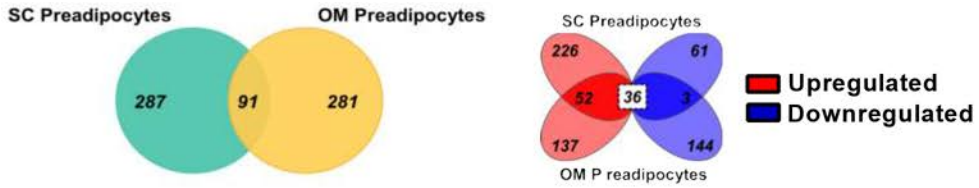

B

T2D Obese *vs.* NG Obese dysregulated pathways in SC Preadipocytes

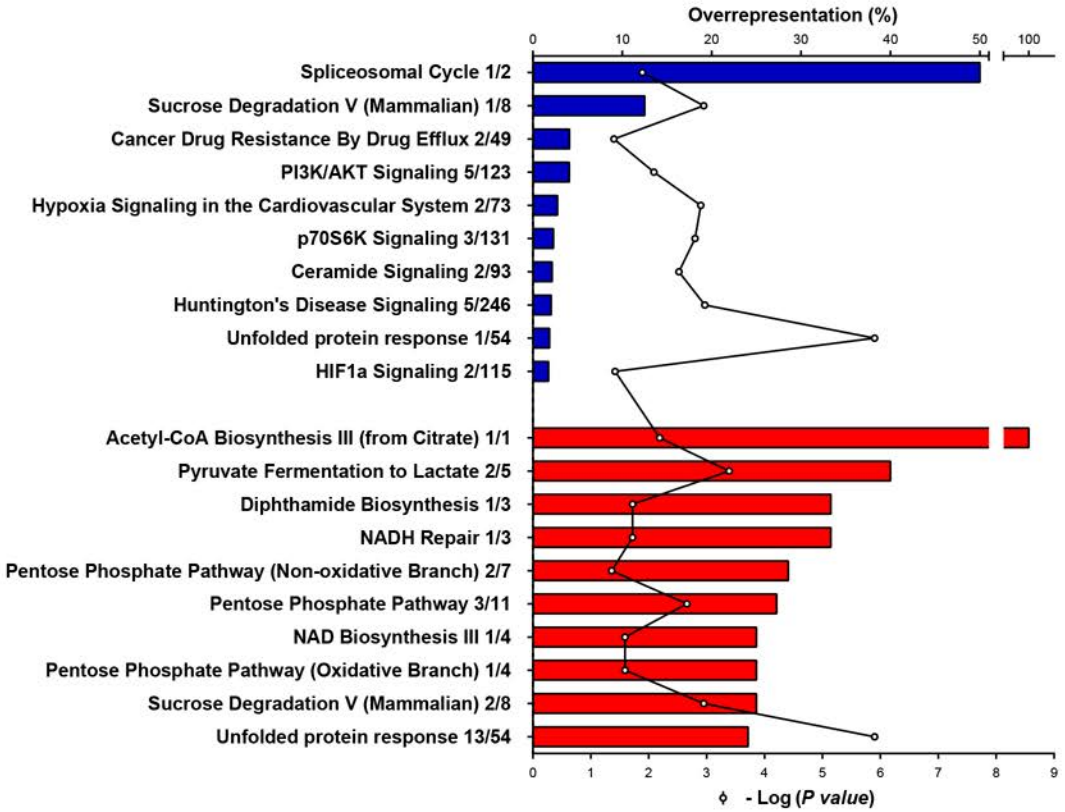

C

T2D Obese *vs.* NG Obese dysregulated pathways in OM Preadipocytes

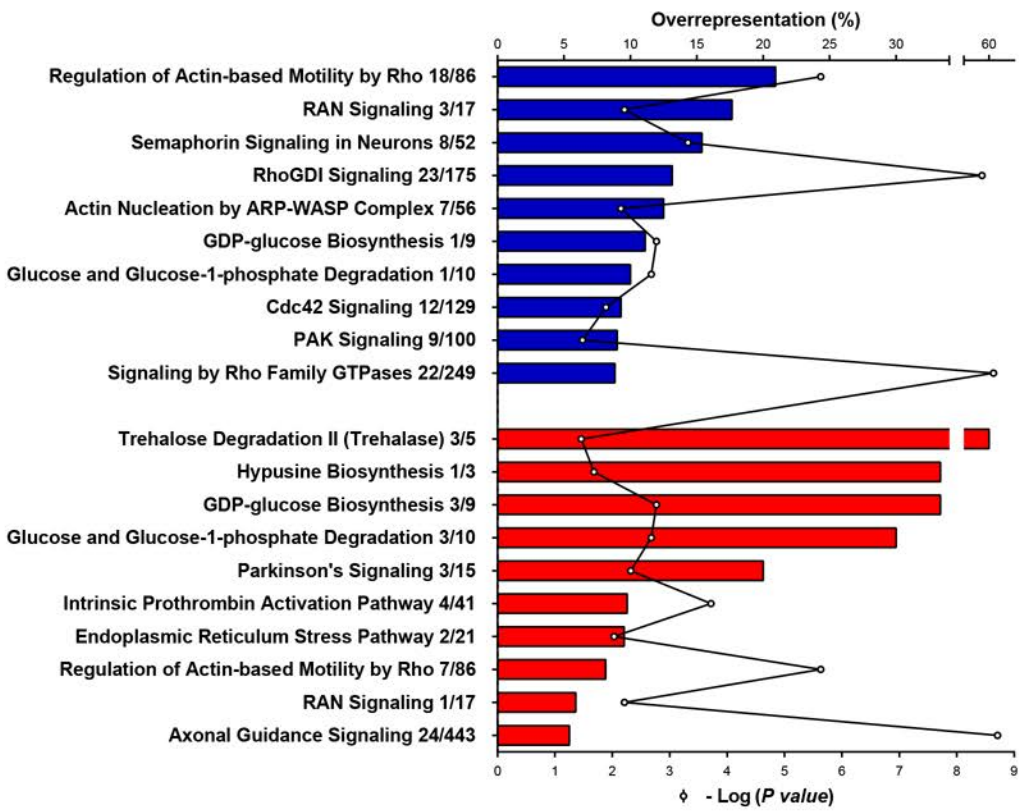

Figure 2

A

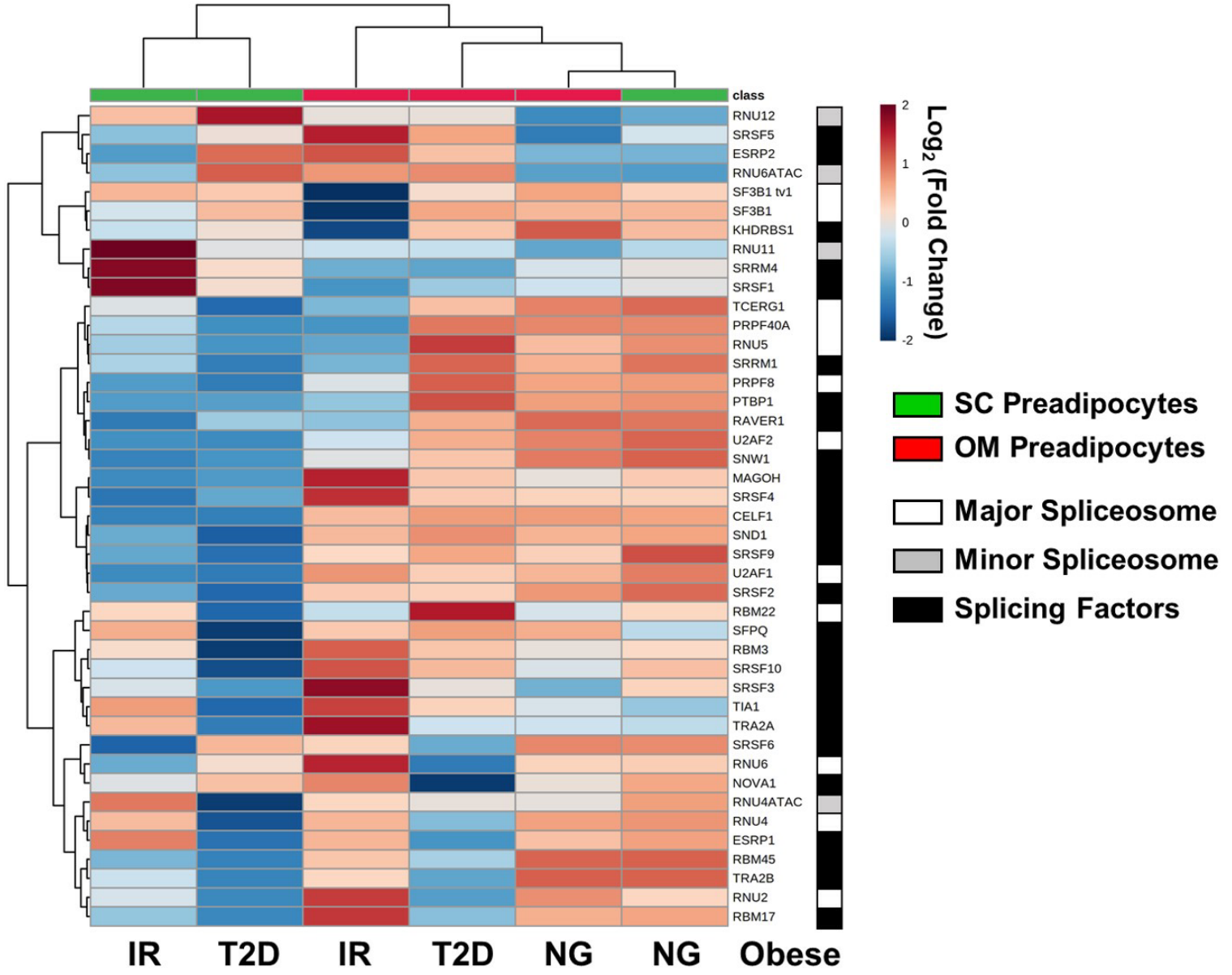

B

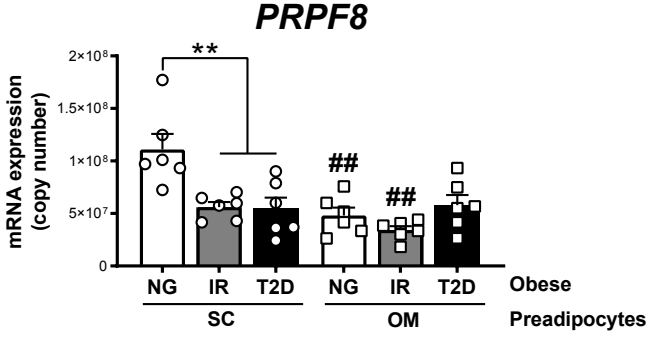

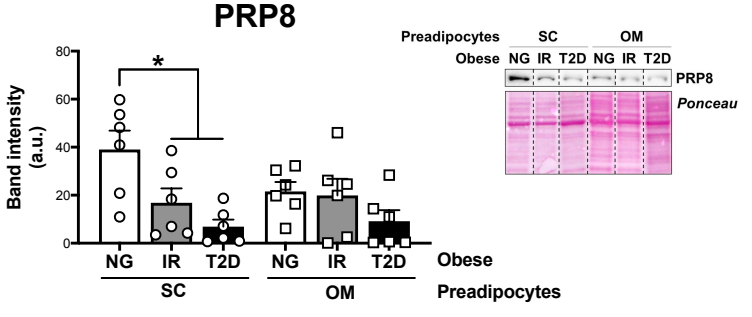

C

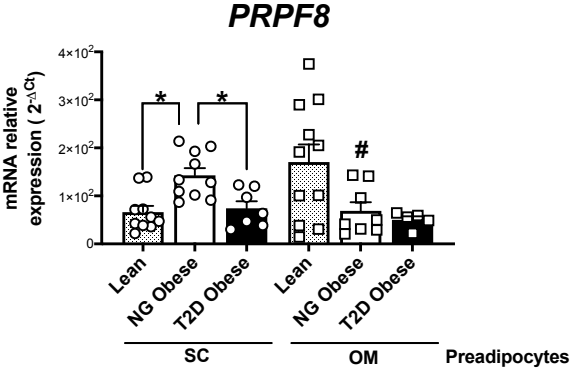

D

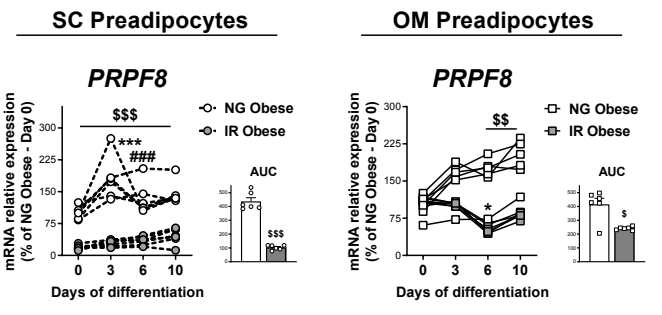

Figure 3

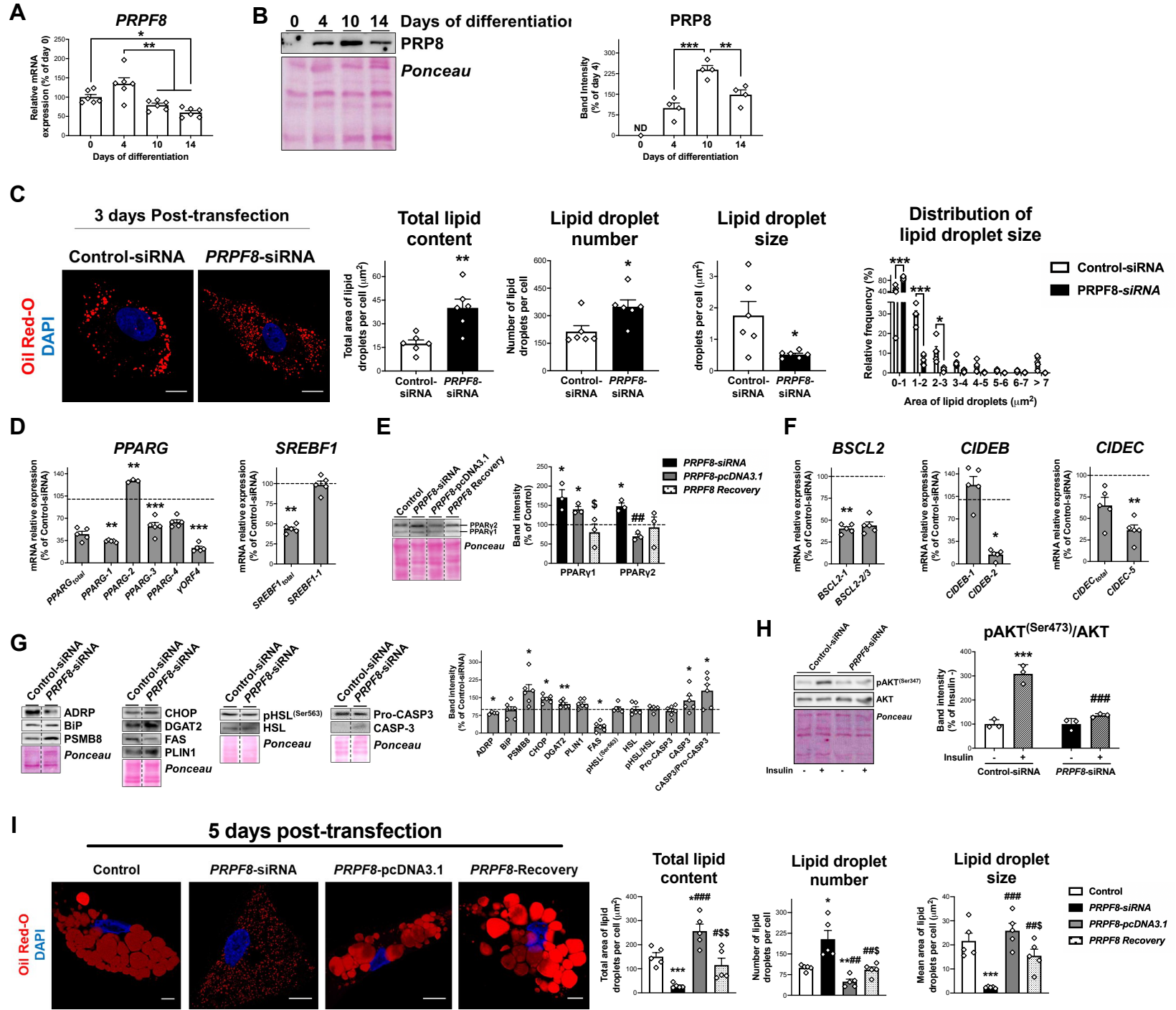
A
PRPF8
Relative mRNA expression (% of day 0)
Days of differentiation
B
0 4 10 14 Days of differentiation
PRP8
Ponceau
PRP8
Band Intensity (% of day 4)
ND
Days of differentiation
C
3 days Post-transfection
Control-siRNA
PRPF8-siRNA
Oil Red-O
DAPI
Total lipid content
Total area of lipid droplets per cell (µm²)
Lipid droplet number
Number of lipid droplets per cell
Lipid droplet size
droplets per cell (µm²)
Distribution of lipid droplet size
Relative frequency (%)
Area of lipid droplets (µm²)
Control-siRNA
PRPF8-siRNA
D
PPARG
SREBF1
mRNA relative expression (% of Control-siRNA)
PPARG-1
PPARG-2
PPARG-3
PPARG-4
YORF4
SREBF1-1
E
Control
PRPF8-siRNA
PRPF8-pcDNA3.1
PRPF8 Recovery
PPARγ2
PPARγ1
Ponceau
Band intensity (% of Control)
PPARγ1
PPARγ2
F
BSCL2
CIDEB
CIDEC
BSCL2-1
BSCL2-2/3
CIDEB-1
CIDEB-2
CIDEC-5
G
ADRP
BiP
PSMB8
CHOP
DGAT2
FAS
PLIN1
pHSL(Ser563)
HSL
Pro-CASP3
CASP-3
Ponceau
Band intensity (% of Control-siRNA)
H
pAKT(Ser473)
AKT
Insulin
pAKT(Ser473)/AKT
Band intensity (% of Insulin -)
Control-siRNA
PRPF8-siRNA
I
5 days post-transfection
Control
PRPF8-siRNA
PRPF8-pcDNA3.1
PRPF8-Recovery
Total lipid content
Lipid droplet number
Lipid droplet size
Mean area of lipid droplets per cell (µm²)

Figure 4

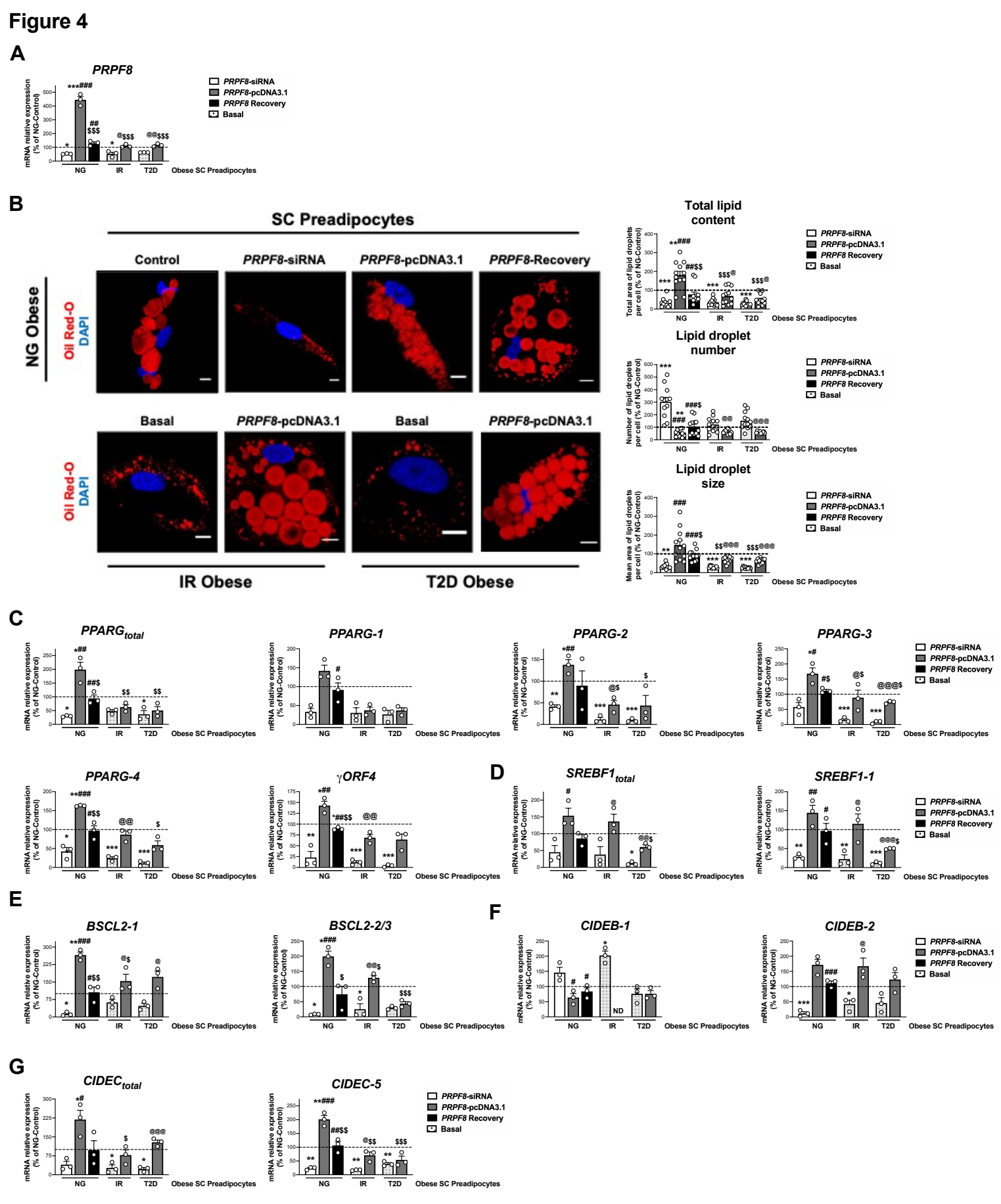
A
PRPF8
mRNA relative expression (% of NG-Control)
PRPF8-siRNA
PRPF8-pcDNA3.1
PRPF8 Recovery
Basal
NG
IR
T2D
Obese SC Preadipocytes
B
SC Preadipocytes
Control
PRPF8-siRNA
PRPF8-pcDNA3.1
PRPF8-Recovery
NG Obese
Oil Red-O
DAPI
Basal
PRPF8-pcDNA3.1
Basal
PRPF8-pcDNA3.1
IR Obese
T2D Obese
Total lipid content
Total area of lipid droplets per cell (% of NG-Control)
Lipid droplet number
Number of lipid droplets per cell (% of NG-Control)
Lipid droplet size
Mean area of lipid droplets per cell (% of NG-Control)
C
PPARG total
PPARG-1
PPARG-2
PPARG-3
PPARG-4
γORF4
D
SREBF1 total
SREBF1-1
E
BSCL2-1
BSCL2-2/3
F
CIDEB-1
CIDEB-2
ND
G
CIDEC total
CIDEC-5

Figure 5

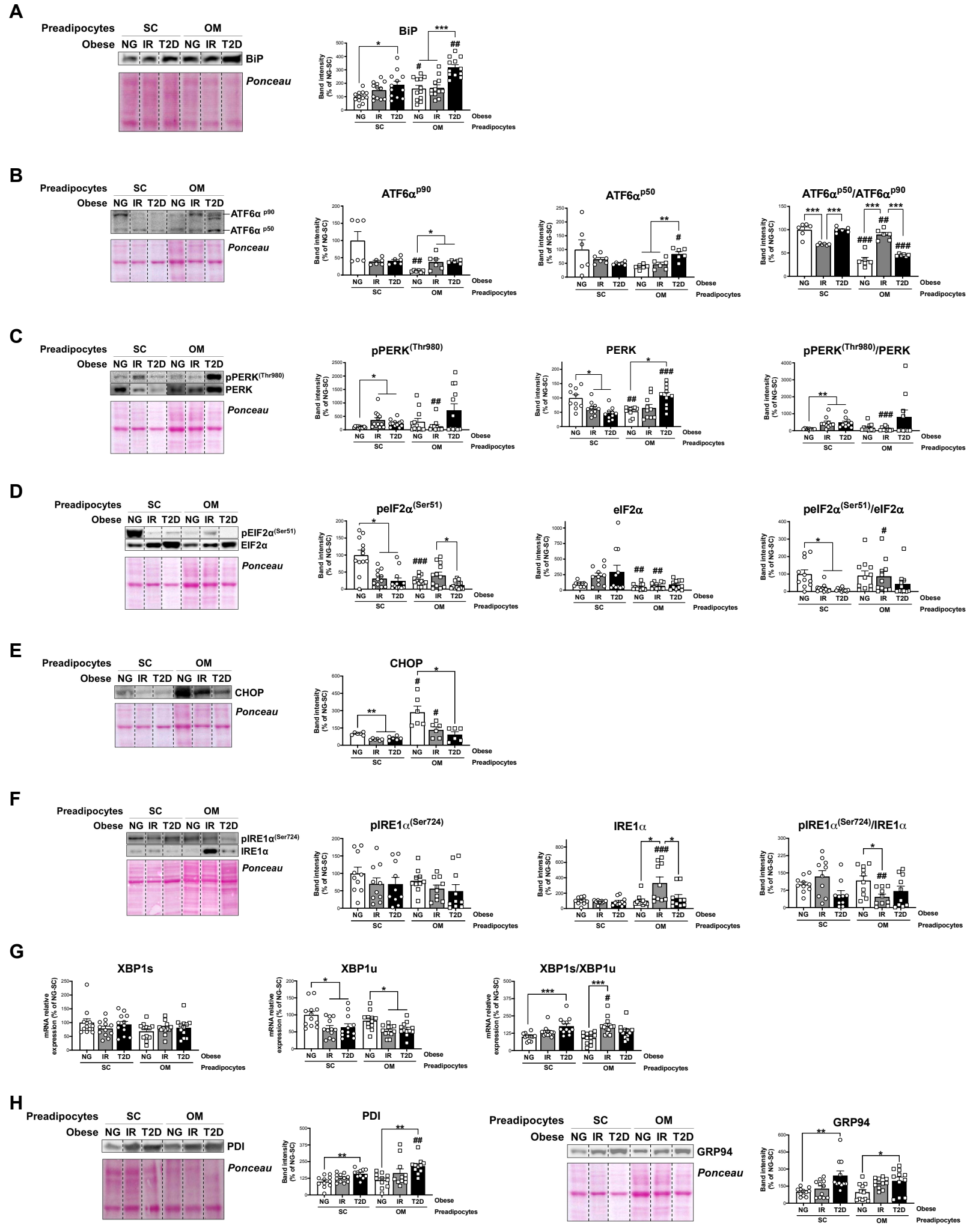
A
Preadipocytes SC OM
Obese NG IR T2D NG IR T2D
BiP
Ponceau
BiP
Band intensity (% of NG-SC)
B
ATF6α p90
ATF6α p50
ATF6α^p90
ATF6α^p50
ATF6α^p50/ATF6α^p90
C
pPERK(Thr980)
PERK
pPERK(Thr980)/PERK
D
pEIF2α(Ser51)
EIF2α
peIF2α(Ser51)
eIF2α
peIF2α(Ser51)/eIF2α
E
CHOP
F
pIRE1α(Ser724)
IRE1α
pIRE1α(Ser724)/IRE1α
G
XBP1s
XBP1u
XBP1s/XBP1u
mRNA relative expression (% of NG-SC)
H
PDI
GRP94
Obese
Preadipocytes

Figure 6

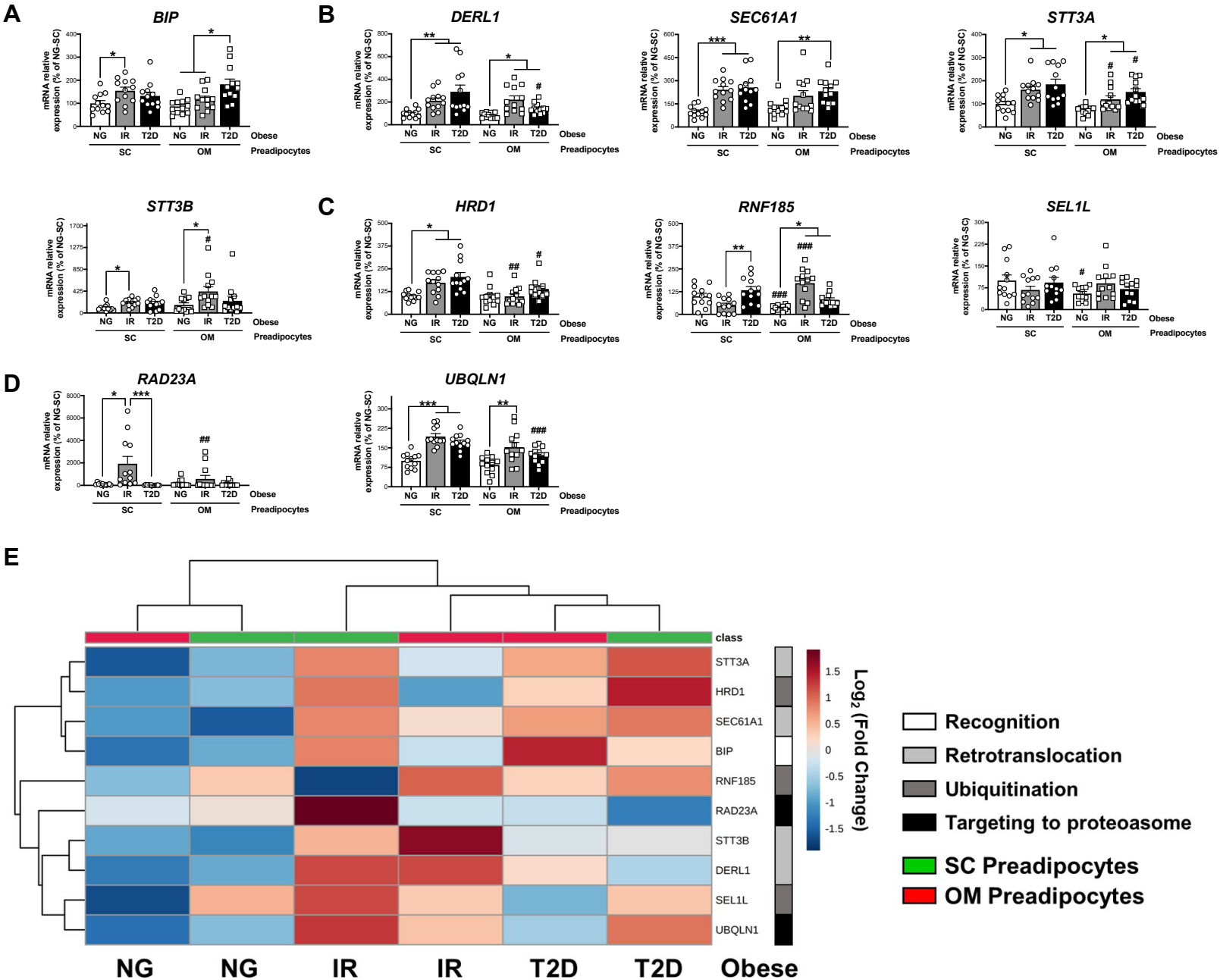
A
BIP
B
DERL1
SEC61A1
STT3A
STT3B
C
HRD1
RNF185
SEL1L
D
RAD23A
UBQLN1
mRNA relative expression (% of NG-SC)
NG
IR
T2D
Obese
SC
OM
Preadipocytes
E
class
STT3A
HRD1
SEC61A1
BIP
RNF185
RAD23A
STT3B
DERL1
SEL1L
UBQLN1
Log2 (Fold Change)
Recognition
Retrotranslocation
Ubiquitination
Targeting to proteoasome
SC Preadipocytes
OM Preadipocytes
NG
NG
IR
IR
T2D
T2D
Obese

Figure 7

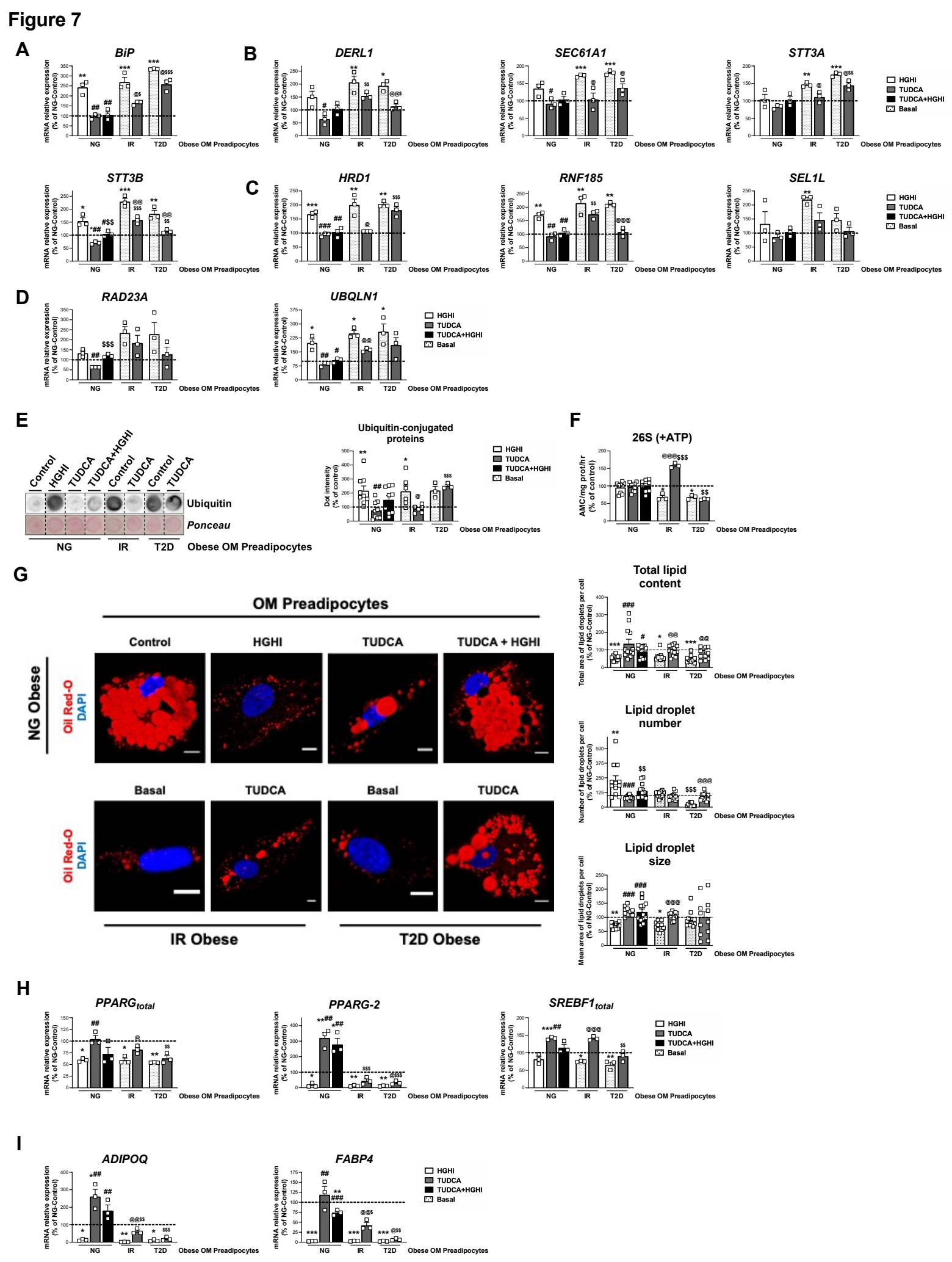
A
BiP
B
DERL1
SEC61A1
STT3A
STT3B
C
HRD1
RNF185
SEL1L
D
RAD23A
UBQLN1
mRNA relative expression (% of NG-Control)
NG
IR
T2D
Obese OM Preadipocytes
HGHI
TUDCA
TUDCA+HGHI
Basal
E
Control
HGHI
TUDCA
TUDCA+HGHI
Control
TUDCA
Control
TUDCA
Ubiquitin
Ponceau
Ubiquitin-conjugated proteins
Dot intensity (% of control)
F
26S (+ATP)
AMC/mg prot/hr (% of control)
G
OM Preadipocytes
Control
HGHI
TUDCA
TUDCA + HGHI
NG Obese
Oil Red-O
DAPI
Basal
TUDCA
Basal
TUDCA
IR Obese
T2D Obese
Total lipid content
Total area of lipid droplets per cell (% of NG-Control)
Lipid droplet number
Number of lipid droplets per cell (% of NG-Control)
Lipid droplet size
Mean area of lipid droplets per cell (% of NG-Control)
H
PPARGtotal
PPARG-2
SREBF1total
I
ADIPOQ
FABP4

Figure 8

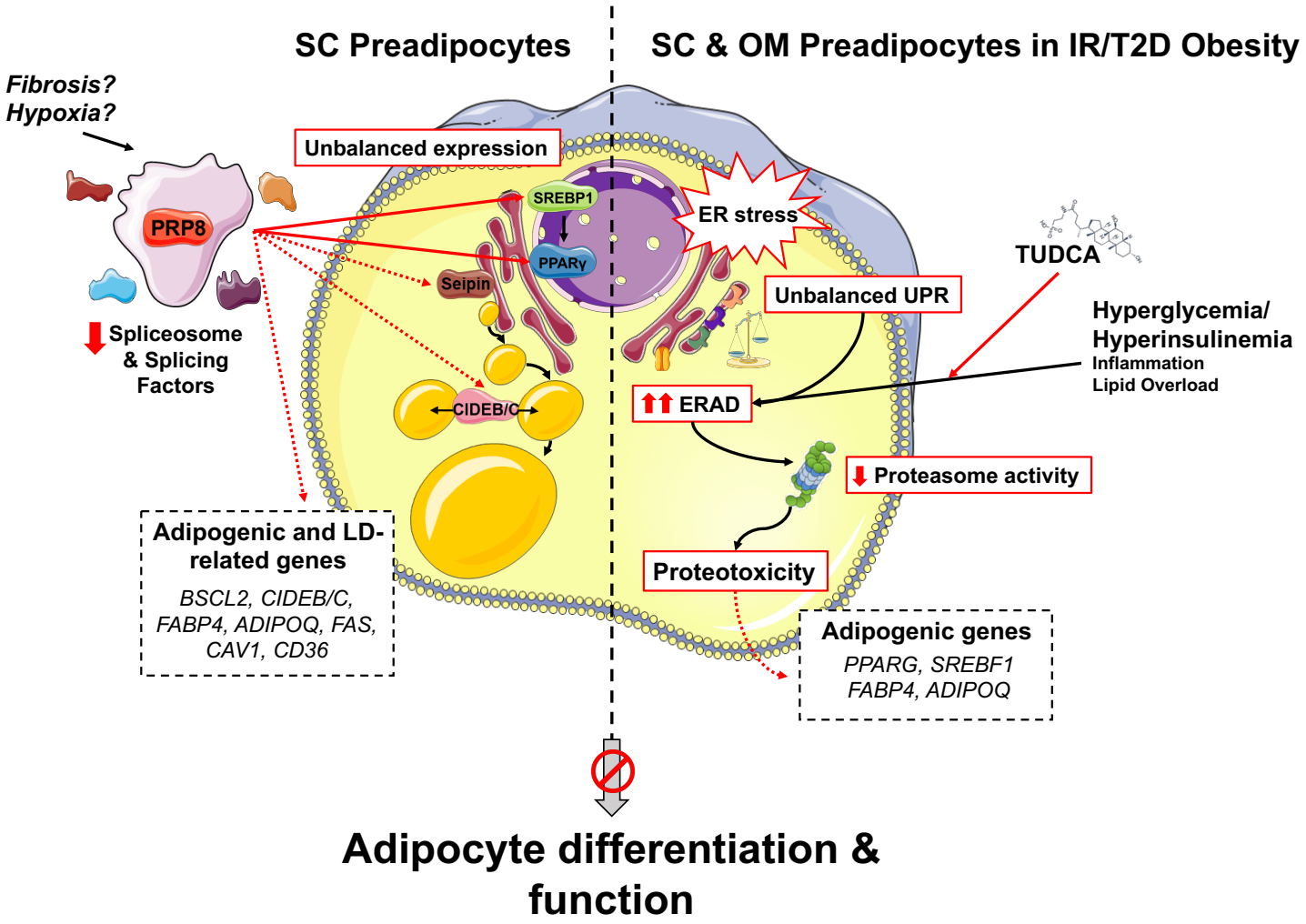
SC Preadipocytes
SC & OM Preadipocytes in IR/T2D Obesity
Fibrosis?
Hypoxia?
PRP8
Spliceosome & Splicing Factors
Unbalanced expression
SREBP1
PPARγ
Seipin
CIDEB/C
ER stress
Unbalanced UPR
ERAD
Proteasome activity
Proteotoxicity
TUDCA
Hyperglycemia/ Hyperinsulinemia
Inflammation
Lipid Overload
Adipogenic and LD-related genes
BSCL2, CIDEB/C, FABP4, ADIPOQ, FAS, CAV1, CD36
Adipogenic genes
PPARG, SREBF1
FABP4, ADIPOQ
Adipocyte differentiation & function

Table 1—Figure supplement 1

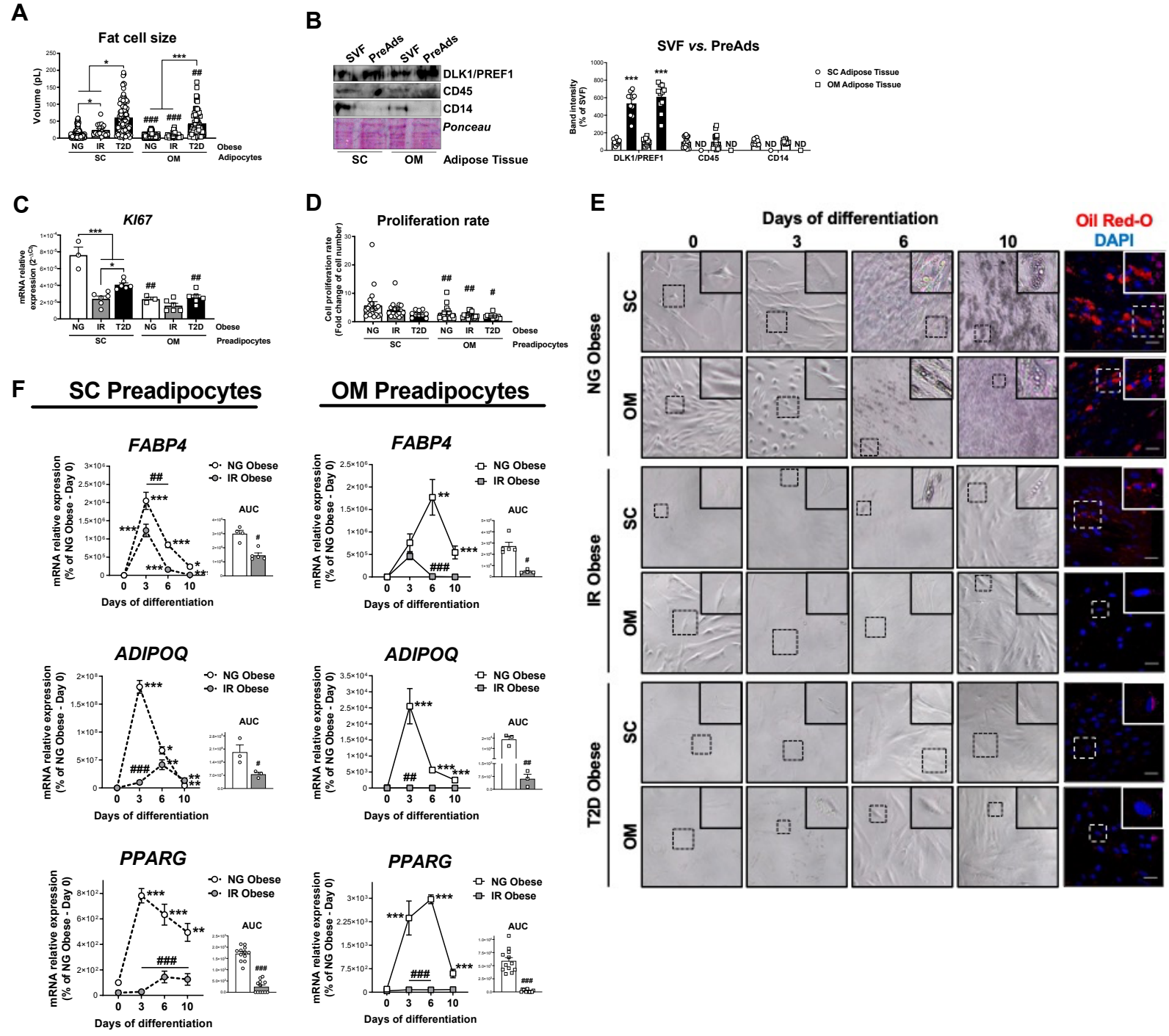

Figure 1—Figure supplement 2

A

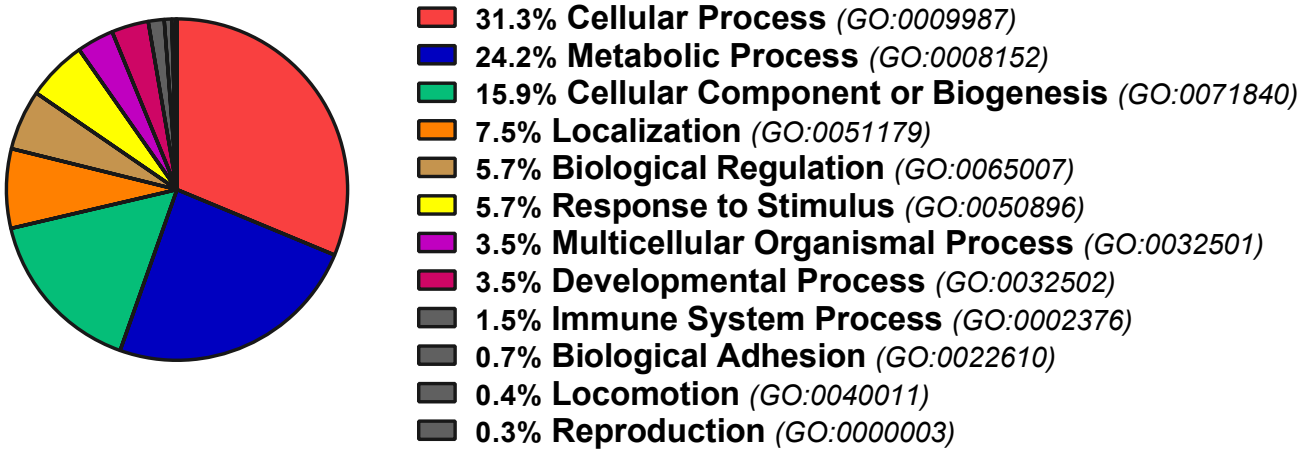

B

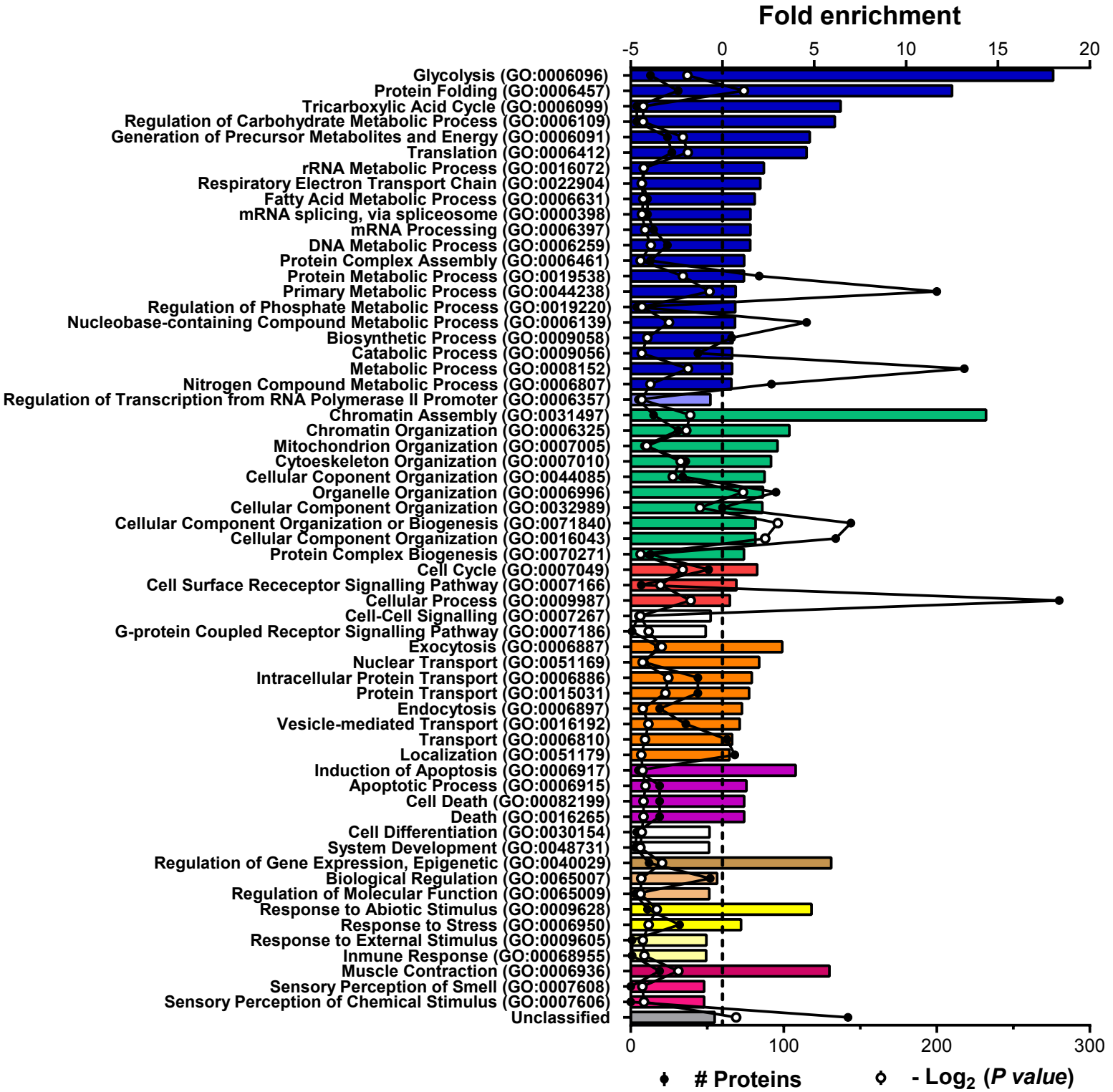

Figure 1—Figure supplement 3

A

SC Preadipocytes *vs.* OM Preadipocytes

B

SC Preadipocytes *vs.* OM Preadipocytes dysregulated pathways in NG Obese

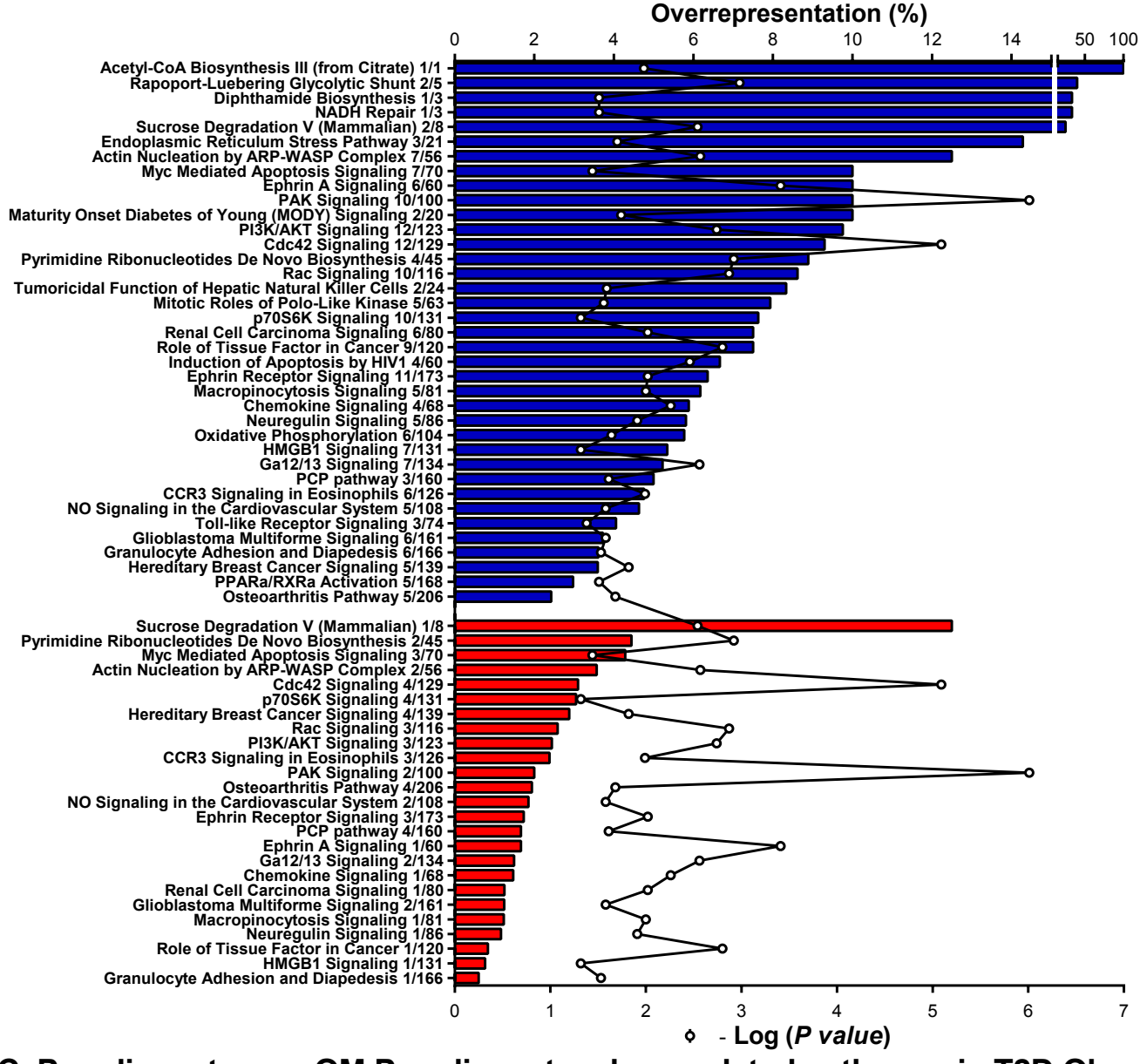

C

SC Preadipocytes *vs.* OM Preadipocytes dysregulated pathways in T2D Obese

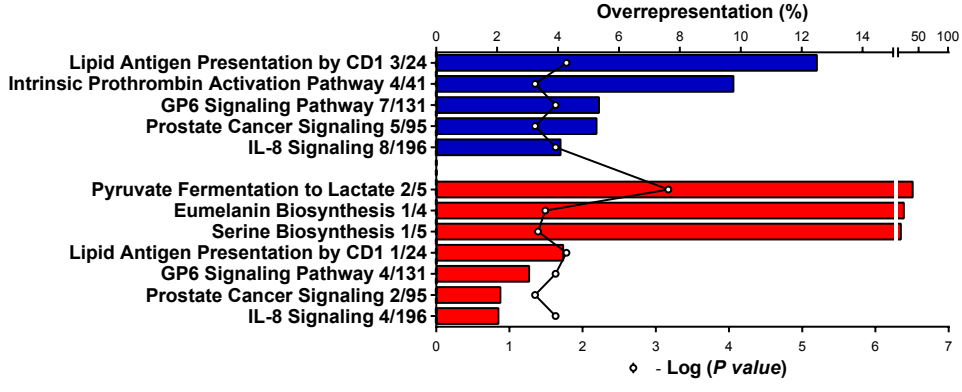

Figure 2—Figure supplement 4

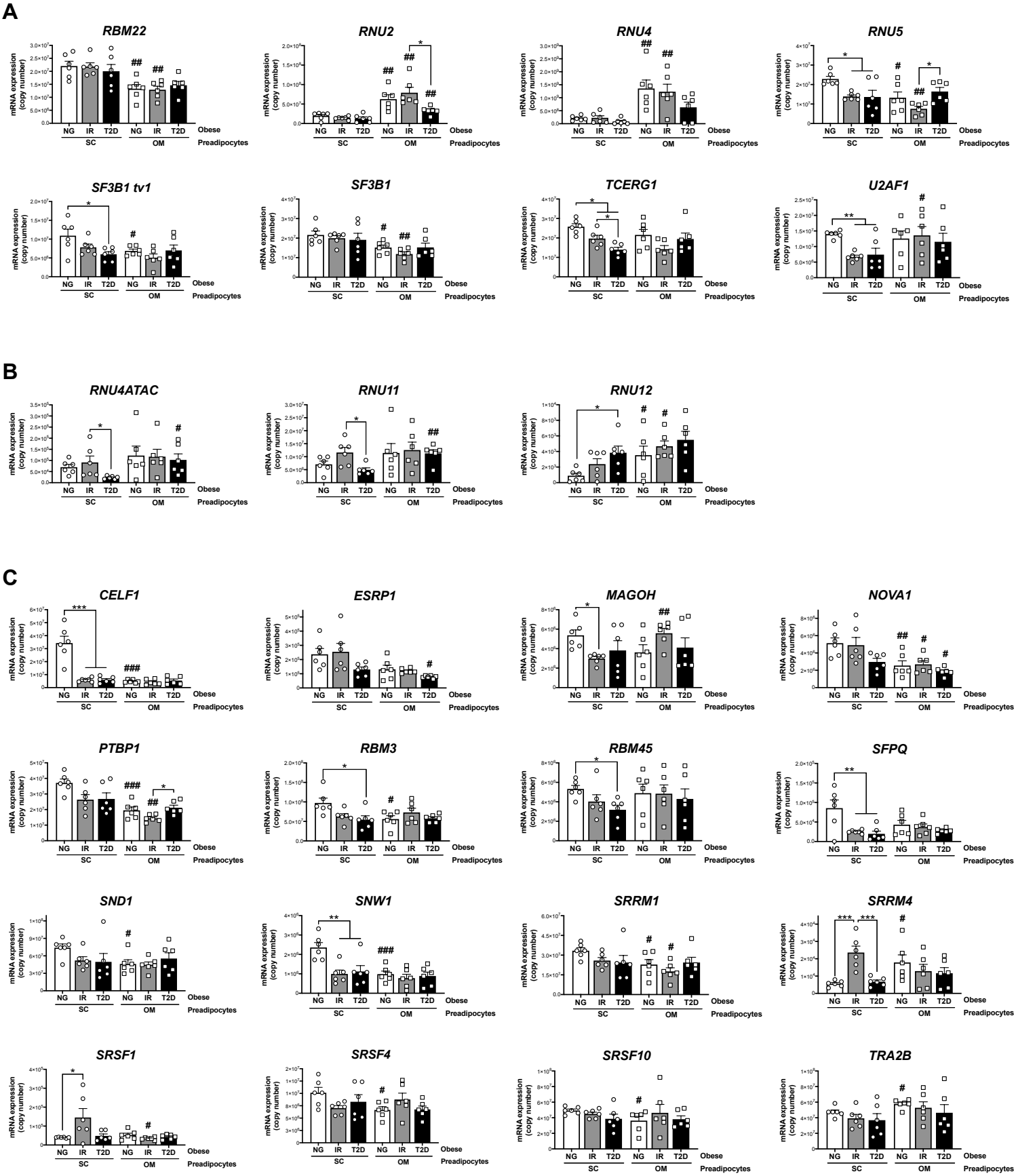

Figure 2—Figure supplement 5

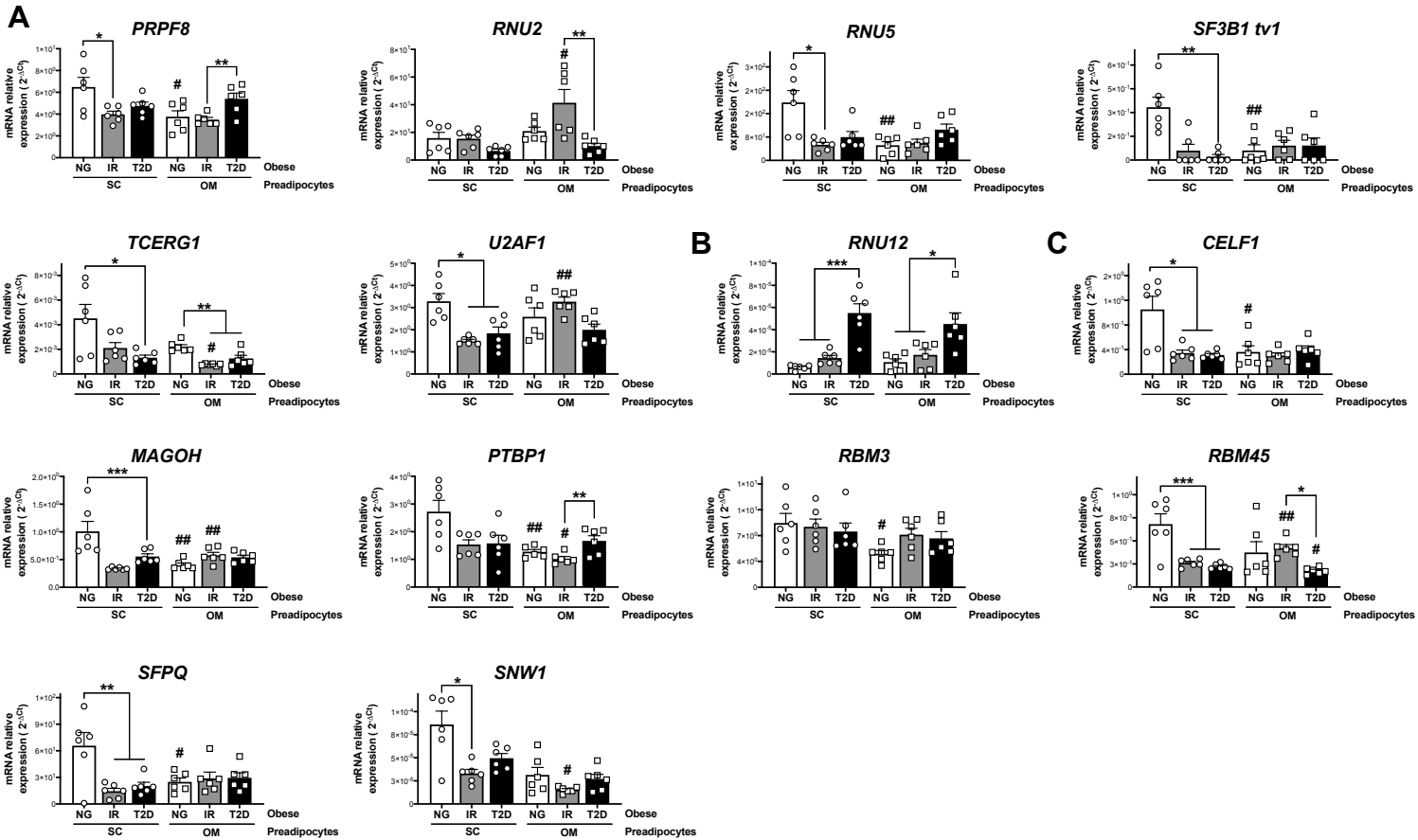

Figure 2 - Figure supplement 6

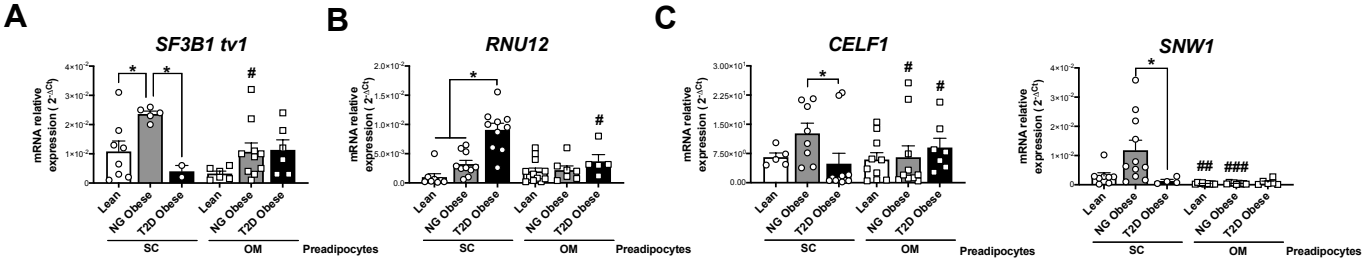

Figure 3—Figure supplement 7

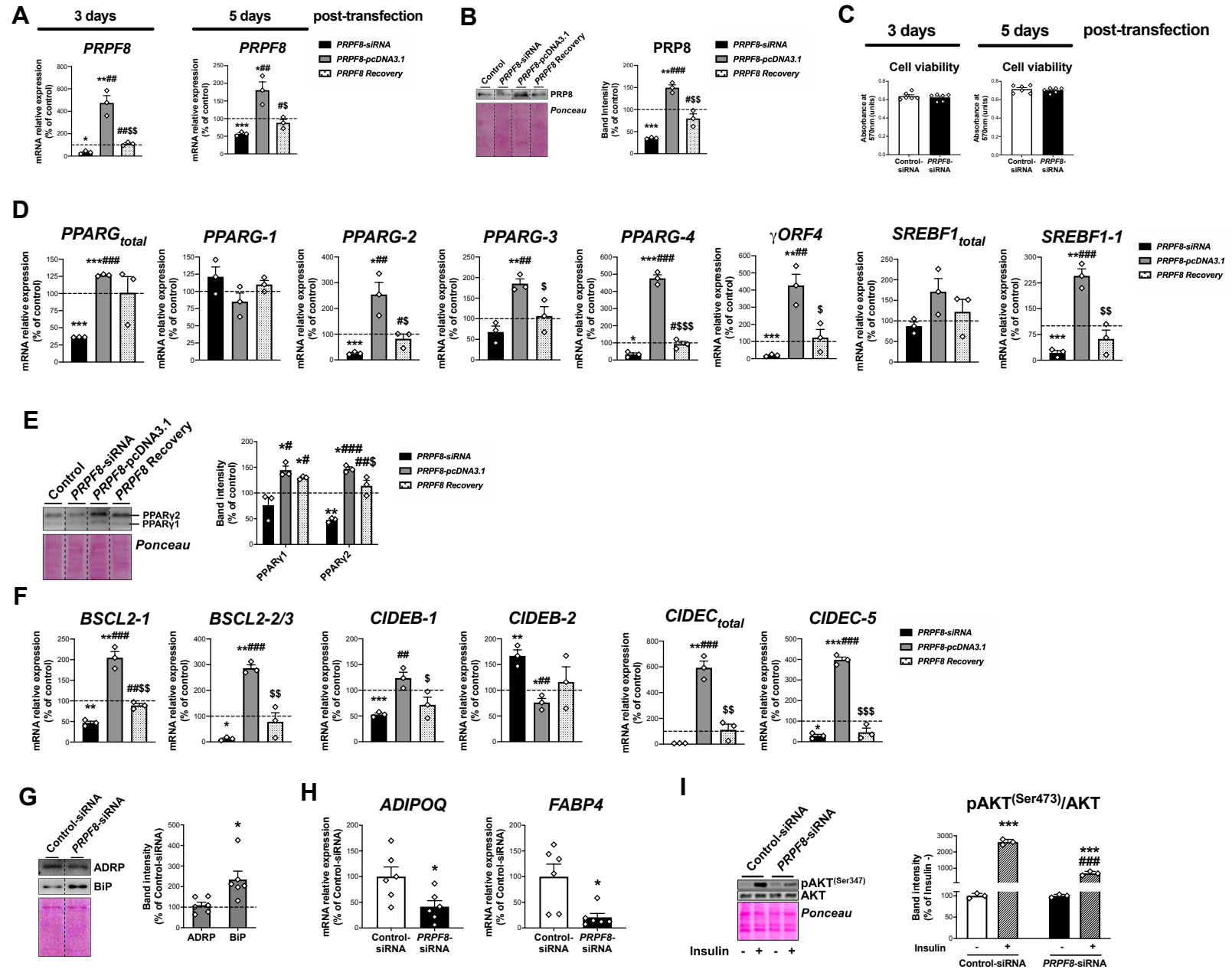

Figure 3—Figure supplement 8

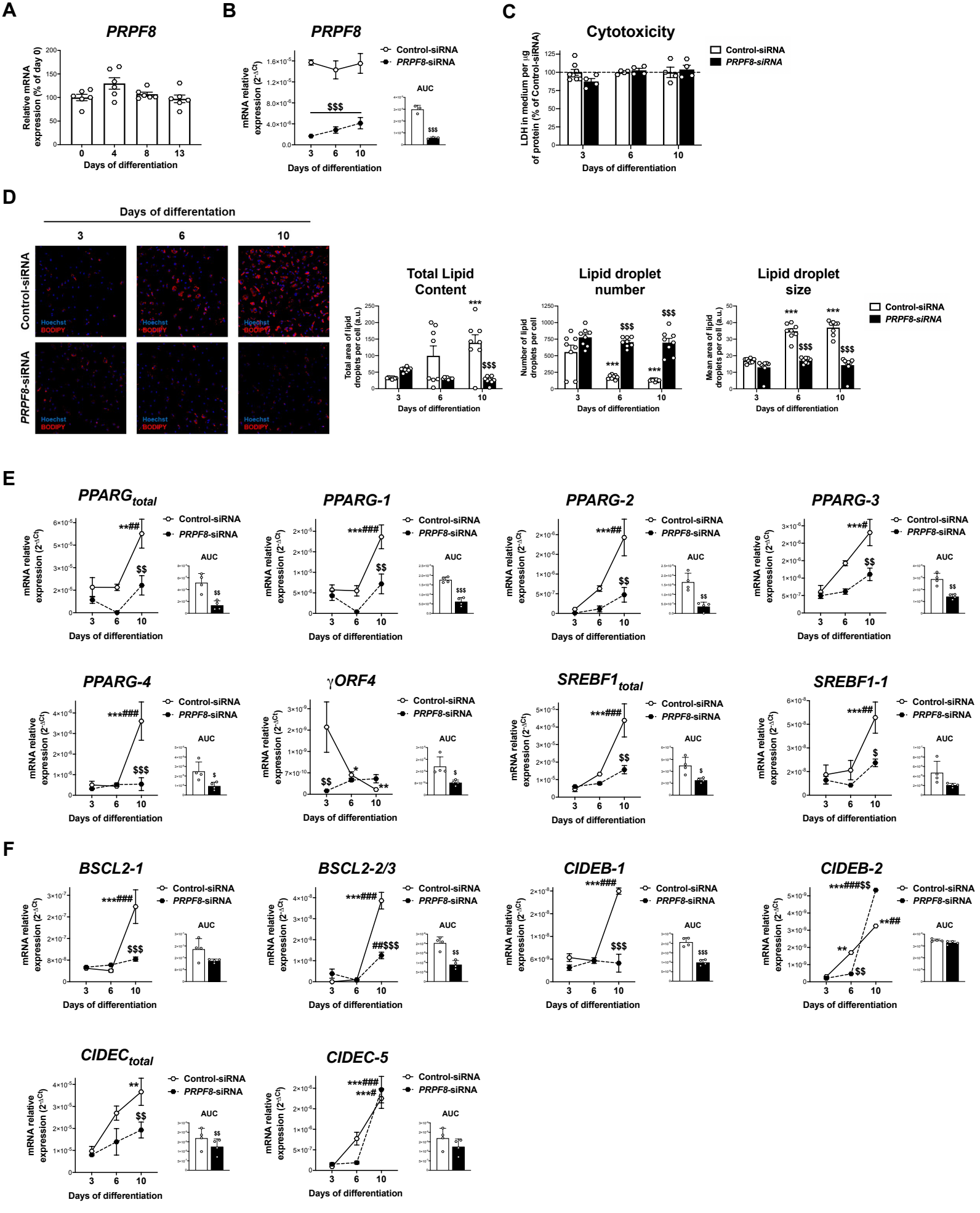

Figure 3 - Figure supplement 9

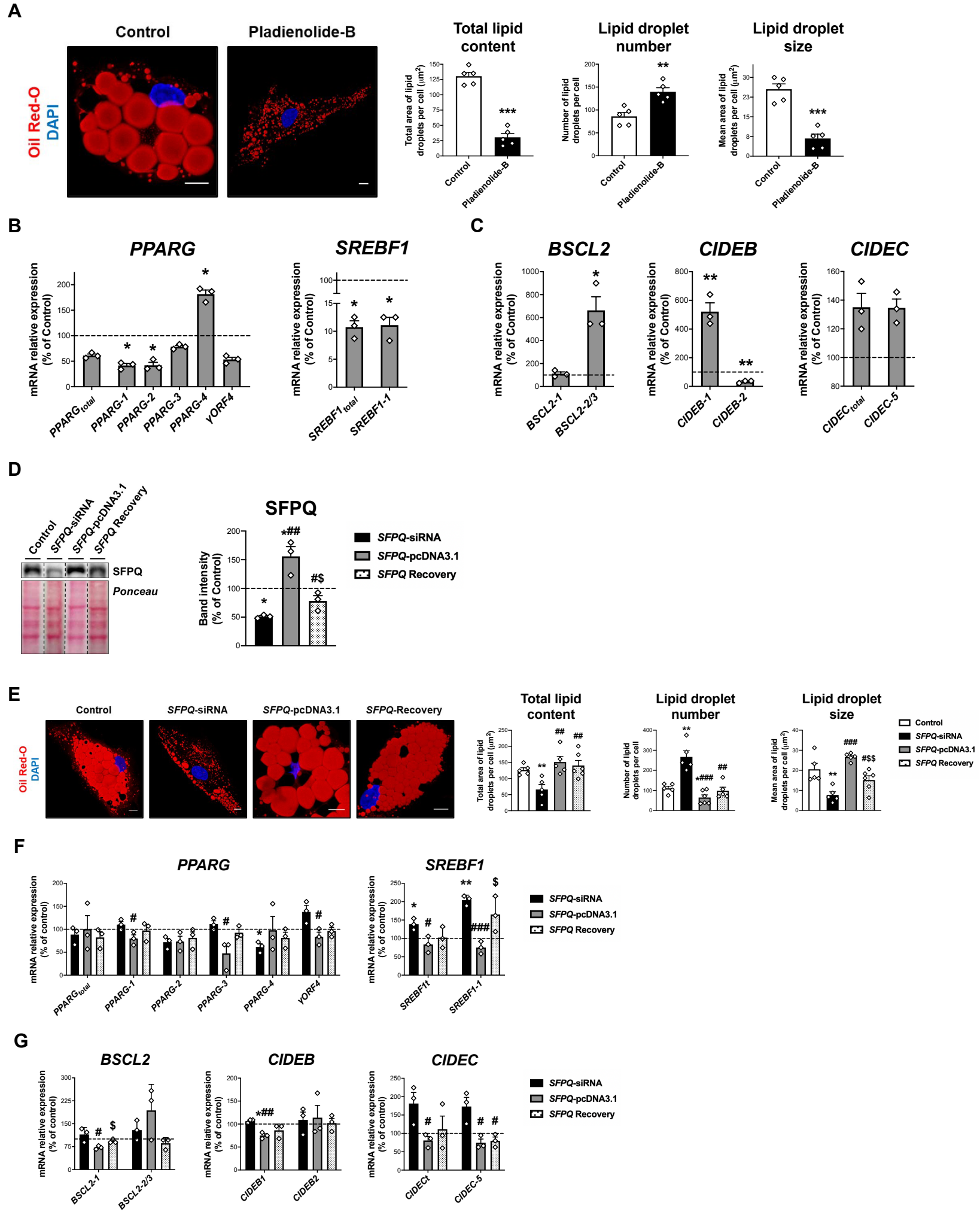

Figure 6—Figure supplement 10

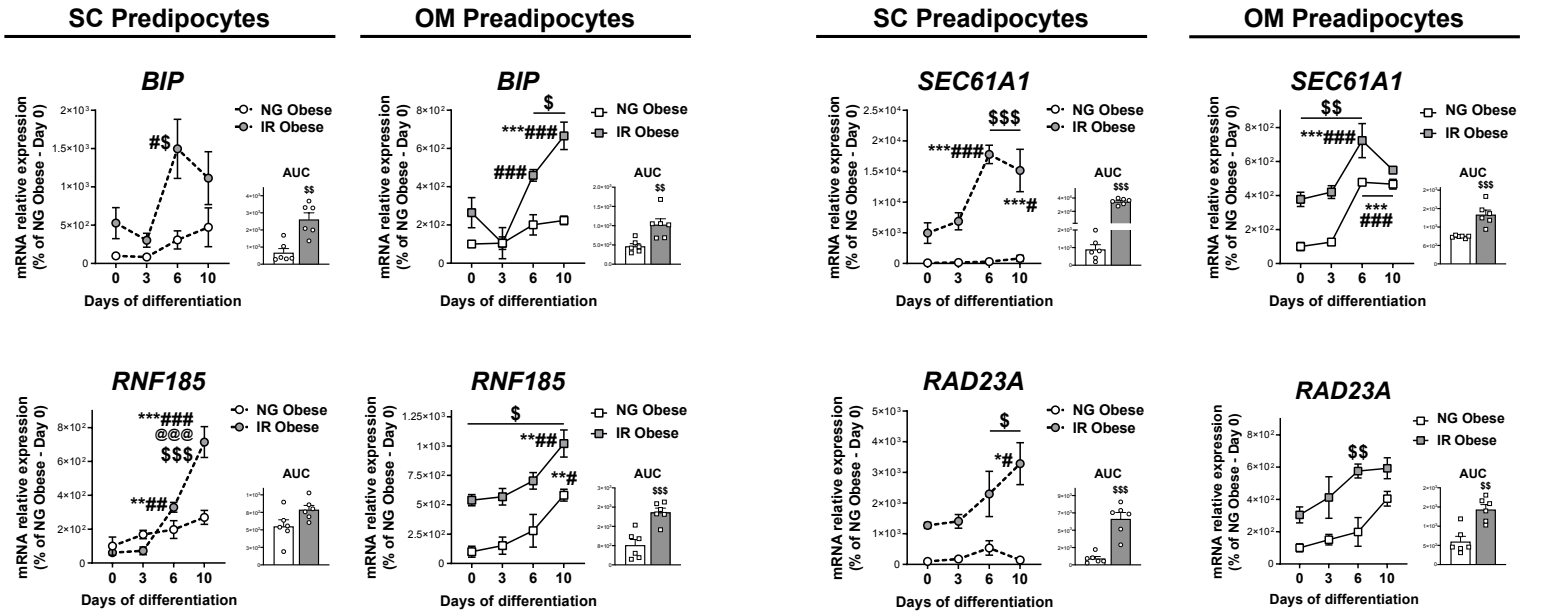

Figure 6—Figure supplement 11

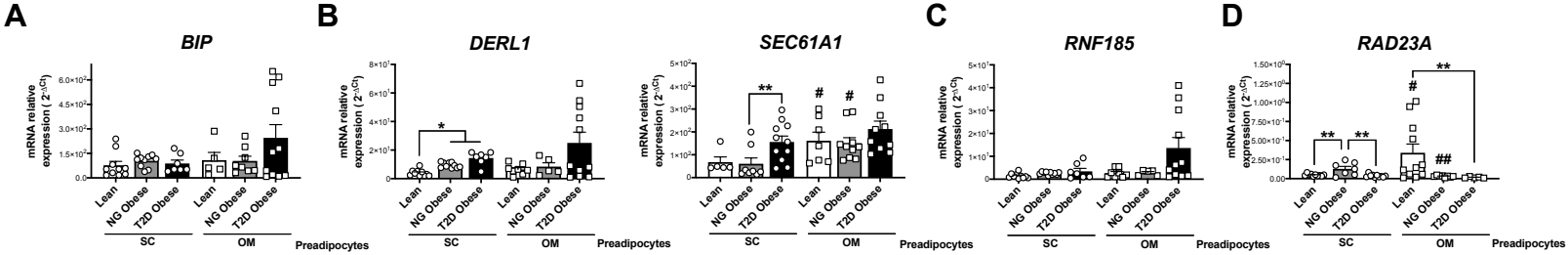

Figure 7—Figure supplement 12

A

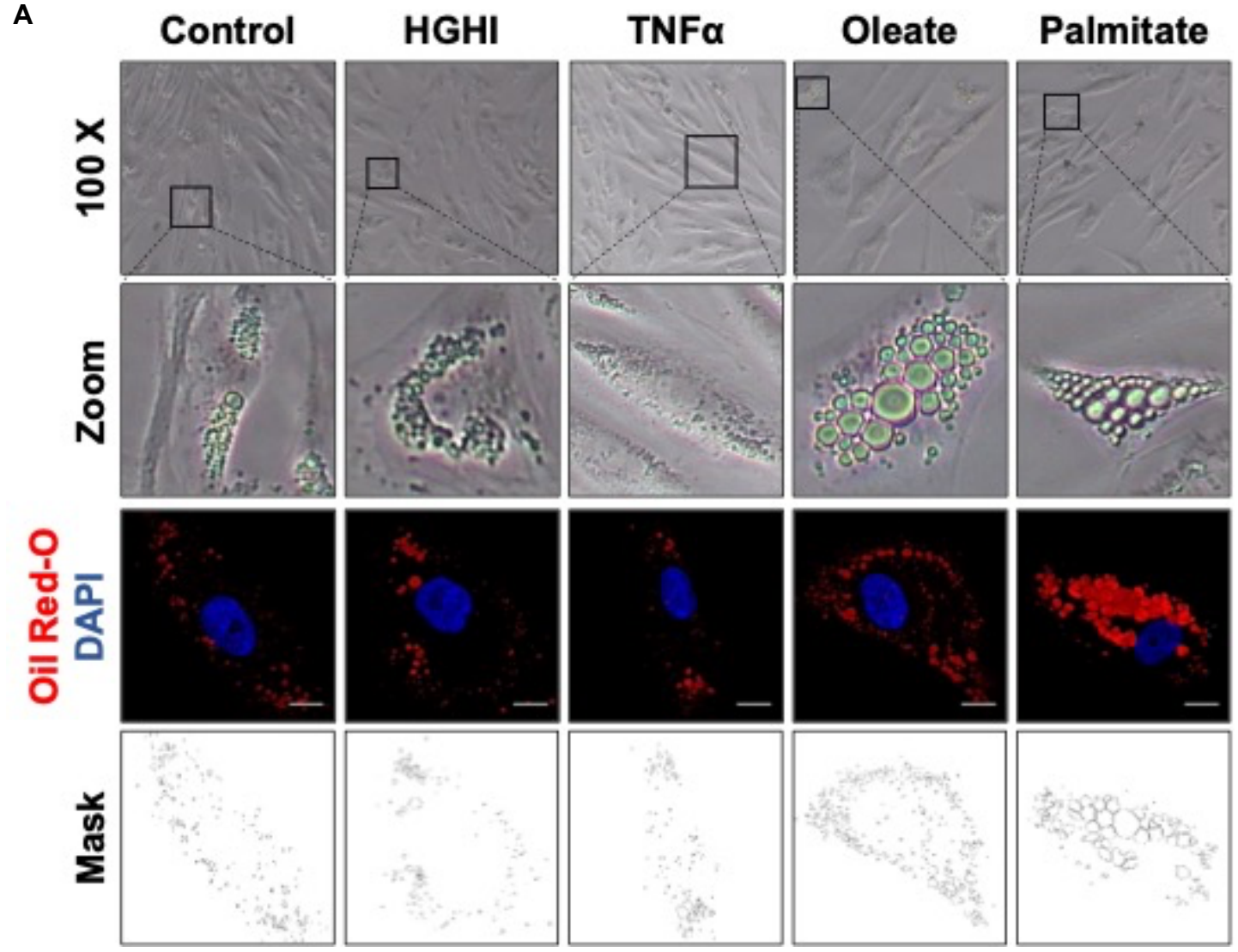

B

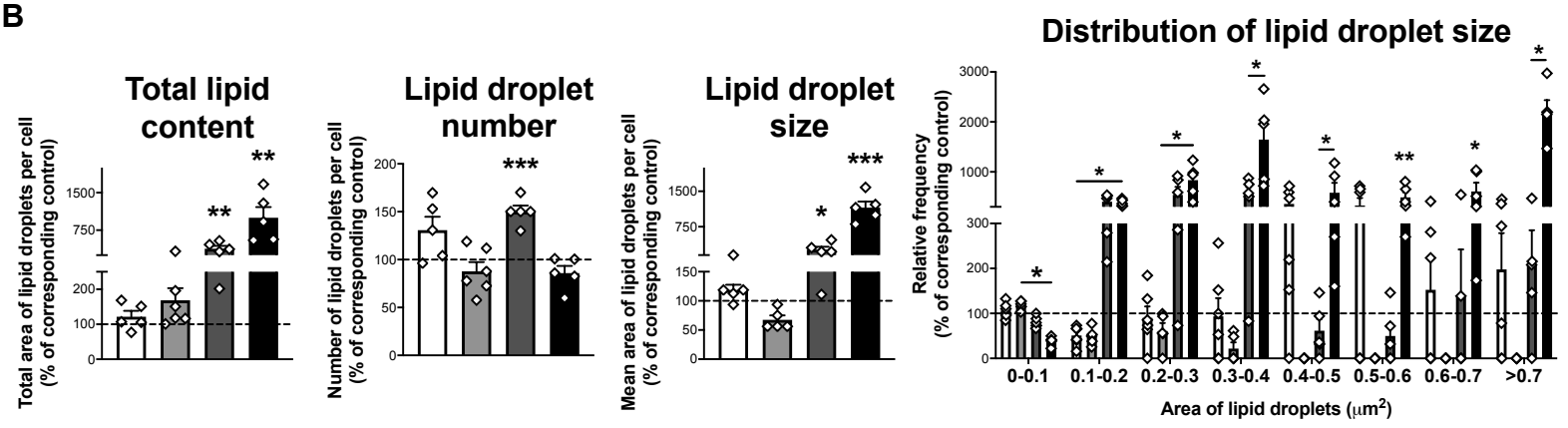

C

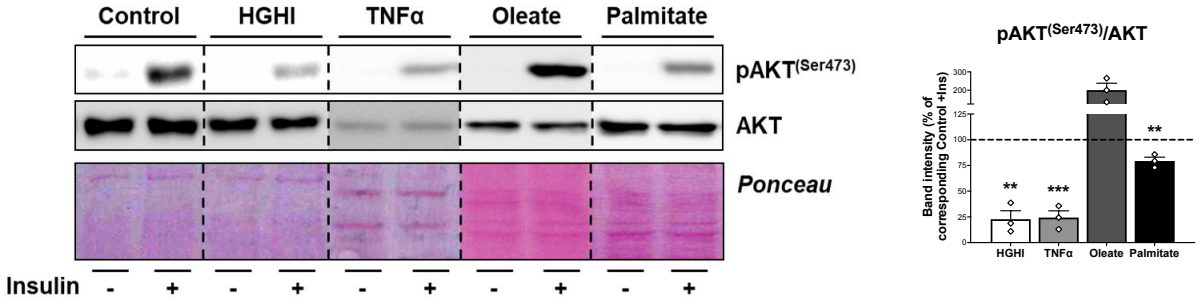

HGHI TNFα Oleate Palmitate

Figure 7—Figure supplement 13

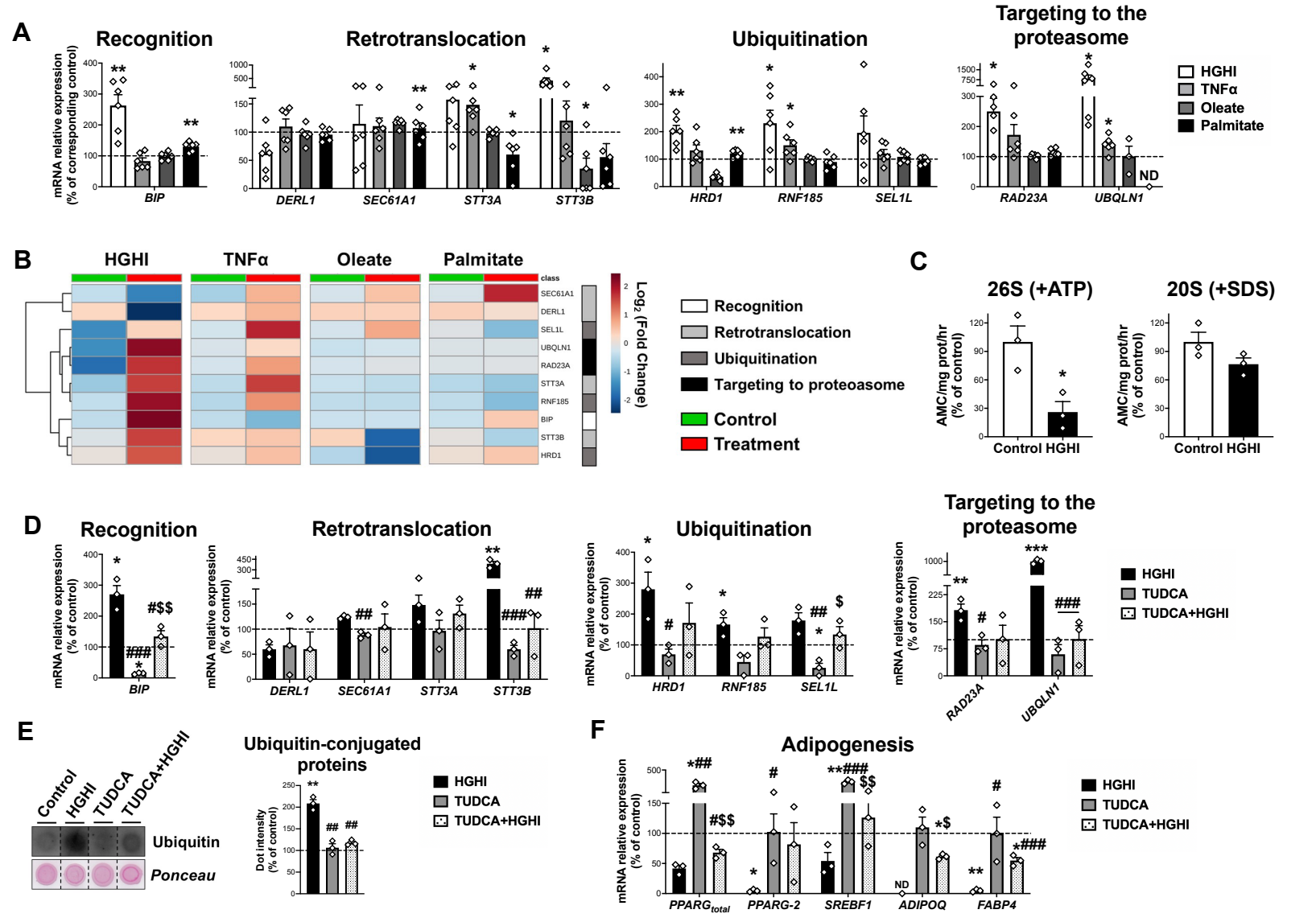
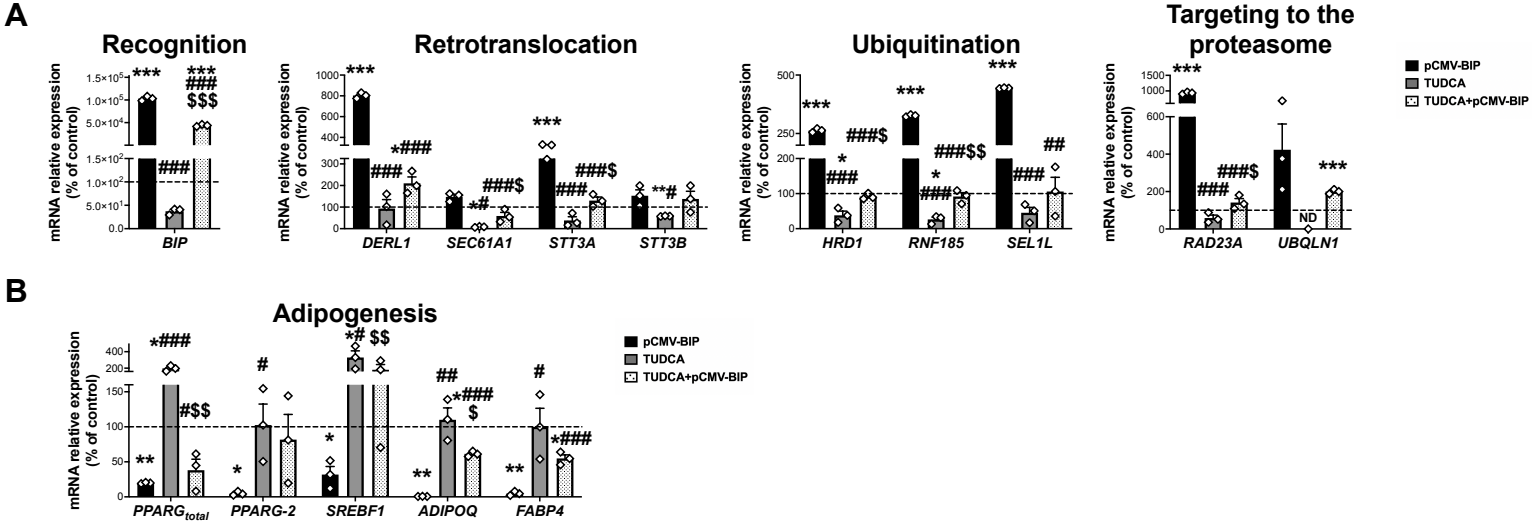
Figure 7—Figure supplement 14